ผลของปริมาณคาร์บอนต่อพฤติกรรมของกรรมวิธีทางความร้อนและความต้านทานการสึกหรอ
แบบขัดสีของเหล็กหล่อขาวธาตุผสมหลายธาตุ
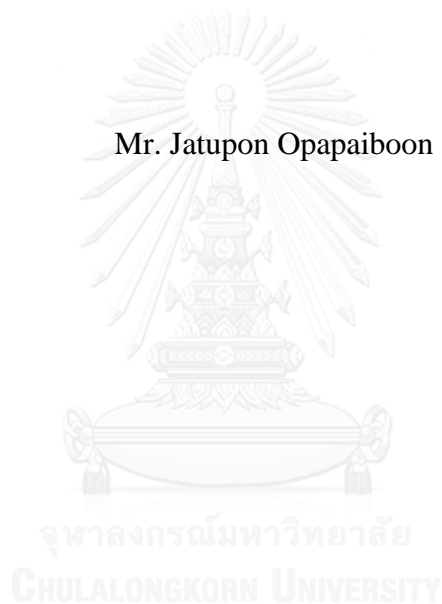
นายจตุพล โอภาไพบูลย์

วิทยานิพนธ์นี้เป็นส่วนหนึ่งของการศึกษาตามหลักสูตรปริญญาวิศวกรรมศาสตรมหาบัณฑิต
สาขาวิชาวิศวกรรมโลหการและวัสดุ ภาควิชาวิศวกรรมโลหการ
คณะวิศวกรรมศาสตร์ จุฬาลงกรณ์มหาวิทยาลัย
ปีการศึกษา 2557

EFFECT OF CARBON CONTENT ON HEAT TREATMENT BEHAVIOR AND
ABRASIVE WEAR RESISTANCE OF MULTI-ALLOYED WHITE CAST IRON

Mr. Jatupon Opapaiboon

A Thesis Submitted in Partial Fulfillment of the Requirements

for the Degree of Master of Engineering Program in Metallurgical and Materials

Engineering

Department of Metallurgical Engineering

Faculty of Engineering

Chulalongkorn University

Academic Year 2014

Thesis Title	EFFECT OF CARBON CONTENT ON HEAT TREATMENT BEHAVIOR AND ABRASIVE WEAR RESISTANCE OF MULTI-ALLOYED WHITE CAST IRON
By	Mr. Jatupon Opapaiboon
Field of Study	Metallurgical and Materials Engineering
Thesis Advisor	Associate Professor Prasonk Sricharoenchai, D.Eng.
Thesis Co-Advisor	Professor Yasuhiro Matsubara, D.Eng.

Accepted by the Faculty of Engineering, Chulalongkorn University in Partial Fulfillment of the Requirements for the Master's Degree

.... Dean of the Faculty of Engineering
(Professor Bundhit Eua-arporn, Ph.D.)

THESIS COMMITTEE

.... Chairman
(Mawin Supradist na ayudhaya, Ph.D.)

.... Thesis Advisor
(Associate Professor Prasonk Sricharoenchai, D.Eng.)

.... Thesis Co-Advisor
(Professor Yasuhiro Matsubara, D.Eng.)

.... Examiner
(Associate Professor Charkorn Jarupisitthorn, M.Eng.)

.... External Examiner
(Assistant Professor Sudsakorn Inthidech, D.Eng.)

จตุพล โอภาไพบูลย์ : ผลของปริมาณคาร์บอนต่อพฤติกรรมของกรรมวิธีทางความร้อน และความต้านทานการสึกหรอแบบขัดสีของเหล็กหล่อขาวธาตุผสมหลายธาตุ (EFFECT OF CARBON CONTENT ON HEAT TREATMENT BEHAVIOR AND ABRASIVE WEAR RESISTANCE OF MULTI-ALLOYED WHITE CAST IRON) อ.ที่ปรึกษาวิทยานิพนธ์หลัก: รศ. ดร. ประสงค์ ศรีเจริญชัย, อ.ที่ปรึกษาวิทยานิพนธ์ร่วม: ศ. ดร. ยาสุฮิโระ มัตสึบาระ, 118 หน้า.

ได้ตรวจสอบผลของปริมาณคาร์บอนต่อพฤติกรรมของกรรมวิธีทางความร้อนของเหล็กหล่อขาวธาตุผสมหลายธาตุที่มีส่วนผสมพื้นฐาน เตรียมเหล็กหล่อขาวธาตุผสมหลายธาตุที่แปรผันปริมาณคาร์บอนตั้งแต่ 1.73% ถึง 2.34% หลังการอบอ่อน ชุบแข็งชิ้นงานจากอุณหภูมิ 1323 เคลวินถึง 1373 เคลวิน แล้วอบคืนตัวที่อุณหภูมิ 673 เคลวินถึง 873 เคลวิน ในสภาพชุบแข็ง ความแข็งเพิ่มขึ้นตามปริมาณคาร์บอนที่เพิ่มขึ้นในช่วงแรก ยกเว้นความแข็งของชิ้นงานที่มีคาร์บอน 2.34% ที่ชุบแข็งจาก 1373 เคลวิน ลดลงอย่างรวดเร็ว

สัดส่วนเชิงปริมาตรของออสเทไนต์เหลือค้าง (Vγ) เพิ่มขึ้นอย่างต่อเนื่องตามปริมาณคาร์บอนที่เพิ่มขึ้น ในสภาพอบคืนตัว เส้นโค้งความแข็งของชิ้นงานแต่ละชิ้นแสดงการแข็งขึ้นทุติยภูมิอย่างชัดเจน เนื่องจากการตกตะกอนของคาร์ไบด์และการแปลงเฟสของออสเทไนต์เหลือค้างเป็นมาร์เทนไซต์ ได้ความแข็งอบคืนตัวสูงสุด (H$_{Tmax}$) จากการอบคืนตัวระหว่าง 798 เคลวินถึง 823 เคลวินที่ซึ่ง Vγ อยู่ในช่วง 4-14%

ประเมินความต้านทานการสึกหรอแบบขัดสีจากการทดสอบการสึกหรอล้อยางของชิ้นงานแต่ละชิ้นที่อบคืนตัวที่อุณหภูมิ 3 ระดับ ความสัมพันธ์ระหว่างน้ำหนักที่หายไป (W$_l$) และระยะการสึกหรอ (W$_d$) แสดงเป็นสมการเส้นตรง และหาอัตราการสึกหรอ (R$_W$) ได้จากความชันของเส้นตรง ในแต่ละสภาวะของกรรมวิธีทางความร้อน ค่า R$_W$ ลดลงหรือความต้านทานการสึกหรอเพิ่มขึ้นเมื่อปริมาณคาร์บอนเพิ่มขึ้น ในสภาพอบคืนตัว ได้ R$_W$ ต่ำสุดหรือความต้านทานการสึกหรอสูงสุดส่วนใหญ่จากชิ้นงาน H$_{Tmax}$ เมื่อค่า V$_g$ น้อยกว่า 5% R$_W$ มีค่าครอบคลุมในช่วงกว้าง แต่พบว่า R$_W$ ลดลงโดยประมาณตามสัดส่วนการเพิ่มขึ้นของความแข็ง ในช่วงที่ Vγ มากกว่า 5% R$_W$ ลดลงตามค่า Vγ ที่เพิ่มขึ้น

ภาควิชา	วิศวกรรมโลหการ	ลายมือชื่อนิสิต	
สาขาวิชา	วิศวกรรมโลหการและวัสดุ	ลายมือชื่อ อ.ที่ปรึกษาหลัก	
ปีการศึกษา	2557	ลายมือชื่อ อ.ที่ปรึกษาร่วม	

5570139021 : MAJOR METALLURGICAL AND MATERIALS ENGINEERING
KEYWORDS: MULTI-ALLOYED WHITE CAST IRON / HEAT TREATMENT / HARDNESS / VOLUME FRACTION OF RETAINED AUSTENITE / ABRASIVE WEAR RESISTANCE / CARBON EFFECT

JATUPON OPAPAIBOON: EFFECT OF CARBON CONTENT ON HEAT TREATMENT BEHAVIOR AND ABRASIVE WEAR RESISTANCE OF MULTI-ALLOYED WHITE CAST IRON. ADVISOR: ASSOC. PROF. PRASONK SRICHAROENCHAI, D.Eng., CO-ADVISOR: PROF. YASUHIRO MATSUBARA, D.Eng., 118 pp.

Effect of carbon content on heat treatment behavior of multi-alloyed white cast irons with basic alloy composition was investigated. The multi-alloyed white cast irons with varying C content from 1.73 to 2.34% were prepared. After annealing, the specimens were hardened from 1323 and 1373 K, and then tempered at 673 to 873 K. In as-hardened state, the hardness increased first as C content rose except that the hardness of 2.34% C specimen hardened from 1373 K decreased remarkably.

The volume fraction of retained austenite ($V\gamma$) increased continuously with increasing C content. In the tempered state, hardness curve of each specimen clearly showed secondary hardening due to the precipitation of carbides as well as the transformation of retained austenite to martensite. The maximum tempered hardness (H_{Tmax}) was obtained by tempering between 798 to 823 K where the $V\gamma$ ranged from 4 to 14%.

Abrasive wear resistance was evaluated by a rubber wheel wear test of each specimen tempered at three levels of temperatures. The relationship between weight loss (W_l) and wear distance (W_d) was expressed by linear function and wear rate (R_W) was obtained from the slope of the straight line. In each heat treatment condition, the R_W value decreased or the wear resistance increased as C content increased. In the tempered state, the lowest R_W or the highest wear resistance was obtained mostly in H_{Tmax} specimens. When the $V\gamma$ values less than 5%, the R_W covered in wide range but it was found that the R_W lowered roughly in proportion to the increase in hardness. In the region of $V\gamma$ over 5%, the R_W decreased with increasing $V\gamma$ value.

Department:	Metallurgical Engineering	Student's Signature	....
Field of Study:	Metallurgical and Materials Engineering	Advisor's Signature	....
		Co-Advisor's Signature	....
Academic Year:	2014		

ACKNOWLEDGEMENTS

CONTENTS

LIST OF TABLES

LIST OF FIGURES

Chapter I

Introduction

1.1 Background

Alloyed white cast irons have been developed for materials resistant to abrasive wear for about haft a century. The main purpose of their researches was to improve the abrasive wear resistance and toughness. At the moment, the alloyed white cast irons have been widely used in steel-making, mining, cement industries and thermal power plant, where various types of machines are working for crushing or pulverizing minerals. In the machines, the surface of the parts and components is heavily damaged by abrasive wear. This failure is directly accessed to the initial cost. Therefore, the technical innovation to increase the wear performance of materials with an acceptable cost has been requested.

The transition of alloyed white cast irons for steel rolling and mineral pulverizing mill rolls is shown in Fig. 1-1. The alloyed white cast iron changed from low-alloyed white cast iron through Ni-hard cast iron to high chromium (Cr) cast iron. The high Cr cast iron was most popular abrasive wear resistance materials for a long time because of superior wear performance. However, a large volume fraction of Cr carbide existing in high Cr cast iron reduces the toughness to cause failure under an addition of impact load. Therefore, the development of a new alloy which has more toughness and higher wears resistance has been requested. To achieve this purpose, the cast iron containing multiple types of carbides with higher hardness has to be designed than the chromium carbides and lower volume fraction of carbides for toughness.

After a lot of researches, the multi-alloyed white cast iron was developed around 30 years ago. This cast iron contains multiple carbide forming elements such as chromium (Cr), molybdenum (Mo), tungsten (W) and vanadium (V). The carbides formed in the multi-alloyed white cast iron were MC, M_2C, M_6C, M_7C_3 and $M_{23}C_6$ types. It is well known that MC, M_2C, M_6C carbides are secondarily precipitated in high speed tool steel, and M_7C_3 and $M_{23}C_6$ carbides precipitate in high Cr cast iron. These complex carbides have extremely high hardness and they improve the abrasive wear resistance. In the cast irons, carbide forming elements form their own special or complex carbides and the rest of them distributes into the matrix. The alloys dissolved in the matrix precipitate as secondary carbides by heat treatment and they promote the secondary hardening.
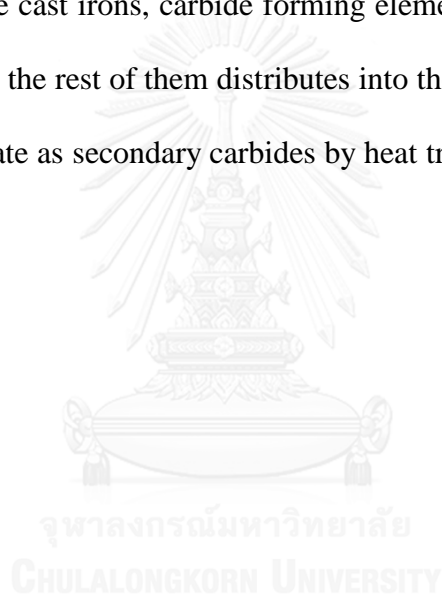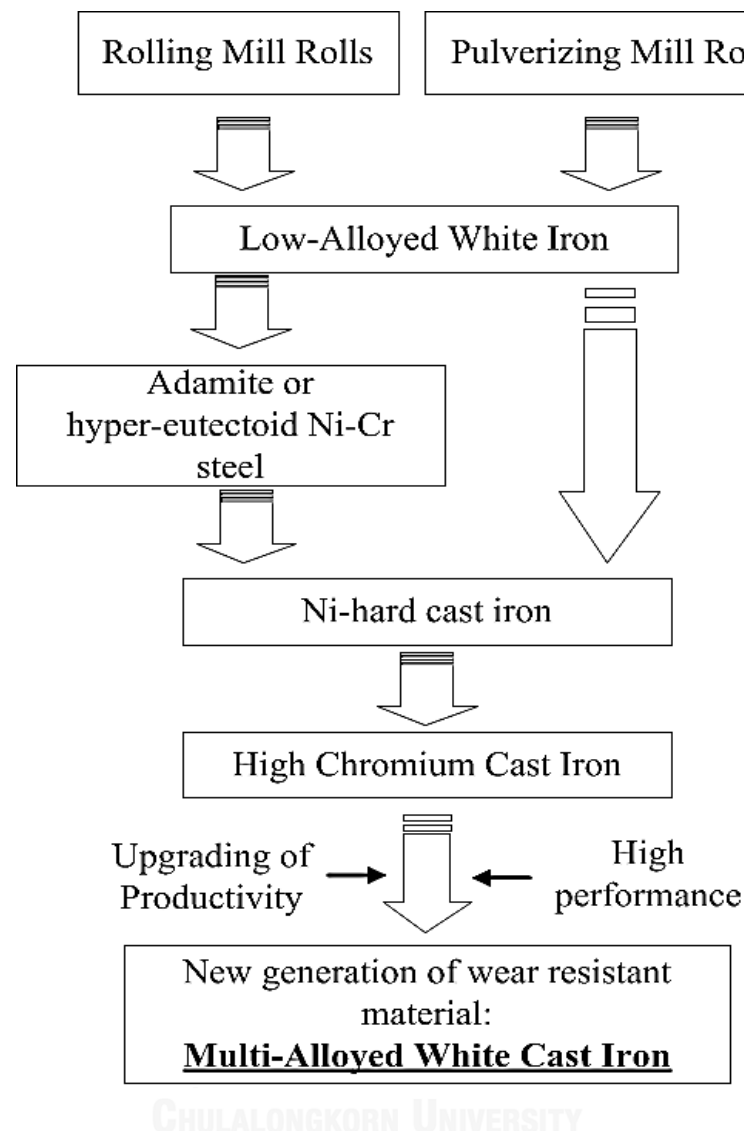
Fig. 1-1 Transition of alloyed white cast iron for steel rolling and mineral pulverizing

mill rolls [1].

The basic alloy composition of multi-alloyed white cast iron was determined by the following reasons. Since the target of the resemble and development was hot rolling mill rolls of which the Cr content ranged from 17% to 22% Cr, the total content of carbide forming elements was set to be 20%, expediently 5 mass% of each Cr, Mo, W and V [1, 2]. In addition, Cobalt (Co), which does not form its carbide, was added in order to improve the high temperature properties, such as hardness and

toughness. In this alloy system, hypoeutectic composition is preferably chosen because of toughness. During solidification, the primary austenite (γ_P) solidifies first and followed by eutectic reaction of (γ+carbide). The carbide structures, that is, type and morphology of crystallized carbides depend on the kind and the amount of carbide forming elements and solidification rate [2]. On the other side, heat treatment of alloys after solidification is very important because the matrix structures that is related to the mechanical or wear properties can be controlled and modified [3].

Generally, the heat treatment of multi-alloyed white cast iron consists of annealing, hardening and tempering processes in the same way as high Cr cast iron or tool steel [4]. During holding at austenitizing temperature, the austenite is destabilized by the precipitation of secondary carbides and then transforms to martensite or bainite during cooling to room temperature. The precipitation of special carbides due to carbides reaction occurs during tempering at high temperature. The retained austenite after holding transforms into martensite in the post cooling. As a result, the matrix with high hardness and better wear resistance are obtained.

After the great efforts of researches, a large number of the multi-alloyed white cast irons have been practically applied to hot strip mill rolls and recently the cast iron is tried to apply to the pulverizing mill materials in the cement and mining industries. It is reported that the rolling mill roll made by multi-alloyed white cast iron shows much higher performance than the conventional roll made by Ni-hard and high Cr cast iron [4]. It is convinced that this cast iron will be applied more and more in many industrial fields in the future.

In industrial applications, the abrasive wear can be classified into two-body and three-body-types [3, 5-7]. In the case of two-body-type abrasive wear, the wear occurs when abrasive materials give the concentrated stress on the surface of machine parts leading to heavy plastic deformation. The parts receiving such a wear are exampled as the frames of jaw crusher and impact crusher. In laboratory test, the abrasives used for the two-body type wear test are emery papers which SiC or Al_2O_3 particles are fixed on the paper by glue. The Suga abrasive wear tester is suitable to evaluate this type of wear resistance. In case of three-body-type abrasive wear, the abrasive particles move freely on the surface of machine parts. The example of such wear circumstances can be seen in the ball mills and tube mills to pulverize the cement clinker, coal and blast furnace slag. In this case, wear stress is normally lower than two-body type wear testing. The suitable test equipment for the three-body-type wear is a rubber wheel abrasive wear tester [5, 7].

The abrasive wear behavior in the industrial application is very complex and varies according to wear environment, type of abrasives, contacting angle, magnitude of load applied and the microstructure of materials [5]. In spite that the wear tests in many laboratories have been carried out, the test data are often invalid for the practical use [5, 8]. Therefore, it is considered that more researches to evaluate the abrasive wear have to be tried using different types of wear testers.

With respect to the multi-alloyed white cast iron for abrasive wear resistant materials, on the other hand, it is necessary that systematic research on the improvement of microstructure should be carried out. From another prospective, it is very interesting and helpful to study the effect of heat treatment on the

microstructures, and this could lead to the practical applications in the industrial field. The researches on solidification sequence and heat treatment behavior of multi-alloyed white cast irons with basic alloy composition have been already reported [9, 10]. However, the systematic research on the abrasive wear behavior related to the heat treatment is not carried out yet.

1.2 Objective of research

In this study, firstly the effect of C content on the behavior of heat treatment, that is, the variation of micro- and macro-hardness and volume fraction of retained austenite ($V\gamma$) of multi-alloyed white cast irons with basic alloy composition will be studied. Next, the abrasive wear tests of multi-alloyed white cast irons heat-treated under the some special conditions are investigated using Rubber wheel (three-body-type) abrasive wear tester. Then, their correlation of abrasive wear resistance, hardness, and volume fraction of retained austenite ($V\gamma$) are clarified.

1.3 Scopes of research

The experiments are carried out as follows:

1. Preparation of test specimens of multi-alloyed white cast irons with various C content and basic chemical composition of carbide forming elements.

2. Heat treatment of annealing at 1123 K, hardening from 1323 and 1373 K austenitizing and tempering at 673-873 K with 50 K intervals.

3. Measurement of micro- and macro-hardness in heat-treated specimens.

4. Measurement of volume fraction of retained austenite (V_{γ}) in heat-treated specimens.

5. Observation of microstructures by OM and SEM.

6. Abrasive wear tests using three-body-type (Rubber wheel) abrasive wear tester.

7. Discussion about the correlation wear resistance, among C content, hardness and $V\gamma$.

1.4 Advantages of research

(1) This research clarifies the effects of C content on heat treatment behavior of multi-alloyed white cast iron.

(2) This research clarifies the relations of abrasive wear resistance vs. hardness and $V\gamma$ of multi-alloyed white cast iron.

(3) These data give helpful guidelines to the practical heat treatment for improvement of abrasive wear resistance of multi-alloyed white cast iron.

Chapter II

Literature Reviews

Multi-alloyed white cast iron contains multiple kinds of strong carbide forming elements such as Cr, Mo, W and V so that they can form their special types of carbides, M_7C_3, M_2C, M_6C and MC during solidification [10]. These carbides have high hardness as shown in Table 2-1 and they are stable at high temperature [10, 11]. Therefore, the multi-alloyed white cast iron in which multiple kinds of carbides exist shows high abrasive wear resistance at room and elevated temperatures. Consequently, this alloy has been preferably applied to the hot rolling mill rolls in the steel industry.

Table 2-1 Hardness of carbides and matrix phases [5, 10].

Carbide or matrix	Hardness (HV)
Fe_3C / M_3C	800-1000
$(Cr,Fe)_7C_3$ / M_7C_3	1200-1800
$(Cr,Fe)_{23}C_6$ / $M_{23}C_6$	1100
$(Mo,Fe)_2C$ / M_2C	1800
$(Mo,Fe)_6C$ / M_6C	1800-2000
WC / MC	2400
$(W,Fe)_2C$ / M_2C	3000
$(W,Fe)_6C$ / M_6C	1900-2100
$(V,Fe)C$ / MC	2800
Ferrite	200-270
Pearlite	250-450
Austenite	250-500
Martensite	300-800

It is well known that Cr plays very important role for the wear performance in high Cr cast iron. In the range over 12% additions, complex Cr carbide of M_7C_3 crystalizes from liquid as a eutectic. This eutectic carbide contributes to excellent wear resistance due to high hardness and preferable toughness because it has an interconnected or discontinuous morphology [3-7]. In addition, Cr is also distributed into the matrix and improves the hardenability. Mo and W are strong carbide formers, and they form complex carbides of M_2C [$(Mo,Fe)_2C$] and M_6C [$(Mo,Fe)_6C$] types. These carbides are harder than M_7C_3 carbide. Mo and W also dissolve in the matrix and promote the hardenability but Mo works more effective than W [4, 7, 12, 13]. Mo and W increase the secondary hardening by tempering. V is well known as grain refiner in steel and it was also clarified in high Cr cast iron [2]. The V forms MC carbide with extremely high hardness as shown in Table 2-1. It seems to reduce hardenability but greatly promotes the secondary precipitation of carbides to increase the secondary hardening [4, 9, 12]. In spite that Co decreases hardenability, it is added to the multi-alloyed white cast iron to improve the resistance to softening and the strength at high temperature, because Co raises the eutectic temperature and decreases the coarsening of grain at the elevated temperature by the effect to decrease the diffusivity of carbon and retarding coarsening of secondary carbides [2, 12-14].

2.1 Alloy designing

The basic alloyed composition of High Cr cast iron for steel rolling mill rolls in the industries are composed 17 - 22% Cr to forming strong carbide such as $M_{23}C_6$ and dissolve into matrix to solid solution strengthened for high hardness and superior wear resistance. To compare the properties of the multi alloyed white cast iron with

those of high Cr cast iron, the total content of strong carbide forming elements is set in the range of %Cr of high Cr cast iron. The basic chemical composition of multi-alloyed white cast iron designed as 5% of each Cr, V, Mo, W and Co was proposed by Matsubara et.al. [9]. On the other side, it is supported for the further research and development of the effect of each alloying element on the heat treatment behavior and abrasive wear resistance. It is known that C in the cast iron melt is combined with carbide forming elements to form their special carbides and the rest distributes into the matrix. In order to estimate C content that dissolves in the matrix, it is convenient to introduce a parameter of carbon balance (C_{bal}) as expressed in the following equation [9, 10, 15].

$$C_{bal} = \%C - C_{Stoich} \quad\quad\quad\quad (2.1)$$

Here, %C is C content of the cast iron and C_{Stoich} is stoichiometric amount of carbon that just combines with all of carbide forming elements in the cast iron. In case that M_7C_3 carbide does not exist in microstructure of the cast iron, the C_{Stoich} can be calculated using the following equation.

$$C_{Stoich} = 0.060\ \%Cr + 0.063\ \%Mo + 0.033\ \%W + 0.235\ \%V \quad\quad (2.2)$$

In case that M_7C_3 carbide precipitates in the cast iron, the equation is expressed as follows,

$$C_{Stoich} = 0.099\ \%Cr + 0.063\ \%Mo + 0.033\ \%W + 0.235\ \%V \quad\quad (2.3)$$

C in the matrix plays important role in phase transformation of matrix or heat treatment. Therefore, C_{bal} is very important factor to determine both of carbide

and matrix structures. Under equilibrium condition, positive value of C_{bal} means that excess of carbon remains in the matrix and negative value means that carbon is not saturated in the matrix. As for the basic alloy composition of multi-alloyed white cast iron, it is desirable in subsequent heat treatment that the C_{bal} is settled around 0% [9, 15].

2.2 Carbides in multi-alloyed white cast iron

As mentioned previously, multiple kinds of eutectic carbides precipitate from the melt in the multi-alloyed white cast iron. The type, morphology and volume fraction of carbides depend on chemical composition of the cast iron and cooling rate during solidification [10]. Low cooling rate promotes formation of coarse solidification structure while high cooling rate provides fine one [16]. An increase in C content makes carbides precipitate more and uniformly in the microstructure and changes the carbide morphology [10, 17, 18].

Types of carbides and alloy concentration in the multi-alloyed white cast iron are illustrated in Table 2-2. As for the configuration of carbide, MC carbide has three morphologies, petal-like or flaky, nodular and coral-like while M_2C carbide has two morphologies, lamellar and plate-like as shown in Fig. 2-1 for MC, Fig. 2-2 for M_2C and Fig. 2-3 for M_7C_3 carbide, respectively.

It was reported that MC carbides are dispersed throughout the matrix but M_2C carbides are unevenly distributed in the region of grain boundary [19-21]. M_7C_3 carbide shows rod-like or ledeburitic morphology. It is known that M_7C_3 carbides appeared in the cast iron with high C content [5, 22, 23]. From Table 2-2, it

is found that MC carbide is mainly composed of V while M_2C carbide consists of Mo and W. M_7C_3 carbide contains mainly Fe and Cr with some other elements.

Table 2-2 Type and alloy concentration in carbides and matrix of multi-alloyed white cast iron with basic chemical composition [10].

Phase	Elements (%)					
	Cr	Mo	W	V	Co	Fe
MC	3.0 ~ 4.1	4.2 ~ 10	4.3 ~ 8.3	49 ~ 65	0.6 ~ 1.0	16 ~ 18
M_2C	10 ~ 15	26 ~ 30	19 ~ 22	6.4 ~ 12	0.8 ~ 1.3	20 ~ 26
M_7C_3	17 ~ 24	5.3 ~ 9.0	3.6 ~ 5.4	3.2 ~ 6.2	2.2 ~ 3.2	59 ~ 66
Matrix	3.5 ~ 4.2	0.2 ~ 1.3	1.8 ~ 3.1	1.0 ~ 2.4	0 ~ 14	82 ~ 85

The comparison in two-dimensional and three-dimensional microstructures of carbides by SEM is shown in Fig. 2-1 for MC carbide, 2-2 for M_2C carbide and 2-3 for M_7C_3 carbide, respectively. As shown in Fig. 2-1 (a), the flat microstructure of the flaky MC carbides observed is string-like or granular and discontinuous, but they have petal-like or cornflake configuration three-dimensionally and that they are interconnected. The nodular MC carbide shown in Fig. 2-1 (b) can be imagined as a sphere crystallized by itself. It is true from the three-dimensional SEM microphotograph, but some of nodular MC carbides could be finally connected to eutectic M_7C_3 carbides precipitated by the eutectic reaction of ($L\rightarrow\gamma+M_7C_3$).

In the case of MC carbides shown in Fig. 2-1 (c), which appears in the hypereutectic cast iron, nodular and flaky or grain carbides co-exist in the matrix

two-dimensionally. However, they have three- dimensionally a configuration like a coral in which primary MC carbides precipitated independently and connected to eutectic MC carbides formed by the eutectic reaction of $(L \rightarrow \gamma + MC)$.

As for microstructures of M_2C carbides in Fig. 2-2 (a) and (b), they show fine or coarse rod-like M_2C carbides two-dimensionally and they have lamellar morphology consisting of many fine or coarse plates of M_2C carbides three-dimensionally.

The comparison of M_7C_3 microstructures are shown in Fig. 2-3 (a) for two-dimensionally and (b) for three-dimensionally. In OM microphotograph (a), it can be understood that M_7C_3 carbides precipitate coexisting with M_2C eutectic carbides in the boundary region of primary austenite, and it seems to be mixed. However, both eutectic solidifications occur separately in the different order. In the three-dimensional microphotograph by SEM, on the other side, it can be obviously found that each eutectic solidification of $(L \rightarrow \gamma + MC)$, $(L \rightarrow \gamma + M_7C_3)$ and $(L \rightarrow \gamma + M_2C)$ takes place independently.

Optical Microscope (Two-dimensionally microstructure)	Scanning Electron Microscope (Three-dimensionally microstructure)
Flaky (a)	Petal-like
Nodular (b)	Sphere
Nodular (c)	Coral-like
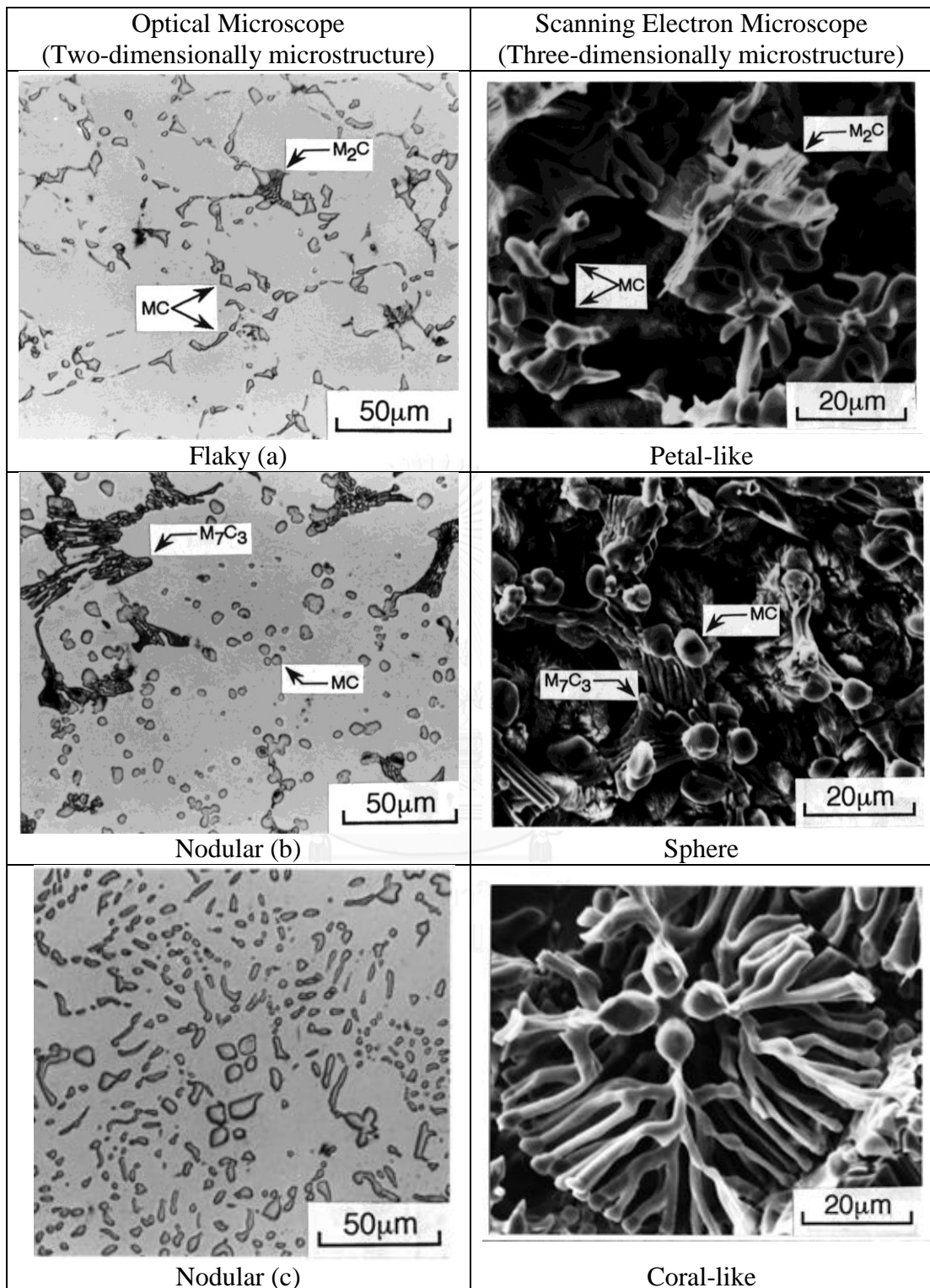
Fig. 2-1 Comparison of two-dimensionally and three-dimensionally microstructures of MC carbides precipitated from the melt in multi-alloyed white cast iron by OM and SEM [10].

Optical Microscope (Two-dimensionally microstructure)	Scanning Electron Microscope (Three-dimensionally microstructure)
Fine rod-like (a)	Lamellar
Coarse rod-like (b)	Coarse plate-like
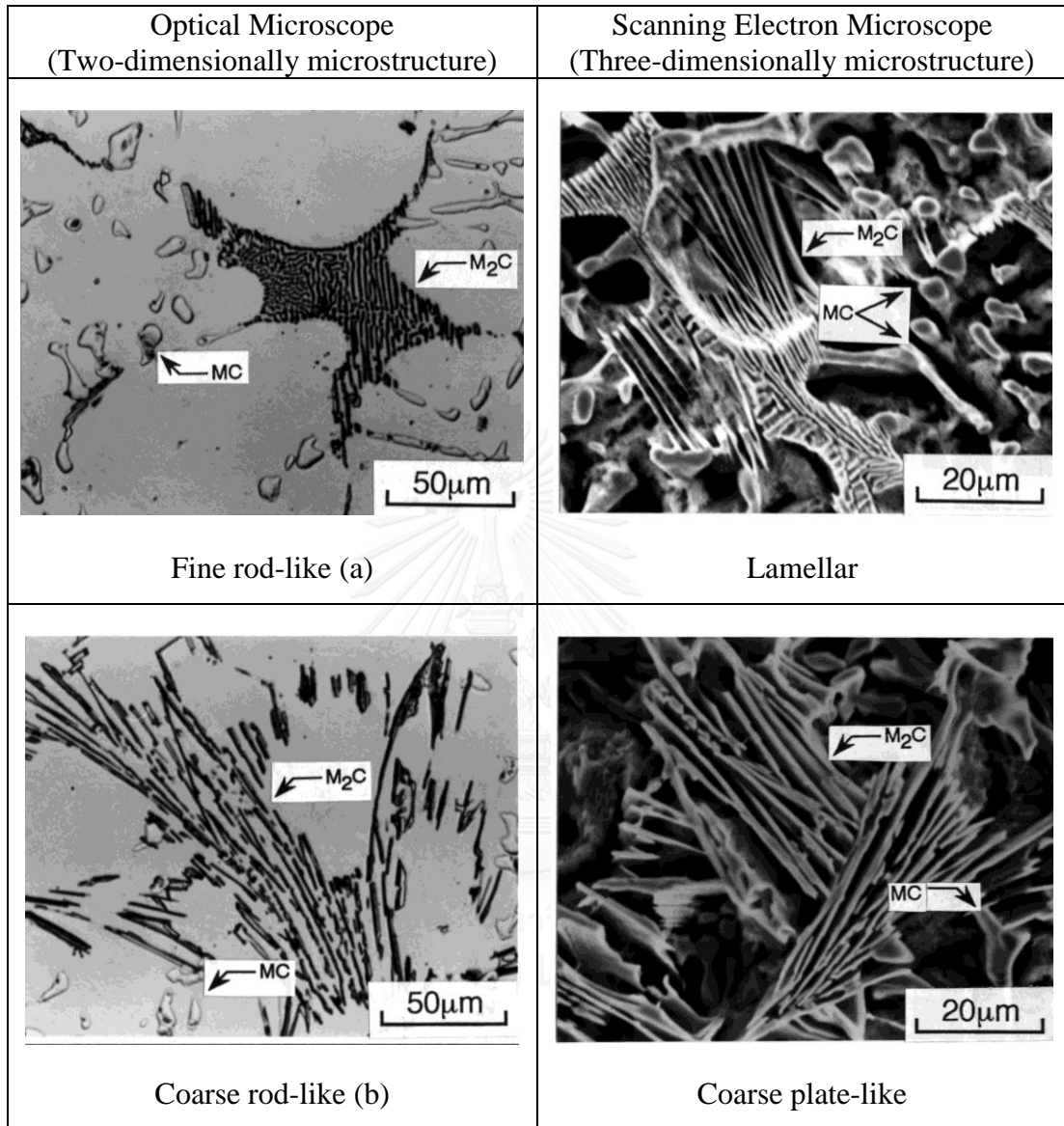
Fig. 2-2 Comparison of two-dimensionally and three-dimensionally microstructures of M_2C carbides precipitated from the melt in multi-alloyed white cast iron by OM and SEM [10].

Optical Microscope (Two-dimensionally microstructure)	Scanning Electron Microscope (Three-dimensionally microstructure)
(a)	(b)
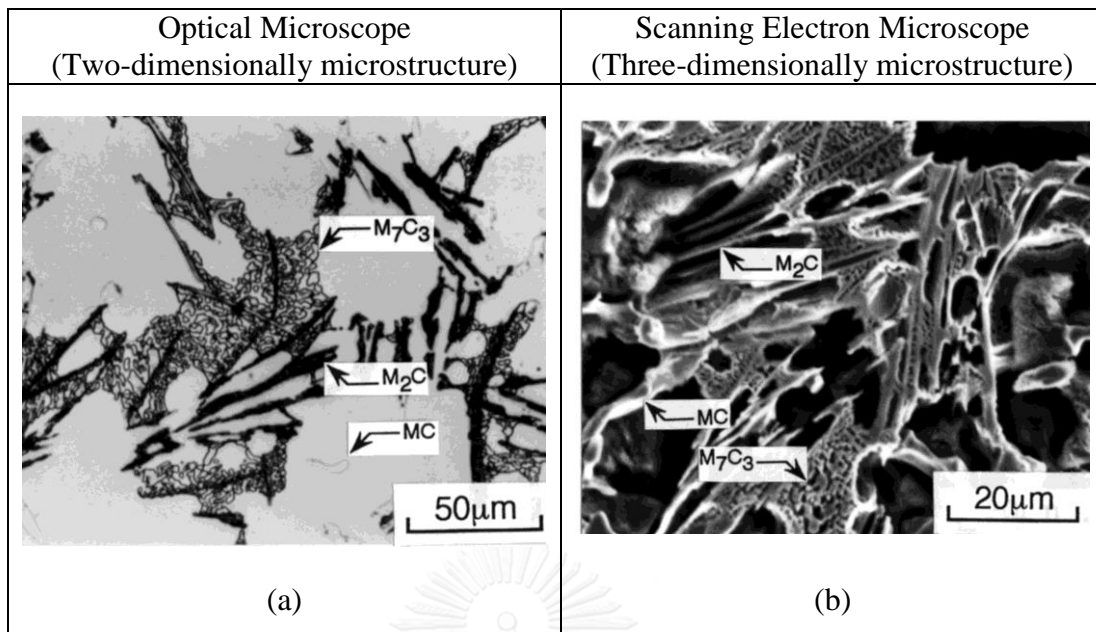
Fig. 2-3 Comparison of two-dimensionally and three-dimensionally microstructures of M_7C_3 carbides precipitated from the melt in multi-alloyed white cast iron by OM and SEM [10].

The diagram of solidification structures related to variation of C and V contents in basic of multi-alloyed white cast iron was reported by Wu et.al. [10, 23, 24]. Influence of V and C contents on type and morphology of eutectic carbide is shown in Fig. 2-4 for Fe-5%Cr-2%Mo-2%W-5%Co alloy system. It is found that morphology of MC carbide differs due to the combination of C and V contents. The nodular MC carbide appears in the area of 1-6% V and over 1.4% C. The petal-like or flaky MC carbide precipitates in low C content less than 1.8% and 1-10% V. The coral-like MC carbide crystallizes in the range of 8-15% V. As the V content increases, more C content is necessary to form M_7C_3 carbide. Therefore, the formation of M_7C_3 carbide occurs in the area of high C content. M_2C carbide exists in the region between MC and M_7C_3 carbides.

Effect of tungsten equivalent (W_{eq}) and C content on eutectic carbide is shown in Fig. 2-5. The W_{eq} can be calculated from the following equation [9, 10].

$$W_{eq} = \% \ W + 2 \ (\%Mo) \quad \text{...}(2.4)$$

It is found from Fig. 2-4 and Fig. 2-5 that the change of V, C and W_{eq} values have effect on formation of type and morphology of carbides. The nodular MC carbides appear when W_{eq} is less than 11% and C content is higher than 1.8%. Out of this region, where W_{eq} is over 11% and C content is more than 1.8%, the petal-like or flaky MC carbide is mostly obtained. As for M_7C_3 carbides, they precipitate co-existing with MC carbides in the region above the straight line in Fig. 2-5. It is clear that the morphology of M_2C carbide can be related to the combination of C content and W_{eq} value. M_2C carbide in the lamellar morphology appears where W_{eq} is less than 15% and the plate-like M_2C carbide does when W_{eq} value is higher than 15%.
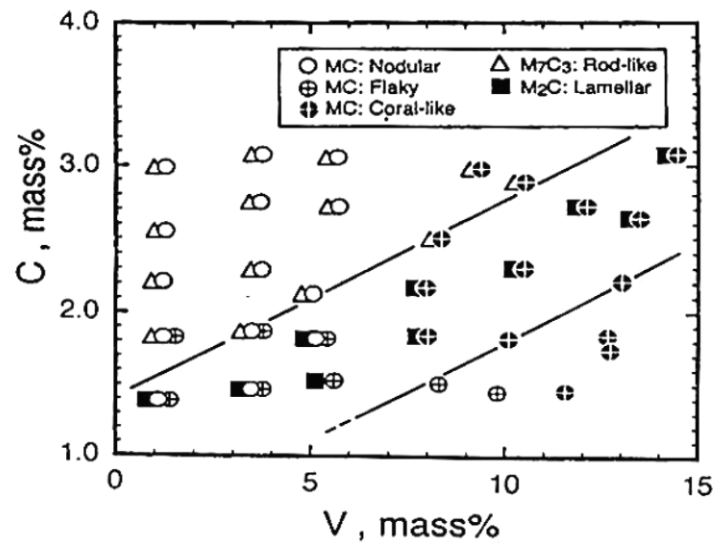
Fig. 2-4 Effect of V and C contents on type and morphology of carbide precipitated

from the melt in multi-alloyed white cast iron [10].
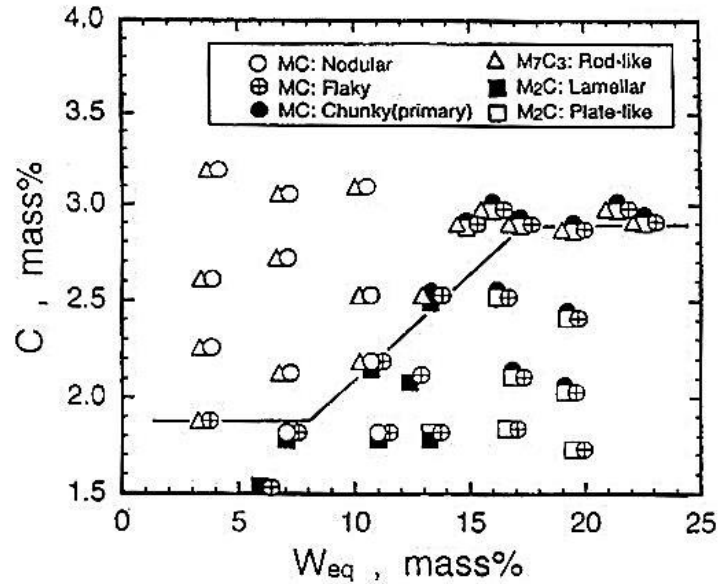
Fig. 2-5 Effect of W_{eq} value and C content on type and morphology of carbides

precipitated from the melt in multi-alloyed white cast iron [10].

Influence of Co and C contents on type and morphology of eutectic carbide in Fe-5%Cr-2%Mo-2%W-5%V alloy system is shown in Fig. 2-6. It is interesting that both type and morphology of carbides do not change even if Co content is varied. Regardless of Co content, the flaky MC carbide and the lamellar M_2C carbide exist when C content is less than 2%. When C content is over 2%, on the contrary, the nodular MC and the rod-like M_7C_3 carbides co-exist. Therefore, it can be said that Co does not effect on the carbide structure.
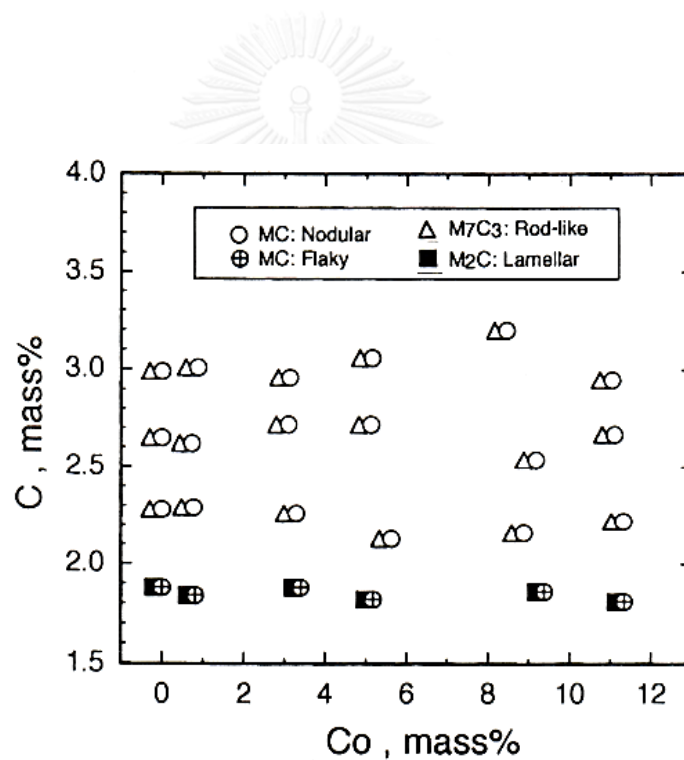
Fig. 2-6 Effect of Co and C contents on type and morphology of carbides precipitated from the melt in multi-alloyed white cast irons [10].

Influence of solidification rate and C content on carbide structure in multi-alloyed white cast iron is shown in Fig. 2-7. MC carbides precipitate at all the solidification rates but the morphology is different. M_7C_3 carbide is formed in the region of high C content and low solidification rate. M_3C carbide appears in a small area at very high C content and very low solidification rate.
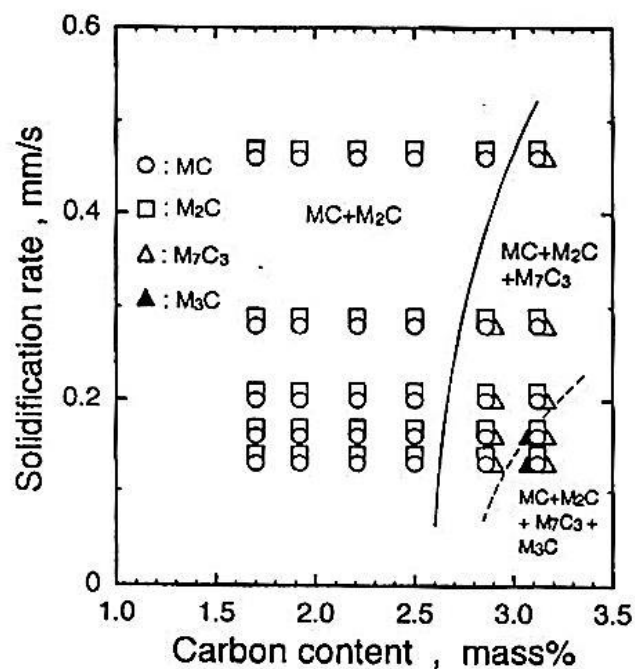
Fig. 2-7 Type of carbide corresponding to solidification rate and C content in multi-alloyed white cast iron [10].

2.3 Matrix of multi-alloyed white cast iron

Matrix in the as-cast state consists of bainite, martensite and some retained austenite [9, 12-24]. Volume fraction of retained austenite ($V\gamma$) ranges widely from 5 to 50% depending on C content of the cast iron [9]. Higher C content contains more retained austenite. This is because C decreases Ms temperature. An increase in

solidification rate reduces amount of retained austenite [9]. However, retained austenite is supposed to transform into the useful phases by heat treatment [9, 19].

2.4 Solidification sequence and phase diagram of multi-alloyed white cast iron

The C content and alloying elements are varied so that several combinations of eutectic carbides can be obtained in multi-alloyed white cast iron. The solidification sequences were investigated by means of quench tests during thermal analysis [10, 23, 24]. As an example, the thermal analysis and the transition of microstructures obtained by quenched specimens during solidification are shown in Fig. 2-8 (a) and (b) for the multi-alloyed white cast iron with basic chemical composition (Fe-5%Cr-5%Mo-5%W-5%V-5%Co-2%C alloy system), in which the petal-like MC and plate-like M_2C carbides co-exist. In the thermal analysis curve (a), quenched positions are shown and the change or transition of microstructure by quench tests is shown in (b). First of all, primary austenite dendrite forms at 1590 K, followed by precipitation of (γ+MC) eutectic at 1558 K, and finally (γ+M_2C) eutectic begins to solidify at 1422 K. Solidification sequences of the other kinds of multi-alloyed white cast irons with various chemical compositions are summarized in Table 2-3.
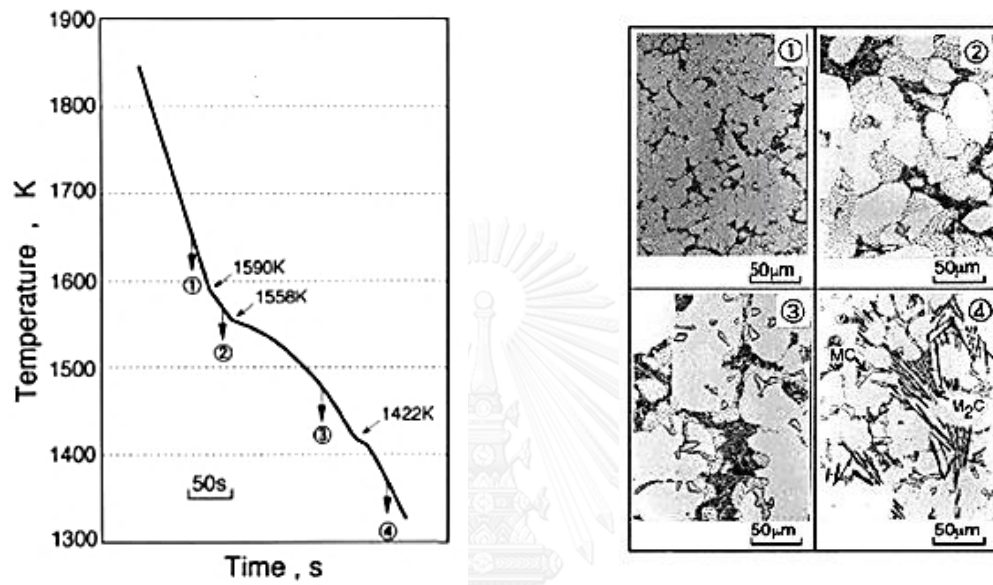
(a) Thermal analysis curve   (b) Transition of microstructure by quench tests

Fig. 2-8 Solidification of multi-alloyed white cast iron with basic chemical composition (Fe-5%Cr-5%Mo-5%W-5%V-5%Co-2%C) [23].

Table 2-3 Solidification sequences of multi-alloyed white cast irons with various

chemical compositions [23].

Number	Chemical composition	Combination of carbide	Solidification Sequence	
1	2%C-5%Cr -2%Mo-2%W -9%V-5%Co	Coral-like MC- Lamellar M_2C	$L_0 \rightarrow \gamma_p + L_1$ $L_1 \rightarrow (\gamma+MC)_E + L_2$ $L_2 \rightarrow (\gamma+M_2C)_E$	at 1651 K at 1631 K at 1498 K
2	3%C-5%Cr -2%Mo-2%W -5%V-5%Co	Nodular MC- Rod-like M_7C_3	$L_0 \rightarrow \gamma_p + L_1$ $L_1 \rightarrow (\gamma+MC)_E + L_2$ $L_2 \rightarrow (\gamma+M_7C_3)_E$	at 1556 K at 1515 K at 1452 K
3	3%C-5%Cr -2%Mo-2%W -9%V-5%Co	Chunky and coral-like MC- Rod-like M_7C_3	$L_0 \rightarrow \gamma_p + L_1$ $L_1 \rightarrow (\gamma+MC)_E + L_2$ $L_2 \rightarrow (\gamma+M_7C_3)_E$	at 1732 K at 1550 K at 1453 K

Section phase diagram of quasi-binary M [Fe-5%Cr-5%Mo-5%W-5%V-Co]-C alloy system and liquidus surface phase diagram of quasi-ternary M [Fe-5%Cr-5%Mo-5%W-5%Co]-V-C alloy system were constructed by Wu et al. [24] and they are shown in Fig. 2-9 and Fig. 2-10, respectively. It is clear in Fig. 2-9 that the high temperature part of the quasi-binary phase diagram has a simple eutectic system of austenite (γ) - MC. Since the eutectic point lies near C content about 2.8%, the cast iron with the basic chemical composition has hypoeutectic microstructure. It is also found that after the eutectic reaction of (L→γ+MC), the remained melt follows

by two other eutectic reactions, $L_1 \rightarrow \gamma + M_7C_3$ and $L_1 \rightarrow \gamma + M_2C$. The order and kind of eutectic reactions vary corresponding to C content.

By contrast, the quasi-ternary liquidus surface phases diagram from Fig. 2-10 shows the construction of liquidus phases when C and V contents are separately changed. On the diagram, precipitations of primary delta-ferrite, austenite, MC carbide as well as M_7C_3 and M_3C carbides are displayed, while the eutectic reaction of $(L \rightarrow \gamma + M_2C)$ can not be displayed on the diagram. The delta-ferrite is found at low C content and MC carbide appears in the region of high C and high V contents. M_7C_3 and M_3C carbides exist in high C and low V region. There are two peritecto-eutectic points, U_1 and U_2, and the temperature of U_1 located at high vanadium and low carbon content. The temperature of U_1 is around 200K higher than that of U_2.

As described here, many researches concerning the multi-alloyed white cast irons have been carried out and reported. However, the researches on heat treatment behavior and abrasive wear resistance of multi-alloyed white cast iron are quit few.
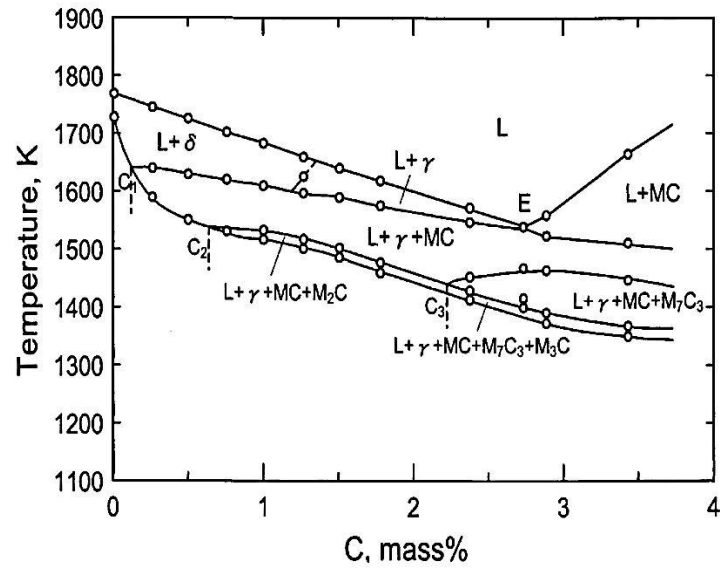
Fig. 2-9 Quasi-binary section phase diagram of basic alloy of M (Fe-5%Cr-5%Mo-
5%W-5%V-5%Co)-C alloy system [24].
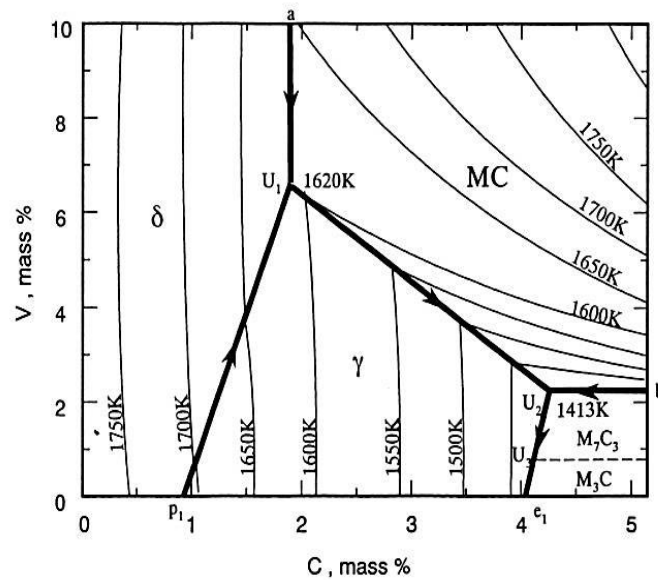
Fig. 2-10 Quasi-ternary liquidus surface phase diagram of M (Fe-5%Cr-5%Mo-5%W-
5%Co)-V-C alloy system [24].

2.5 Heat treatment behavior of multi-alloyed white cast iron

As mentioned before, as-cast matrix of multi-alloyed white cast iron consists of multiple kind of phases; bainite, austenite, ferrite and martensite. It is known that retained austenite and ferrite decrease hardness and wear resistance. It is said that high hardness or better abrasive wear resistance is obtained in case of martensitic matrix. In general, hardness in the as-cast state is low because more austenite remains. Under a certain wear circumstance, therefore, the martensitic matrix is requested for superior wear performance. In order to get the matrix with more martensite, the multi-alloyed white cast iron needs to be heat-treated.

Heat treatment processes given to multi-alloyed white cast iron are generally hardening and tempering in the same way as tool steel or high Cr cast iron [9, 21]. Hardening is that the stable austenite in which alloying elements is supersaturated in the as-cast state is destabilized at high temperature and allowed to transform into martensite during post cooling. Also, tempering is aimed to make the martensite matrix transform to useful and desirable microstructures and at the same time to reduce retained austenite and residual stress caused by hardening. The purposes of heat treatment research in multi-alloyed white cast iron are to clarify the behavior of phase transformation and to utilize the results for improvement of mechanical properties including most important wear resistance.

In order to understand the transformation behavior during heat treatment, continuous cooling transformation (CCT) curves were constructed [21]. As examples, CCT diagrams of multi-alloyed white cast irons with basic alloy composition and two levels of C contents were obtained by two austenitizing temperatures of 1273 and

1373 K and they are shown in Fig. 2-11 for 1.95% C (a) and 2.81% C (b) cast irons. In spite of the difference in C content, pearlite and bainite transformations are separated up and down independently. The nose temperatures of both the pearlite and bainite transformations range from 920 to 980 K and 570 to 610 K for low C cast iron, and 900 to 950K and 590 to 640 K for high C cast iron, respectively. With respect to the start of each transformation, in other words, each nose time, the low C cast iron shows great difference in pearlite and bainite transformations and the pearlite transformation is located at the long time side more than the bainite transformation.

(a) 1.95% C   (b) 2.81% C
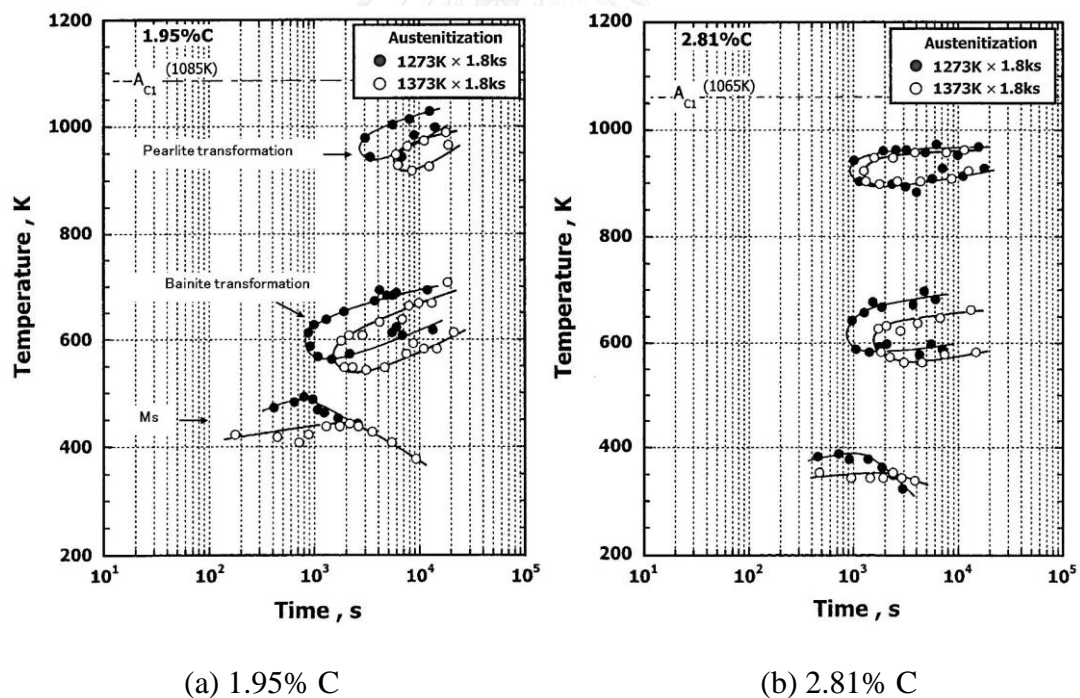
Fig. 2-11 Continuous cooling transformation (CCT) curves of multi-alloyed white cast irons with basic alloy composition [21].

Heat treatment behavior of multi-alloyed white cast iron with Fe-5%Cr-5%W-5%Mo-5%Co-V-C alloy system was studied by Matsubara et al. [9]. From Ms temperature higher austenitizing temperature provides more Vγ because Ms points are lower in the case of 1373 K austenitizing. There is a report investigating the tempering behavior of a semi multi-alloyed white cast iron with 1%C-1%V-5%Cr-5%Mo and it is shown in Fig. 2-12. The curve of tempered hardness shows great secondary hardening obtained near 800 K tempering. On the other side, after hardening from 1323 K retained austenite (Vγ) decrease as the tempering temperature is elevated and it also found that there is a critical temperature at which the Vγ begins to reduce greatly.
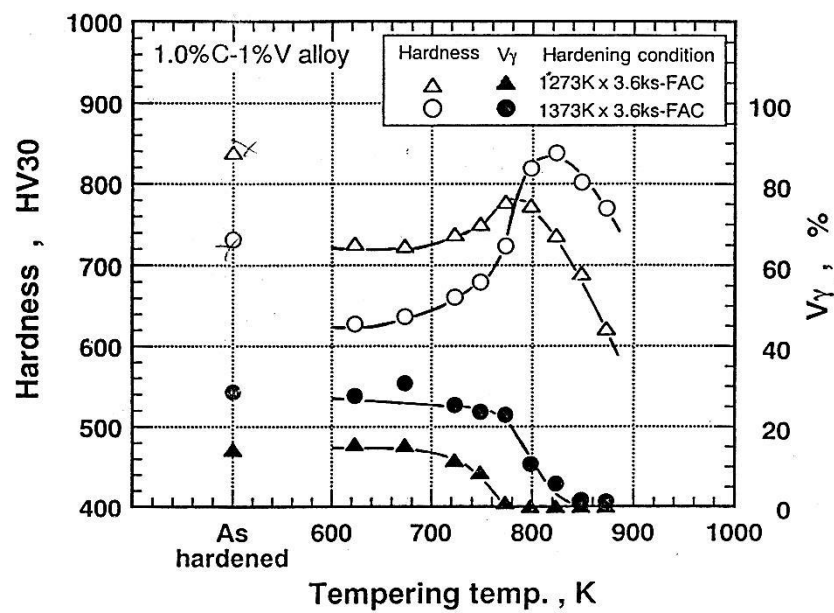
Fig. 2-12 Tempering behavior of alloy with 1%C-1%V-5%Cr-5%Mo [9].

2.6 Abrasive wear resistance

Abrasive wear of materials is caused by repeated contacts of the materials with hard abrasive particles which are frequently seen in the contact between parts or components of materials and minerals. One of important properties for parts or components is high resistance to abrasive wear. It is known that the wear resistance of cast iron is determined by microstructures consisting of carbide and matrix structure. If the matrix is soft, it can't support the hard carbides and the cast iron could be worn away from matrix easily. In order to solve this problem, some alloying elements to strengthen the matrix have been added to cast iron [25-28].

In the industries of mining, cement, steel making, electric power plant, various kinds of machines are used for digging, crushing or milling and pulverizing. According to wear conditions, abrasive wear can be classified as followed [5],

(1) Gouging abrasion which occurs when the surface of materials is scooped out by a large mass of abrasives such as ores or stones with heavy impact load, i.e. wear of hammer materials in an impact crusher.

(2) Grinding or high-stress abrasion which takes place when mineral or cements clinker is pulverized between two moving metals, i.e. wear of balls and liners, crushing discs and rolls in the mills.

(3) Scratching abrasion or low-stress abrasion which occurs when small abrasives are rolling over or scratching on the surface of working parts and in the case that low stress is sufficient to crush or grind the abrasives, i.e. wear in sand mill, sand and shot blasts and slurry pump.

In general, combination wear of two or three-body type occurs simultaneously on the surface of parts during working. As we know, wear resistance of alloyed white cast iron is related to the microstructure, that is, type, morphology, amount of carbide and matrix structure, which are factors to determine hardness of cast iron. These factors may also determine mechanical properties, particularly hardness, strength and toughness. Since eutectic carbide changes little in both quantity and morphology after solidification, the control of matrix structure is very important to improve wear resistance [27, 28].

In high Cr cast irons, many results concerning abrasive wear have been reported. In case that eutectic carbides in high Cr cast irons have higher hardness than the abrasive materials like quartz and garnet, the cast irons shows high abrasive wear resistance. Addition of alloying elements such as V, Mo, Nb and Ti, which form very hard carbides, can improve abrasive wear resistance [25]. It is reported that the rate of wear decreases with increasing hardness of materials and size of abrasive particles [18, 27]. Doğan et al. [27] reported that carbides aligned parallel to the wear surface of high Cr cast iron produced higher wear resistance in pin abrasive wear test. However, Sare [28] showed that an increase of carbide volume fraction (CVF) in high Cr cast iron had little effect upon the spalling rate and then provides some improvement in abrasive wear resistance.

Chapter III

Experimental Procedures

3.1 Preparation of test specimens

Charge calculations of each specimen for target chemical compositions showing in Table 3-1 were carried out. The ingots for test specimens were produced using a 30 kg capacity high frequency induction furnace with alumina lining. Raw materials such as mild steel, pig iron, ferro-alloys and pure metals used as charge materials. The charge materials were melted down and superheated up to 1853 K. After holding at the temperature, each melt is poured from the temperature between 1763 and 1793 K into preheated CO_2 molds of which cavity shape is round bar with 25 mm in diameter and 65 mm in length as shown in Fig. 3-1 and Y-block with the cavity size of 50x50x200 mm shown in Fig. 3-2(a). The surface of the top riser is immediately covered with dry exothermic powder to prevent the liquid of riser from fast cooling.

Table 3-1 Target chemical compositions of test specimens.

Specimen No.	Element (mass%)							
	C	Si	Mn	Cr	Mo	W	V	Co
No.1	1.75	0.50	0.50	5.00	5.00	5.00	5.00	2.00
No.2	2.05	0.50	0.50	5.00	5.00	5.00	5.00	2.00
No.3	2.35	0.50	0.50	5.00	5.00	5.00	5.00	2.00

The chemical compositions of the ingot are shown in Table 3-2.

Table 3-2 Chemical compositions and carbon balance (C_{bal}) of test specimens.

Specimen No.	Element (mass%)								C_{bal}
	C	Si	Mn	Cr	Mo	W	V	Co	
No.1	1.73	0.50	0.49	5.09	5.05	4.98	5.05	2.03	-0.25
No.2	2.00	0.53	0.49	4.96	4.98	4.98	5.01	2.03	0.05
No.3	2.34	0.54	0.49	4.98	5.02	4.98	5.04	1.98	0.38
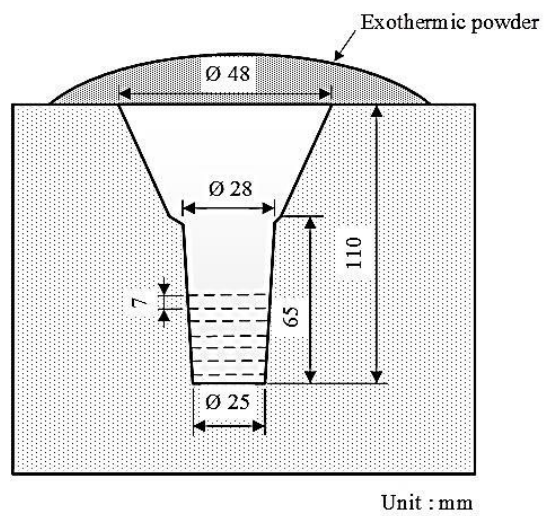
Fig. 3-1 Schematic drawing of CO_2 mold for round bar specimen.
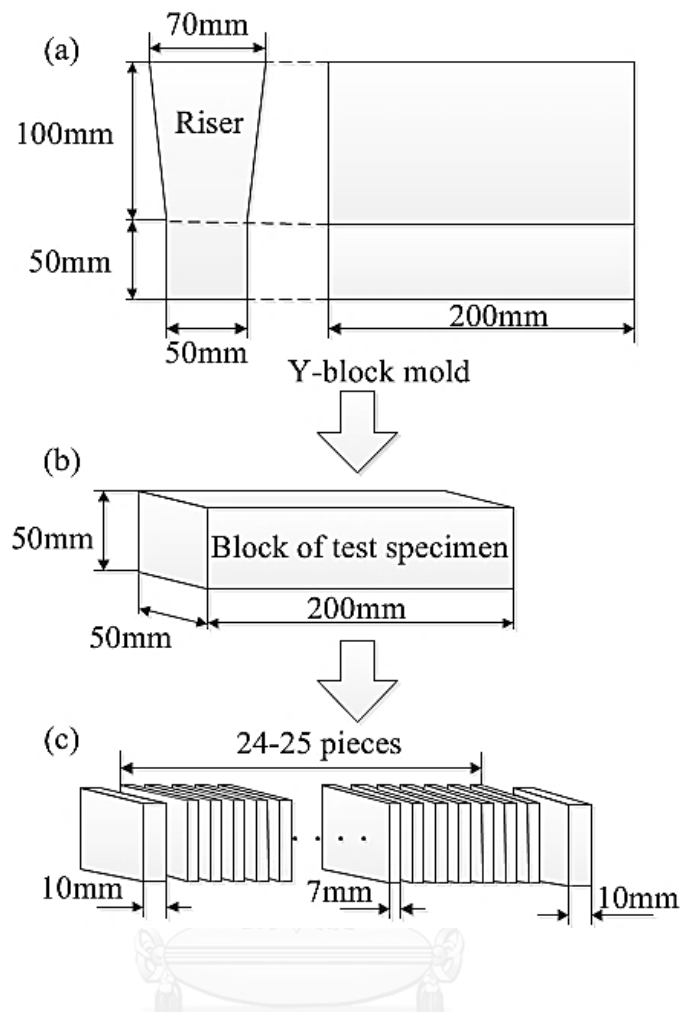
Fig. 3-2 Process of making test pieces for abrasive wear test.

In order to investigate the heat treatment behavior, the round bar specimens were cut by a wire-cutting machine to disk-shape test pieces with 7 mm in thickness. As for the Y-block ingot, the riser portion was cut off and the substantial block (b) was supplied to annealing to remove the casting stress and micro-segregation produced during solidification. The substantial block was coated with an anti-oxidation paste to prevent the block from oxidation and decarburization during annealing. The annealing condition is 1223 K for 18 ks and then furnace cooling (FC). After annealing, the block is sectioned at 7 mm in thickness by a wire-cutting machine to obtain test pieces for rubber wheel abrasive wear test.

When type and morphology of each test specimen are estimated from the previous literature shown in Fig. 2-5, specimen No.1 with 1.73% C and 15% W_{eq} should have MC and M_2C carbides. Specimen No.2 with 2.00% C and No.3 with 2.34% C at 15%W_{eq} could contain the same kinds of carbides as specimen No.1. As-cast microstructure observed by OM is placed in Fig. 4-1. It is evident that the carbides in the microstructure of each specimen follow with those estimated from previous paper.

3.2 Heat treatment

3.2.1 Investigation on heat treatment behavior

Heat treatment conditions of each specimen are summarized in Table 3-3.

In annealing, test pieces were coated with an anti-oxidation paste to prevent oxidation and decarburization. They were put in an electric furnace and heated up to 1223 K (950 ^{o}C) and held for 18 ks (5 hours). After holding, the specimens were cooled in the furnace to room temperature (FC). The annealed test pieces were austenitized at 1323 K (1050 ^{o}C) and 1373 K (1100 ^{o}C) and held for 3.6 ks (1 hour), and then they were hardened by fan air cooling (FAC) to room temperature. The hardened specimens were tempered at 50 K intervals in the range of 673-873 K (400-600 ^{o}C) for 12 ks (200 minutes). After holding at each tempering temperature, the test piece was cooled in air (AC) to room temperature.

The tempered test pieces made of each round bar specimen were supplied to the examination of properties, macro-hardness and volume fraction retained austenite

(Vγ) and the relationships between hardness, Vγ and tempering temperature were obtained.

Table 3-3 Conditions of each heat treatment process.

Heat treatment	Temperature (K)	Holding Time (ks)	Cooling Condition
Annealing	1223	18	Furnace Cooling (FC)
Hardening	1323 1373	3.6	Fan Air Cooling (FAC)
Tempering	673 723 748 773 798 823 873	12	Air Cooling (AC)

3.2.2 Heat treatment for abrasive wear test pieces

Heat treatment conditions of test pieces for abrasive wear test, which were made of the rectangular ingots, were decided referring to the relationships between macro-hardness, Vγ and tempering temperature described in the section 3.2.1. They are summarized in Table 3-4. The tempering temperature was adopted from the combination of hardness and Vγ. The hardened test pieces were tempered in an

electric furnace at three levels of temperatures selected based on the tempered hardness curve obtained experimentally in each specimen, the temperature at which the maximum tempered hardness (H_{Tmax}) was obtained, the lower and higher temperatures than that at H_{Tmax} (L-H_{Tmax} and H-H_{Tmax}, respectively) where the hardness are almost same. The holding time was taken for 12 ks and cooled to room temperature in air. The test pieces tempered at L-H_{Tmax} should have higher Vγ than that at H_{Tmax}, while those tempered at H-H_{Tmax} should have much lower Vγ than that at H_{Tmax}.

Table 3-4 Heat treatments condition of specimens for abrasive wear test.

Heat treatment	Annealing	Hardening	Tempering
Temperature	1223 K	1323 K and 1373 K	3 levels between 673 and 873 K
Holding time	18 ks	3.6 ks	12 ks
Cooling condition	Furnace cooling (FC)	Nitrogen quench in vacuum (N_2 Quench)	Air cooling (AC)

3.3 Observation of microstructure

3.3.1 Optical Microscopy (OM)

Optical microscopy (OM) was used to observe the two-dimensional microstructure of specimen. After tempering, the specimen was polished using SiC emery papers in the order of 80, 120, 180, 320, 400 and 600 meshes and finally buffing with alumina powder of 0.3 micron in grain size. Etchants were used to reveal the microstructures and the etching method is shown in Table 3-5. The etchant type A is generally used to reveal the microstructure.

Table 3-5 Etchants and etching methods.

Type	Etchant	Etching method	Observation
A	Vilella's reagent Picric acid 1 g. HCl 5 cc. Ethanol 100 cc.	Immersion at room temperature	Microstructure

3.3.2 Scanning Electron Microscopy (SEM)

Scanning Electron Microscopy (SEM) was used to observe the microstructure, precipitated carbides and worn surface appearance by high magnifications. The operating conditions were accelerating voltage of 25 kV and filament current of 80 mA. Polished and a little deep etched specimen was supplied to investigate the

detailed microstructure three-dimension alloy. This characterization is very helpful for discussion of experimental results.

3.4 Hardness measurement

Macro-hardness of specimen was measured using Vicker hardness tester with a load of 294.2 N (30 kgf) and measurement of micro-hardness in matrix was performed using Micro-Vicker hardness tester with a load of 0.98 N (100 gf). The hardness was measured at random more than five points and the average values were adopted.

3.5 Measurement of volume fraction of retained austenite

Volume fraction of retained austenite (V_γ) are obtained by X-ray diffraction method using a special goniometer with automatic rotating and swinging sample stage. Mo-Kα characteristic line with a wavelength of 0.007 nm (0.0711 Å) filtered by Zr foil is utilized as a source of X-ray beam. The diffraction peaks used for V_γ calculation are (200) and (220) planes for ferrite (α) or martensite (M), and (220) and (311) planes for austenite (γ). The X-ray diffraction method is convenient because a block specimen can be available [9, 21, 29]. The measuring conditions are shown in Table 3-6.

In this experiment, the simultaneously rotating and swinging sample stage is employed to cancel the influence of preferred orientation or textural configuration of austenite existed in the cast specimen. The four diffraction peaks are selected from crystal planes for calculation of Vγ; (200), (220) of ferrite or martensite and (220), (331) of austenite because these diffraction peaks are independent or not interfering

from peaks of other phases such as carbides. The reason why the strong α_{211} peak is not taken into account is that this peak is overlapped with the strong peak of chromium carbide (M_7C_3). The integrated areas of each adopted peaks are obtained using an image analyzer. The calculation of V_γ is done by the three combinations of peaks, $\alpha_{200} - \gamma_{311}$, $\alpha_{200} - \Sigma\gamma(220,311)$ and $\Sigma\alpha(200,220) - \gamma_{311}$. The $V\gamma$ values calculated from the three combinations are averaged.

Table 3-6 Measurement conditions of volume fraction of retained austenite (V_γ) by X-ray diffraction method.

Target metal	Mo
Tube voltage · current	50 kV · 30 mA
Slits	Divergence slit: 1°, Receiving slit: 1.5 mm, Scattering slit: 1°
Filter	Zr
Scanning range(2θ)	24-44 deg
Scanning speed	0.5 deg/min
Step/Sampling	0.01 deg

3.6 Abrasive wear test

Before abrasive wear test, the surface roughness of each test piece was controlled less than 3 μm (R_{max}) using a grinding wheel machine. The surface roughness was measured more than three times at random in the direction perpendicular to the last grinding direction.

3.6.1 Rubber wheel abrasive wear tester

Picture of tool and schematic drawing of rubber wheel abrasive wear tester is shown in Fig. 3-3 and 3-4. The rubber wheel abrasive wear tester is widely used to simulate the abrasive wear performance. Abrasives of silica sand of ASTM 6 grade is fed to the contacting face between the rotating rubber wheel and the surface of test piece. The rubber wheel is rotated in the same direction as abrasives flow. Mass loss of test piece is measured before and after test using a high precision digital balance with 0.1 mg accuracy. Wear distance (W_d) can be calculated by the following equation.

$$\text{Wear distance } (W_d) = 2 \times \pi \times r \times N_r \quad \text{............(3.1)}$$

$$= 2 \times 3.1416 \times 0.125 \times 10000$$

$$= 785 \text{ m}$$

Here, W_d = wear distance (m)

  r = radius of rubber wheel (m)

  N_r = number of revolution
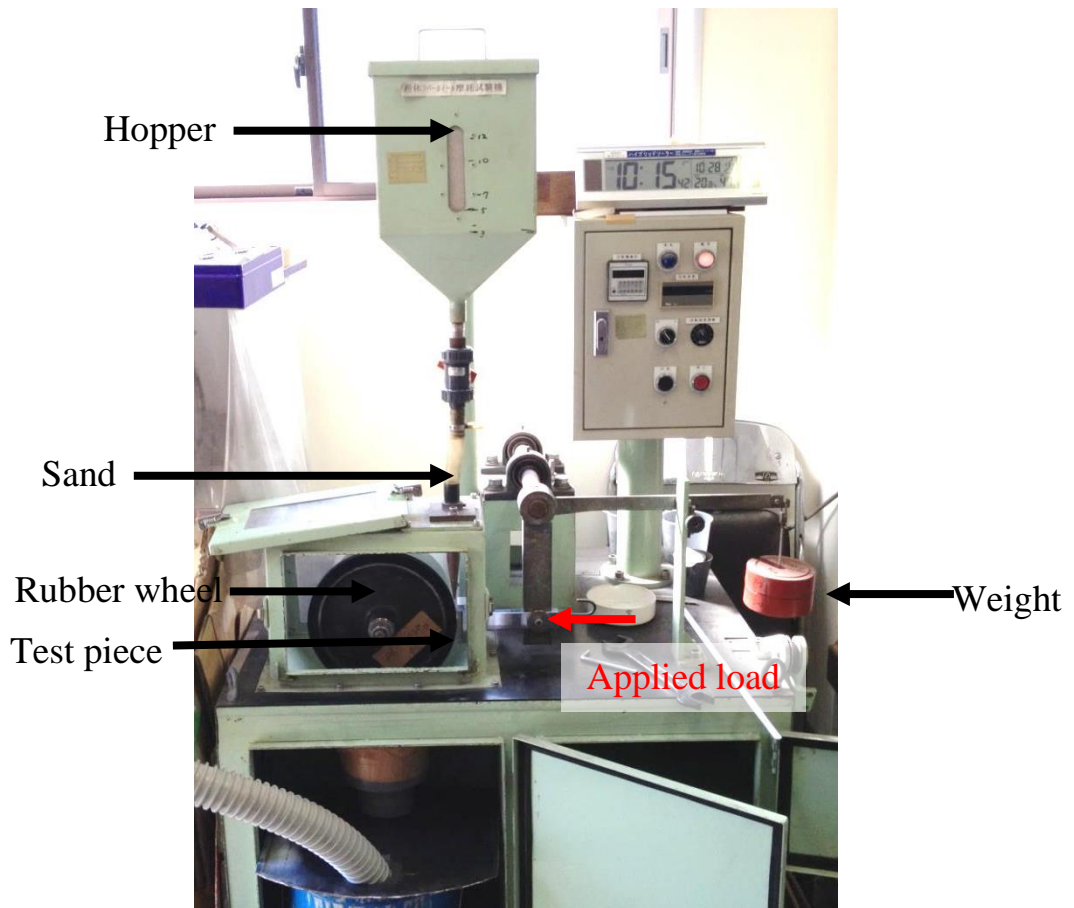
Fig. 3-3 Rubber wheel abrasive wear tester.
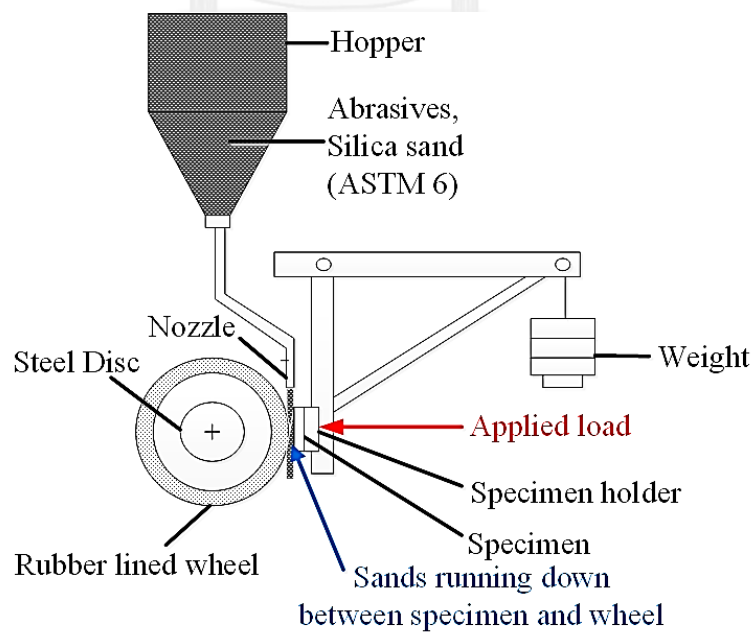
Fig. 3-4 Schematic drawing of Rubber wheel abrasive wear tester.

3.6.2 Abrasive test method and test conditions

A specimen is fixed on the right hand side of specimen holder. The specimen holder is installed to the loading flame first and then rubber wheel is fitted to the axis space between specimen holder and wheel is adjusted to about 3 mm. More detailed setting of a test pieces is shown in Fig. 3-5. All the settings finish, the beam for load supplying is released and then, the surface of specimen and the wheel are touched. After the abrasives of sand begin to run, the wear test starts under the test conditions shown in Table 3-7. One cycle of test takes about 15 minutes. After one wear test is over, the nozzle is closed and rubber wheel and specimen holder are taken out. Tested specimen is cleaned in an ultrasonic acetone bath and dried by dryer, and then, the test piece is weighted repeatedly for 4 times. The worn surface appearance of test piece after rubber wheel abrasive wear test is drawn schematically as illustrated in Fig.3-6.
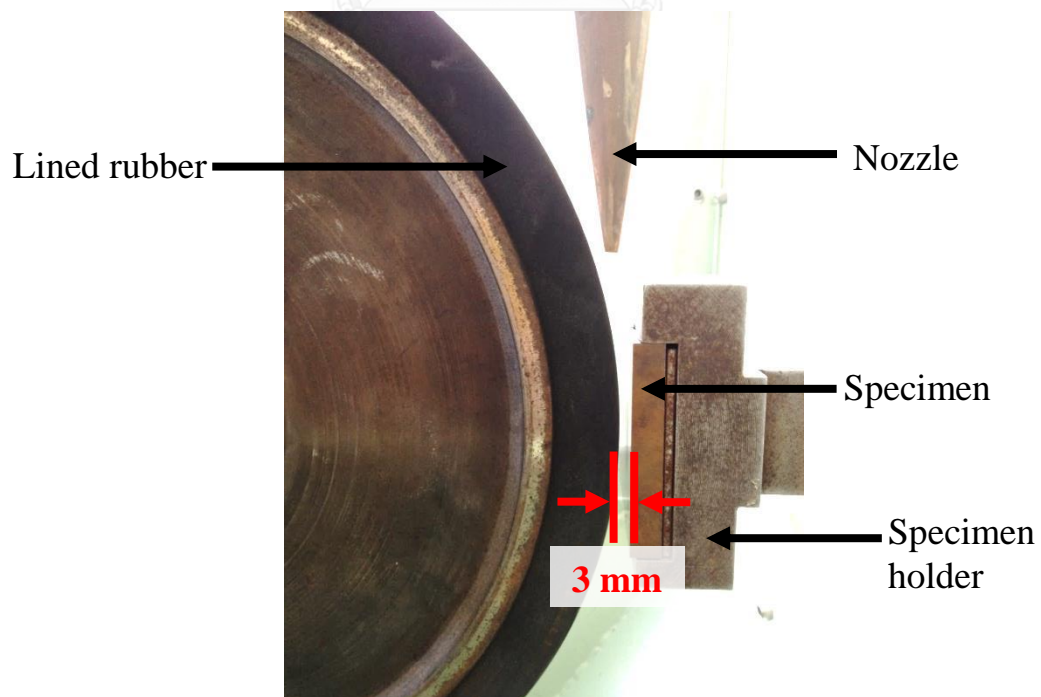
Fig. 3-5 Schematic drawing main portion of Rubber wheel abrasive wear tester.
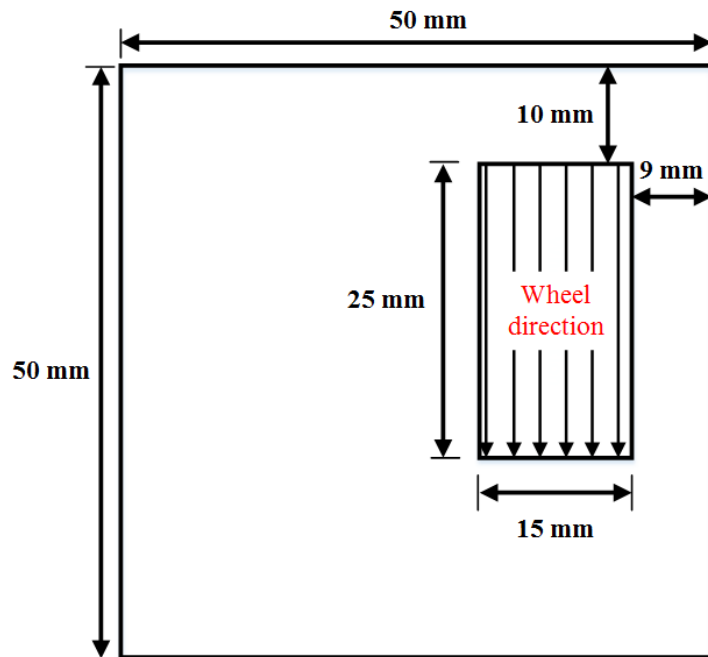
Fig. 3-6 Schematic drawing of worn surface appearance of specimen after Rubber wheel abrasive wear testing.

Table 3-7 Test conditions of rubber wheel abrasive wear test.

Abrasives	Silica sand of ASTM 6 grade
Feeding rate	250 - 300 g/min
Applied load	85.32 N (8.7 kgf)
Number of revolution	1000
Rotating speed	120 r.p.m

The abrasives of silica sand of ASTM 6 grade was used for rubber wheel abrasive wear test. During test, silica sand can freely move and rotate on the surface of test pieces. The kind of compound silica sands, size and their volume fraction are shown in Table 3-8.

Table 3-8 Kind of compound, size of silica sand (ASTM# 6) and their volume fractions.

Chemistry	Volume fraction , %
SiO_2	97.03
Al_2O_3	1.62
Fe_2O_3	0.03
Size (mesh)	Volume fraction , %
35	2.3
48	59.3
60	31.8
80	6.2
100	0.3
-100	0.1

Chapter IV

Experimental Results

4.1. Microstructure of test specimens

Microstructures of test specimens in the as-cast state are shown in the Fig. 4-1. All of specimens show hypoeutectic structure consisting of primary austenite dendrite and eutectic structures. The types of eutectic carbides are mainly MC in granular or string-like shape and M_2C in plate-like or lamellar one. The eutectic carbides appear at boundary region of austenite dendrite. In addition, area fraction of eutectic in the as-cast state measured by an image analyzer increases with an increase in C content, 40.9% in specimen No.1 with 1.73% C, 47.7% in No.2 with 2.00% C and 59.4% in No.3 with 2.34% C. This result tells that volume fraction of the eutectic increases with a rise of C content, that is to say, the amount of eutectic carbide is also increased by increasing the C content.

Matrices of all the specimens are mostly austenite. This is because C dissolved into matrix stabilized austenite and lowered Ms temperature [30]. However, small amount of martensite could exist in the matrix microstructure.
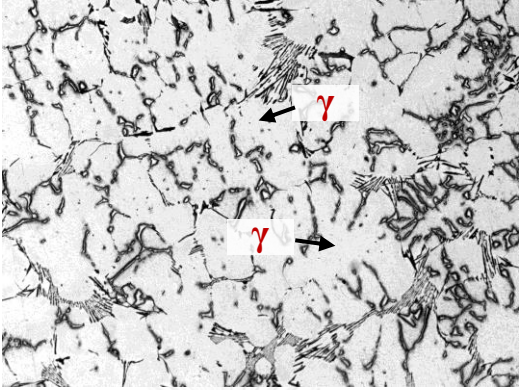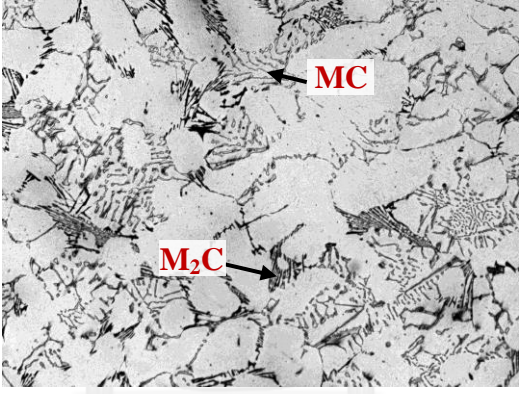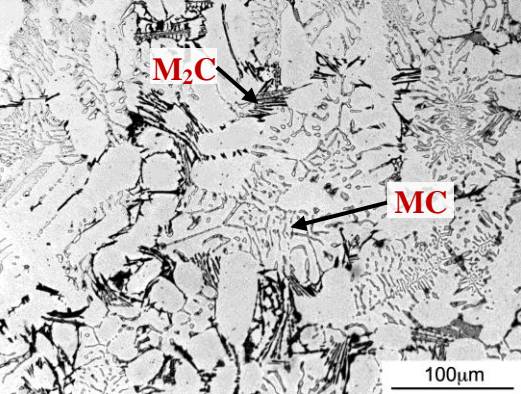
Specimen	OM	Area fraction of eutectic (%)
No.1 (1.73% C)		40.9
No.2 (2.00% C)		47. 7
No.3 (2.34% C)		59.4

Fig. 4-1 Microstructures of as-cast specimens with different C contents and area fraction of eutectic.

4.2 Effect of C content on heat treatment behavior

4.2.1 Effect of C content on as-hardened state

4.2.1.1 Microstructure of as-hardened specimens

As-hardened microstructures of test specimens are shown two-dimensionally in Fig. 4-2 for 1323 K and Fig.4-3 for 1373 K austenitizing, respectively. It is well known that the configuration of eutectic carbide changes little from the as-cast state by hardening process. The matrices of all the specimens are composed of fine carbides, martensite (M) and retained austenite (γ_R). When compared with the as-cast matrix structure, austenite is reduced greatly. Instead, more carbide can be observed in the matrix. This proves that the destabilization of austenite, i.e., precipitation of secondary carbides (Sc) occurred during austenitizing and then decomposed austenite transformed into martensite. However, it can not be clear to find the differences in the amount of secondary carbides among the specimens with different C contents.

In order to investigate the details of precipitated carbides in the matrix, the SEM microphotographs were taken focusing on the matrix areas and the representatives are shown in Fig.4-4 for 1323 K and Fig. 4-5 for 1373 K austenitizing, respectively. It can be understood that the finely precipitated carbides are clearly revealed and they rather decrease in number with increasing the C content. On the other hand, the retained austenite seems to reduce and the martensite is observed clearly in the specimens No.2 and No.3 with higher C content than No.1. When compared the matrix structures hardened from 1323 K with those hardened from 1373 K austenitizing, the number of precipitated carbides are very less in the

specimens in hardening from 1373 K austenitizing, and instead, the retained austenite is increased. This is because the austenite was stabilized due to more dissolution of C and alloying elements at higher austenitizing temperature.
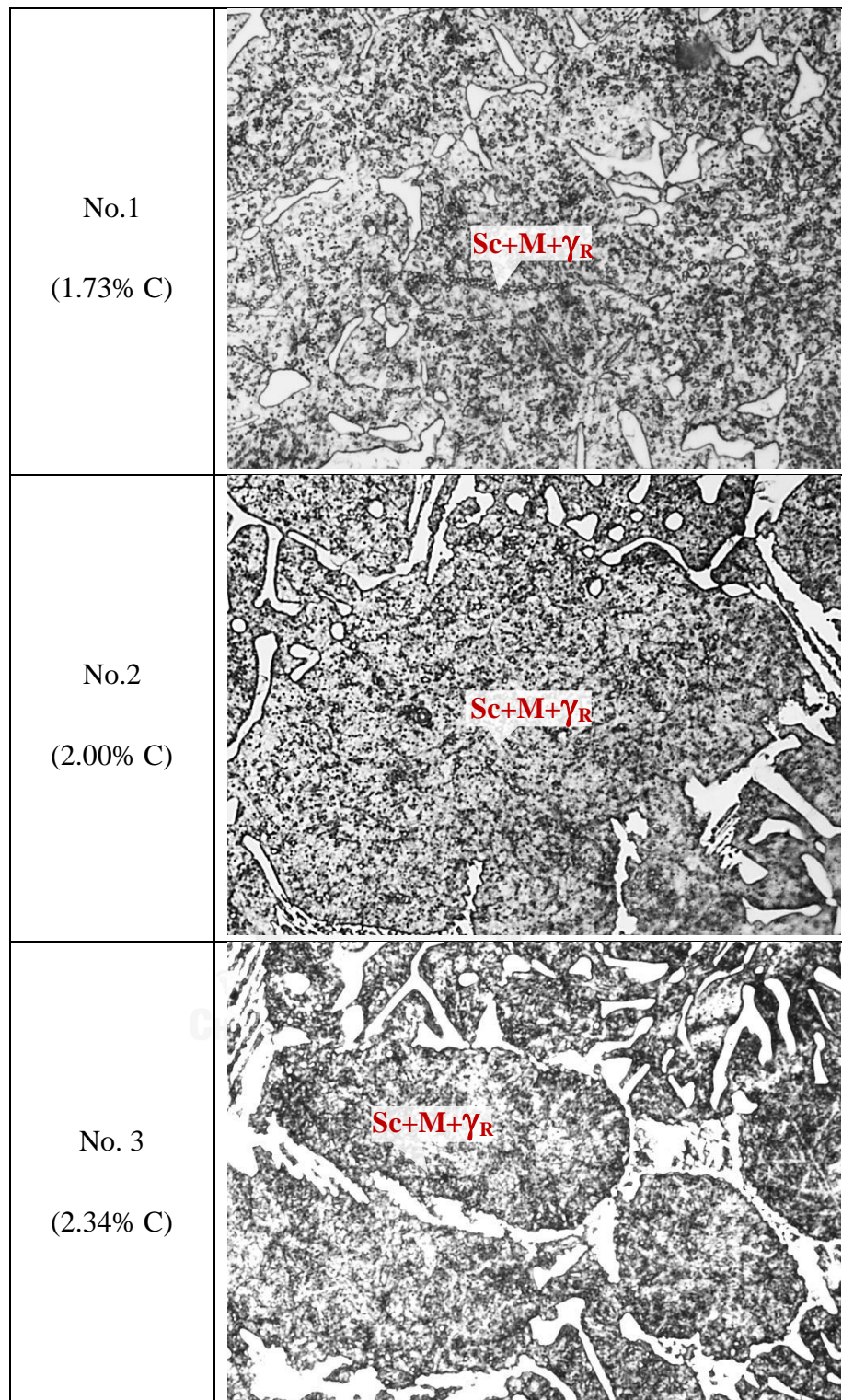
No.1 (1.73% C)	
No.2 (2.00% C)	
No. 3 (2.34% C)	

Fig. 4-2 Two-dimensional microstructures of as-hardened specimens with different C contents in 1323 K austenitizing by optical microscope. Etchant : Vilella's reagent.

No.1 (1.73% C)	Sc+M+γ_R
No.2 (2.00% C)	Sc+M+γ_R
No. 3 (2.34% C)	Sc+M+γ_R

Fig. 4-3 Two-dimensional microstructures of as-hardened specimens with different C contents in 1373 K austenitizing by optical microscope. Etchant : Vilella's reagent.

No.1 (1.73% C)	
No.2 (2.00% C)	
No. 3 (2.34% C)	

Fig. 4-4 SEM microstructures of as-hardened specimens with different C contents in

1323 K austenitizing. Etchant : Vilella's reagent

No.1 (1.73% C)	
No.2 (2.00% C)	
No. 3 (2.34% C)	
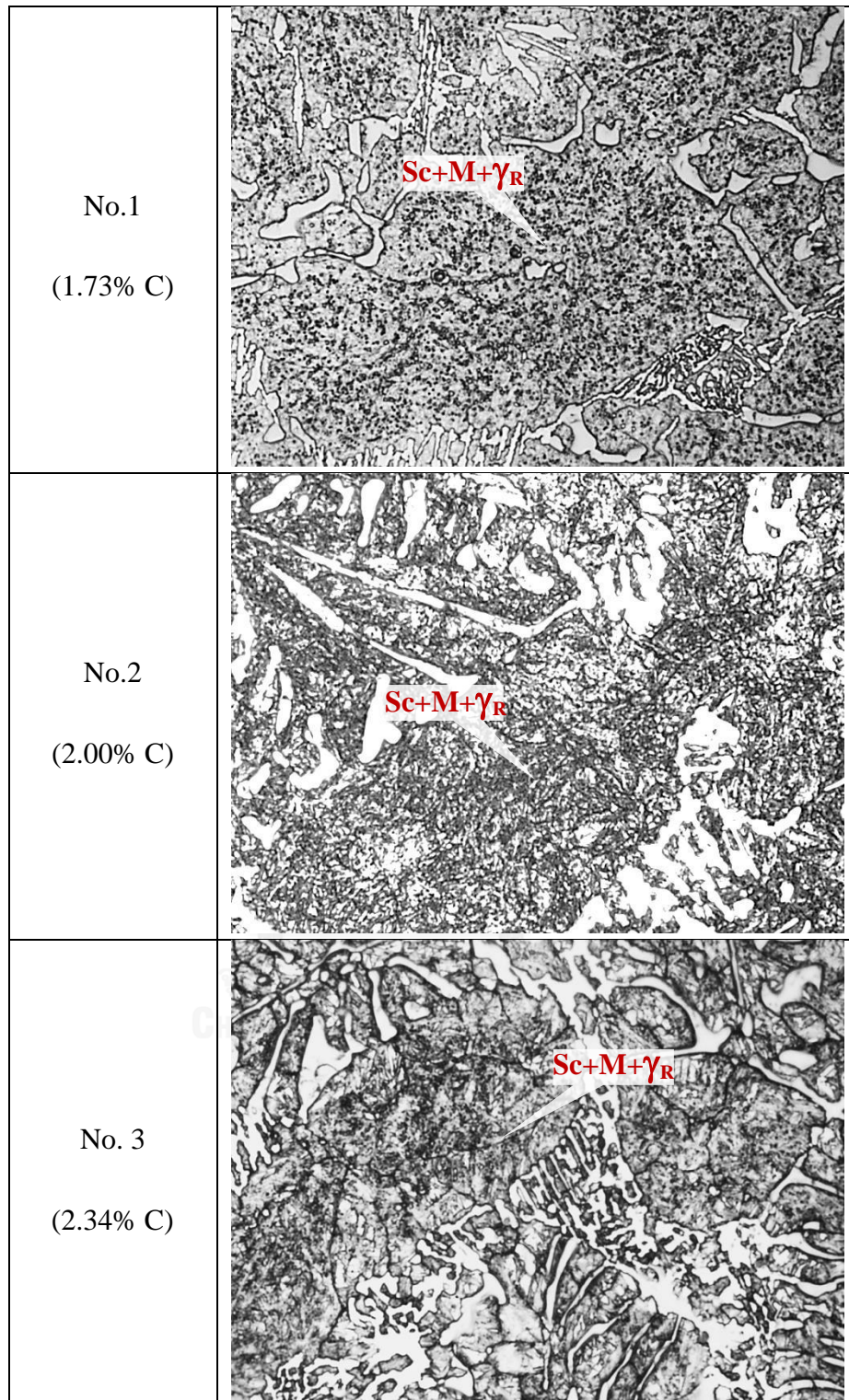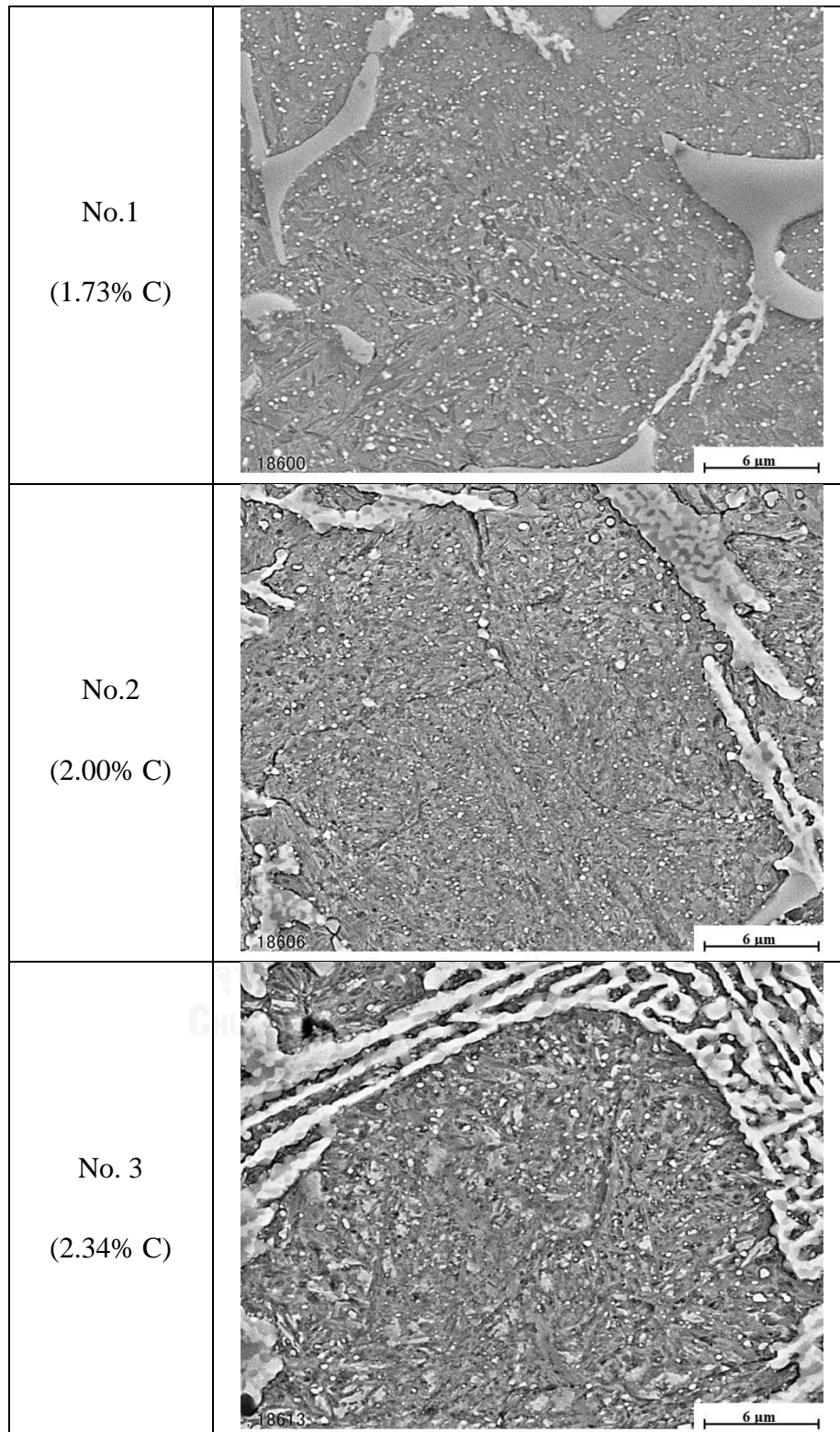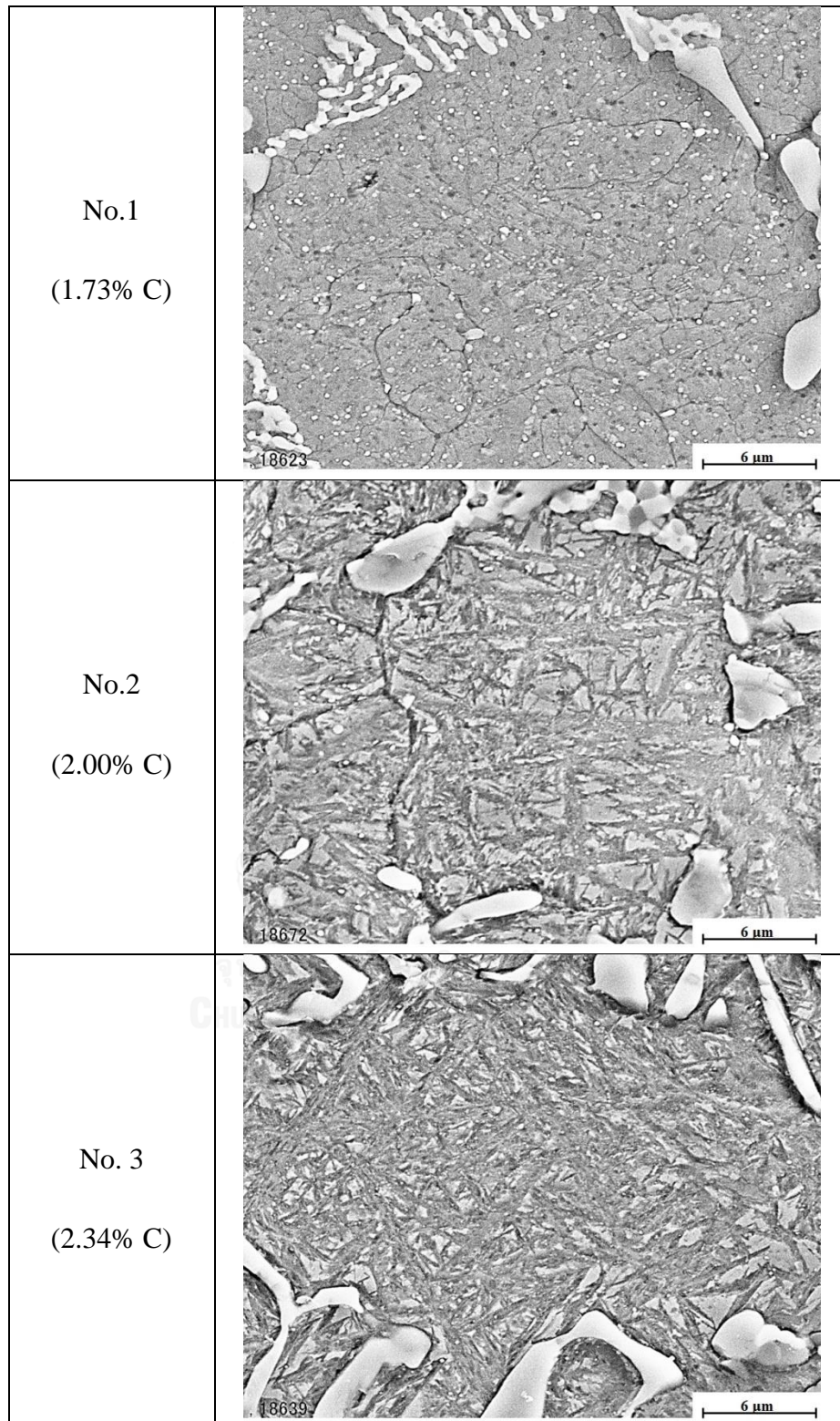
Fig. 4-5 SEM microstructures of as-hardened specimens with different C contents in

1373 K austenitizing. Etchant : Vilella's reagent.

4.2.1.2 Hardness and volume fraction of austenite (Vγ) in as-hardened
specimens

Macro- and micro-hardness and volume fraction of austenite (Vγ) in as-hardened state are summarized in Table 4-1. The hardness of specimen No.1 with 1.73% C was 747.4 HV30 in case of 1323 K and 821.8 HV30 in 1373 K austenitizing. In specimen No.2 with 2.00% C, the hardness was 922.4 HV30 and 856.6 HV30 in the case of hardening from 1323 K and 1373 K austenitizing, respectively. As for specimen No.3 with 2.34%C, the hardness obtained was 937.2 HV30 and 758.2 HV30 in 1323K and 1373K austenitizing, respectively.

Table 4-1 Macro- and micro-hardness and volume fraction of austenite (Vγ) of as-hardened specimens with different C contents.

| Specimen | Austenitizing temperature | | | | | |
| | 1323 K (1050 ^{o}C) | | | 1373 K (1100 ^{o}C) | | |
	Macro-hardness , HV30	Micro-hardness , HV0.1	Vγ , %	Macro-hardness , HV30	Micro-hardness , HV0.1	Vγ , %
No.1	747.4	684.8	6.13	821.8	772.5	11.3
No.2	922.4	857.0	16.83	856.6	781.6	33.41
No.3	937.2	897.2	37.37	758.2	667.7	57.86

4.2.2 Effect of C content on tempered state

After hardening from 1323 K and 1373 K austenitizing, specimens were tempered at 50 K interval between 673 and 873 K and 25 K interval near the high hardness to find out the peaks of hardness. The relationships between macro-hardness, volume fraction of retained austenite ($V\gamma$) and tempering temperature are shown in Fig. 4-6 (a), (b) for No.1, Fig. 4-7 (a), (b) for No.2 and Fig. 4-8 (a), (b) for No.3 specimen, respectively. In each specimen, tempered hardness curves show secondary hardening obviously, regardless of austenitizing temperatures.

In the specimen No.1, maximum tempered hardness (H_{Tmax}) of 800.6 HV30 and 829.2 HV30 were obtained at tempering temperature of 798 K, in both of hardenings from 1323 K and 1373 K. In each specimen, the H_{Tmax} value in tempered state is higher than that in as-hardened state. The hardness increases with increasing the tempering temperature to the highest hardness (H_{Tmax}). As the tempering temperature is elevated over that at H_{Tmax}, the hardness decreases markedly with an increase in the temperature.

On the other side, the $V\gamma$ in specimen No.1 reduces in a small rate as the tempering temperature increases, irrespective of austenitizing temperature, and finally, it converges to nil when the tempering temperature approaches 900 K. The $V\gamma$ values at H_{Tmax} were less than 5% in both the specimens hardened from two different austenitizing temperatures.

In the case of specimen No.2, the H_{Tmax} values of 914.8 HV30 and 931.2 HV30 were obtained by hardening from 1323 K and 1373 K and tempering at

the same temperature of 798 K. It can be said that high austenitizing temperature provides higher H_{Tmax} as same as the specimen No.1. Compared the hardness of specimen No.2 with No.1, the hardness of specimen No.2 are overall higher.

The Vγ values in specimen No.2 begin to decreases greatly when the tempering temperature increases over 748 K and those at H_{Tmax} were around 5%, regardless of austenitizing temperatures. When tempering temperature rises over 880 K, the Vγ becomes nil in both the austenitizing temperatures.

With respect to specimen No.3, the H_{Tmax} of 922.2 HV30 was obtained in the specimen hardened from 1323 K austenitizing and tempered at 798 K, while that of 901.2 HV30 was in the specimen hardened from 1373 K and tempered at 823 K.

From the results mentioned in this section, it can be said that the high austenitizing temperature provides higher H_{Tmax} value except for specimen No.3 with 2.34% C. On the other side, 10% and 14% Vγ still remained at H_{Tmax} of specimen No.3 when hardening from 1323 K and 1373 K, respectively. In this specimen hardened from 1373 K, the Vγ did not reduce to nil even tempered at 880 K.
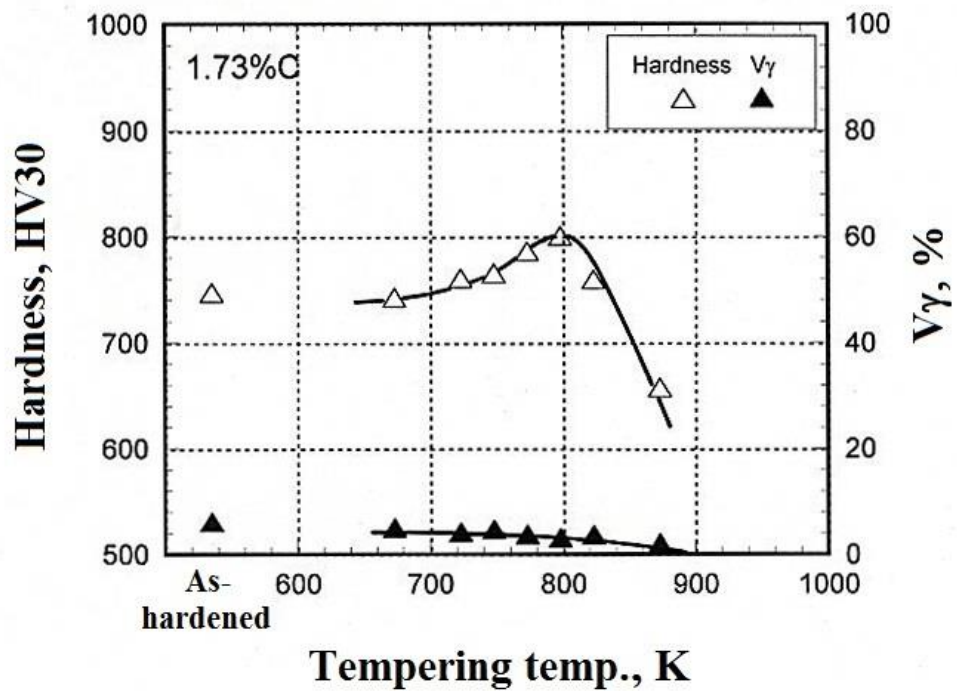
(a) Austenitizing temperature : 1323 K
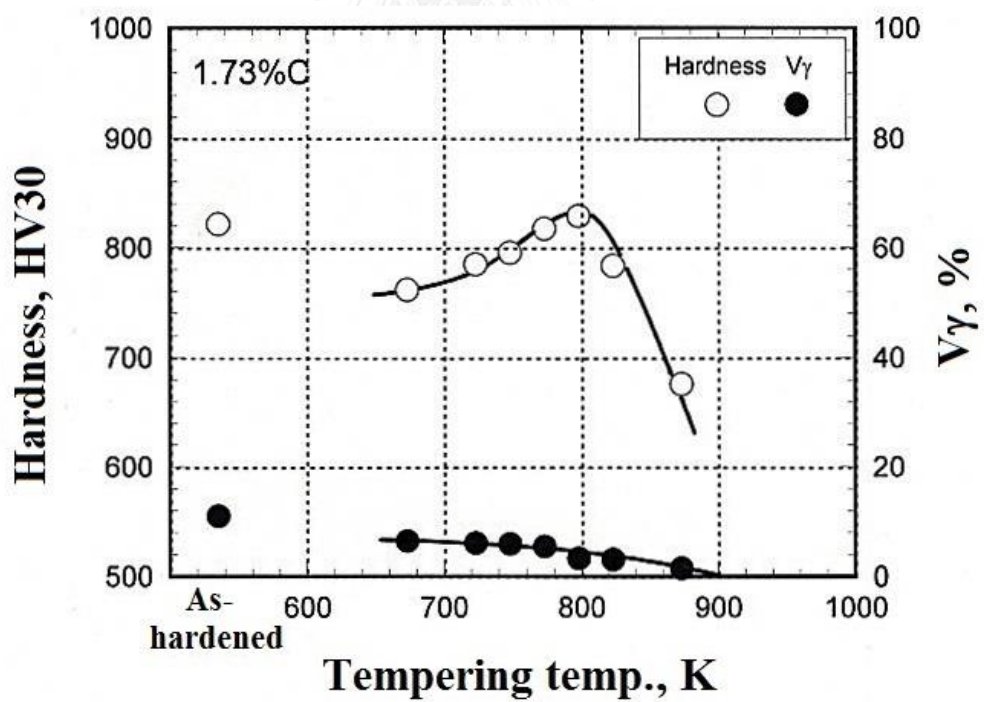
(b) Austenitizing temperature : 1373 K

Fig. 4-6 Relationship between macro-hardness, volume fraction of retained austenite

(Vγ) and tempering temperature. Specimen : No.1.
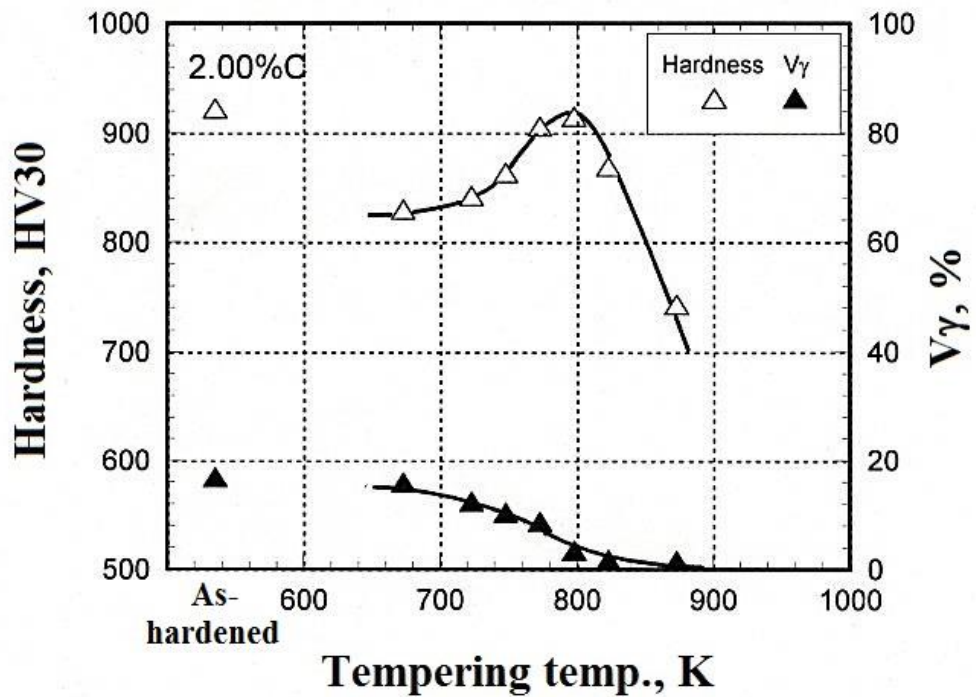
(a) Austenitizing temperature : 1323 K
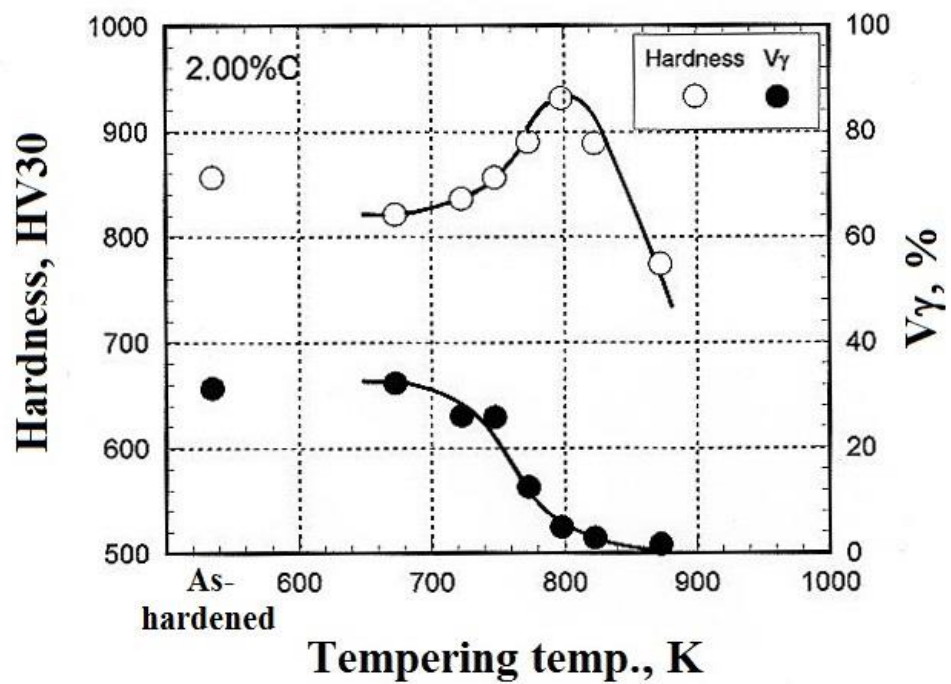
(b) Austenitizing temperature : 1373 K

Fig. 4-7 Relationship between macro-hardness, volume fraction of retained austenite

(Vγ) and tempering temperature. Specimen : No.2.
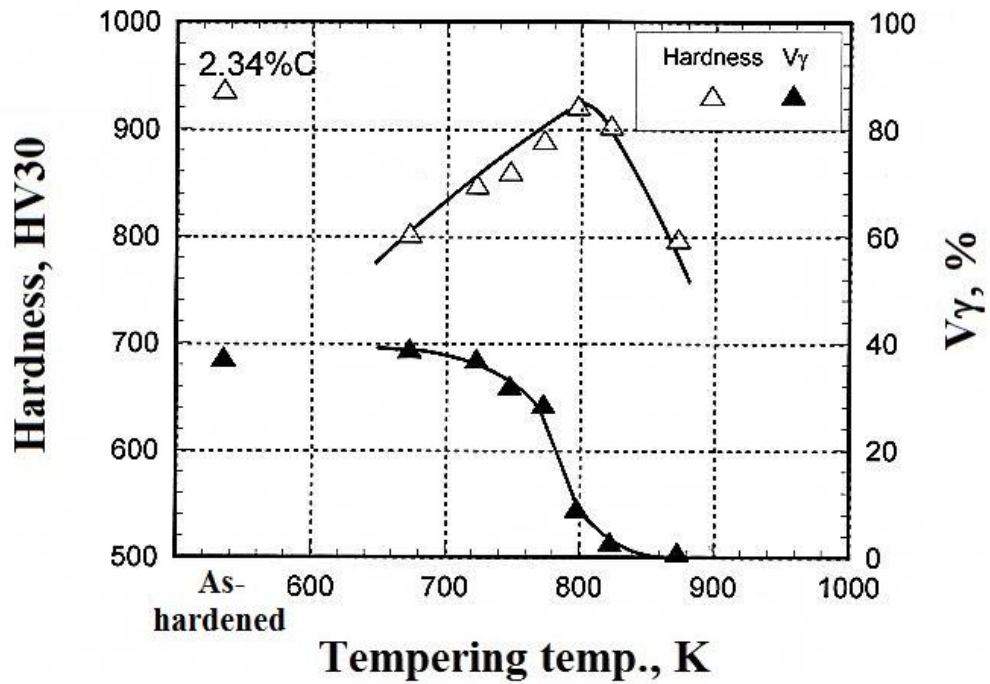
(a) Austenitizing temperature : 1323 K
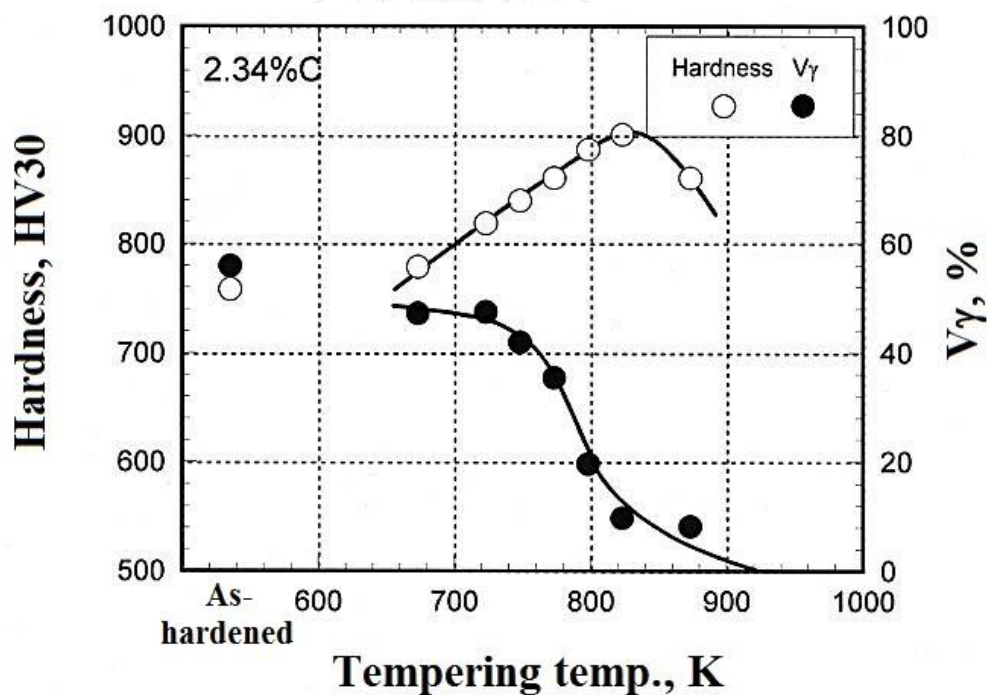
(b) Austenitizing temperature : 1373 K

Fig. 4-8 Relationship between macro-hardness, volume fraction of retained austenite

(Vγ) and tempering temperature. Specimen : No.3.

4.2.3 Microstructure of tempered specimens

Microstructures of tempered specimens with different C contents were observed by an optical microscope (OM). In order to clarify the effect of C content on tempered matrix structure, the microphotographs of each specimen tempered at same temperature of 798 K were selected as an example and they are shown in Fig. 4-9. The particles of precipitates or carbides and some retained austenite can be seen in the matrix of each specimen. However, martensite phase (M) can not be clearly distinguished.

The effect of tempering temperature, in other ward, the effect of Vγ value on the matrix structure of specimen No.2 tempered at 723 K (L-H$_{Tmax}$), 798 K (H$_{Tmax}$) and 873 K (H-H$_{Tmax}$) were chosen representatively and their microphotographs are displayed in Fig. 4-10. As the tempering temperature was increased, fine precipitates or carbides were coarsened in particle size from L-H$_{Tmax}$ via H$_{Tmax}$ to H-H$_{Tmax}$ specimens. However, martensite phases can not be still distinguished.

In the order to investigate the matrix microstructure in detail, the specimens were observed by SEM and their microphotographs are displayed in Fig. 4-11 for the effect of C content and Fig.4-12 for the effect of tempering temperature. In the SEM microphotographs, the phases existing in the matrix are revealed more clearly and distinguished. An increase in the secondary carbide in matrix can be seen comparing with the as-hardened state. The martensite was observed obviously in the specimens with high C content. However, the precipitated carbides decreases as the C content rises. From SEM microphotographs of specimen No.2 tempered at different temperatures (L-H$_{Tmax}$, H$_{Tmax}$ and H-H$_{Tmax}$) after hardening from 1323 K

austenitizing, it is found that the matrix microstructures was revealed with higher resolution by relating to the tempering temperature.
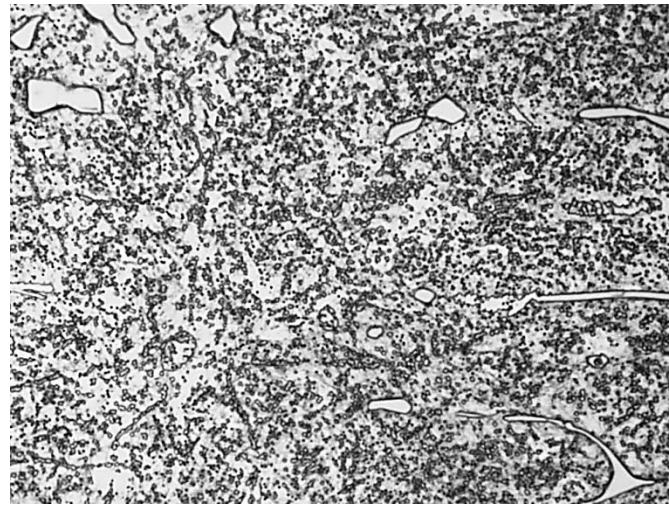
No.1 (1.73% C)

No.2 (2.00% C)
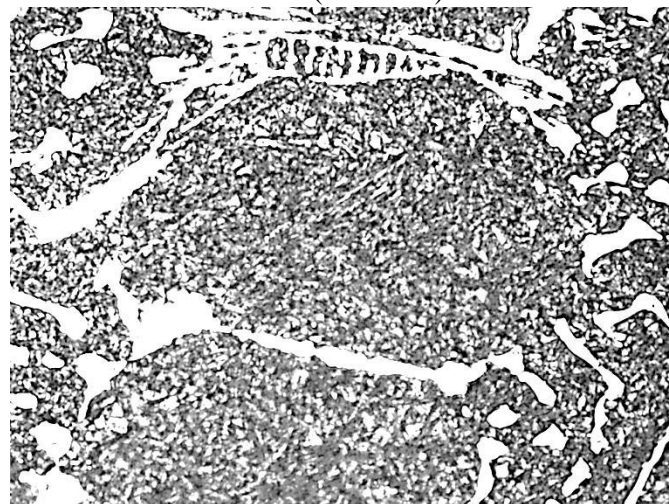
No.3 (2.34% C)

Fig. 4-9 Effect of C content on microstructures of H_{Tmax} specimens tempered after

hardening from 1323 K austenitizing. By optical microscope.

L-H$_{Tmax}$ (723 K)

H$_{Tmax}$ (798 K)

H-H$_{Tmax}$ (873 K)

Fig. 4-10 Comparison of microstructures of L-H$_{Tmax}$, H$_{Tmax}$ and H-H$_{Tmax}$ specimens in

No.2 with 2.00% C tempered after hardening from 1323 K austenitizing.
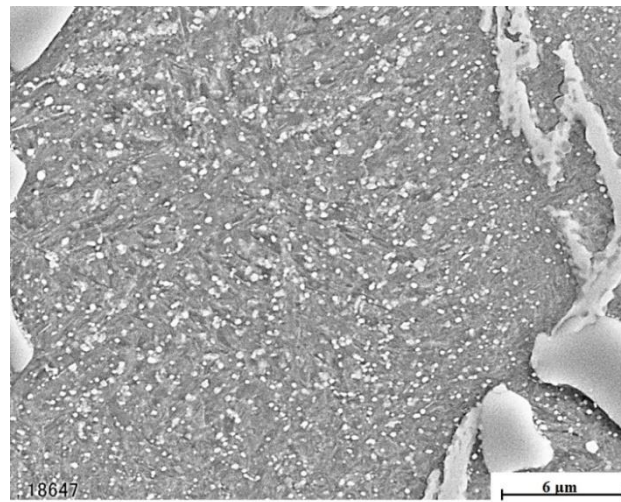
No.1 (1.73% C)
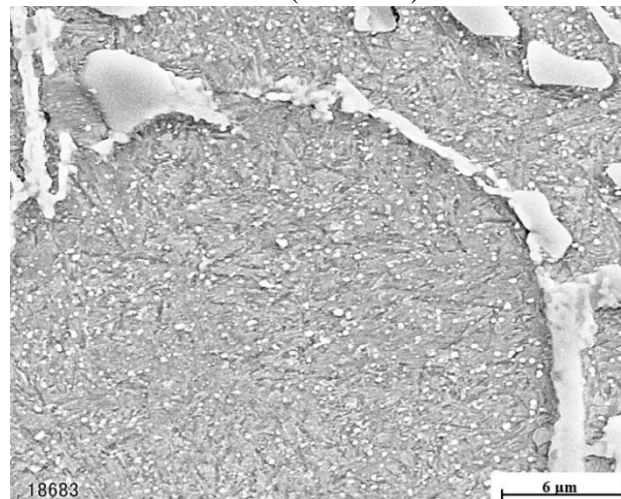
No.2 (2.00% C)
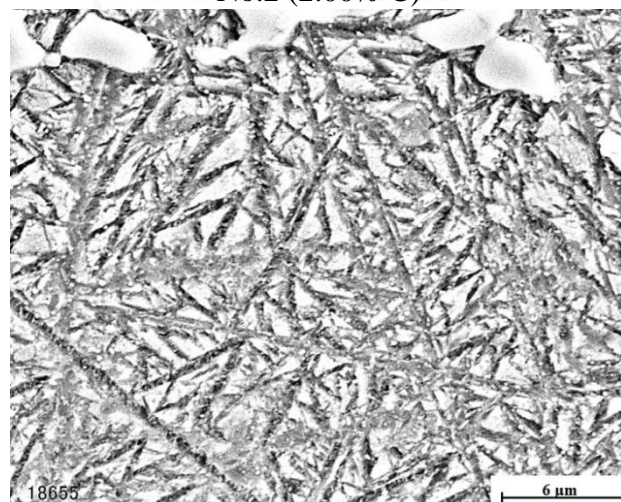
No.3 (2.34% C)

Fig. 4-11 SEM microphotographs of H_{Tmax} specimens with different C contents tempered after hardening from 1323 K austenitizing.

L-H$_{Tmax}$ (723 K)

H$_{Tmax}$ (798 K)

H-H$_{Tmax}$ (873 K)
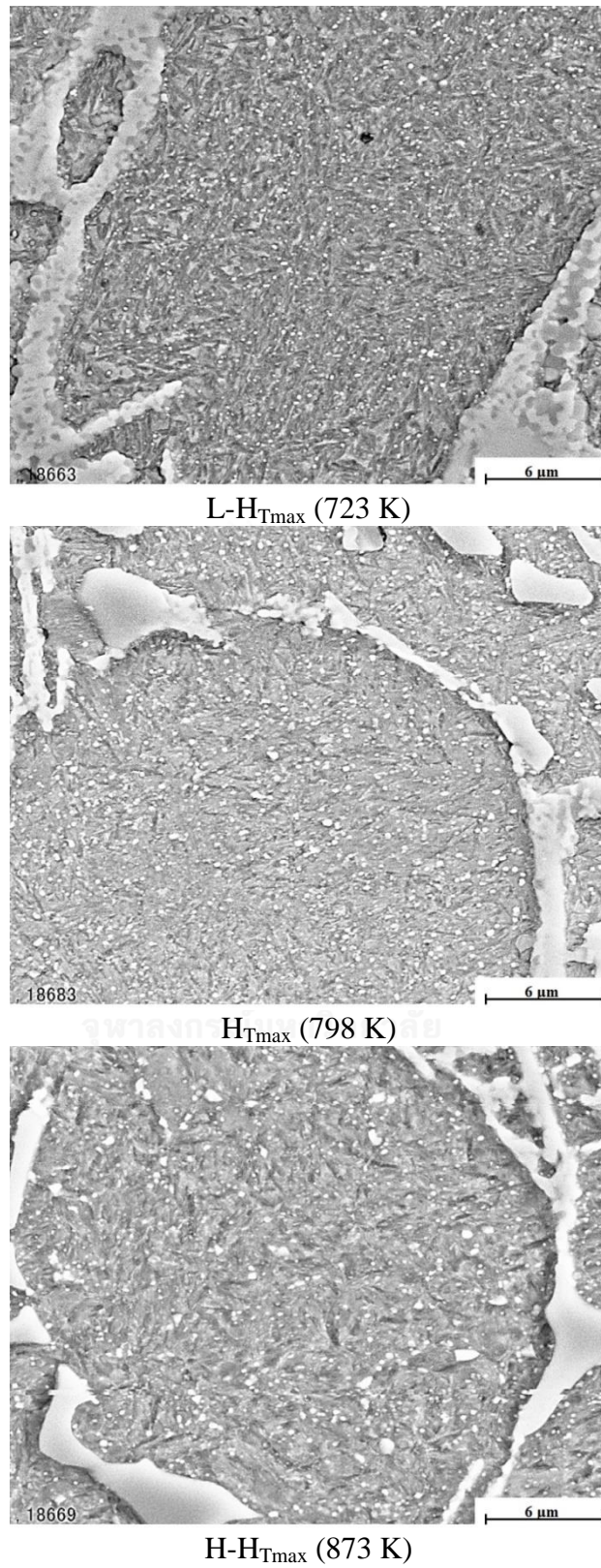
Fig. 4-12 SEM microphotographs of L-H$_{Tmax}$, H$_{Tmax}$ and H-H$_{Tmax}$ specimens in No.2

with 2.00% C tempered after hardening from 1323 K austenitizing.

4.3 Effect of heat treatment on abrasive wear behavior

Rubber wheel (three-body-type) abrasive wear test was introduced to evaluate the wear resistance of multi-alloyed white cast irons with different C content and basic alloy composition. The tempering temperatures for wear test pieces were determined referring to L-H_{Tmax}, H_{Tmax} and H-H_{Tmax} on the tempered hardness curves which had been previously made by the experiments (Section 4.2.2). Fig. 4-13 illustrates how to determine the tempering temperatures referring to the results of specimen No.2 hardening from 1373 K austenitizing.
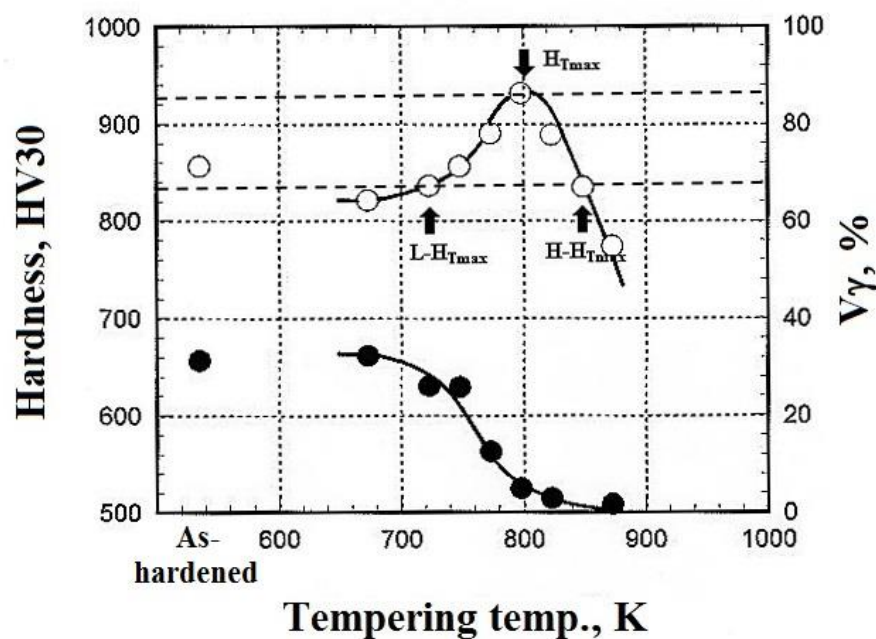
Fig. 4-13 Schematic illustration showing the tempering temperatures.

By selections of the temperatures, it becomes possible to evaluate the effect of Vγ on the wear resistance under the same hardness by comparing the wear rates of L-H_{Tmax} and H-H_{Tmax} specimens.

4.3.1 In case of hardening from 1323 K austenitizing

Relationships between wear loss (W_l) and wear distance (W_d) of specimens No.1, No.2 and No.3 which were tempered after hardened from 1323 K austenitizing are shown in Fig. 4-14, 4-15 and 4-16, respectively. It is clear that the wear loss is in proportion to the wear distance in every specimen even if it was tempered by different temperatures. The relations of W_l vs. W_d are displayed by the equations in the table shown below the figure and the coefficient or slope of each linear function means the wear rate (R_W).

For the specimens hardened from 1323 K and 1373K austenitizing, the total wear loss (W_l) at 3140 m of rubber wheel abrasive test are summarized in Table 4-2 (a) for 1323 K, and 4-2 (b) for 1373 K austenitizing specimens, respectively. In specimen No.1 with 1.73% hardened from 1323 K, the total W_l was the smallest 444 mg of H_{Tmax}, followed by the order of low wear losses of 469 mg of H-H_{Tmax}, 491 mg in as-hardened and the largest of 557 mg of L-H_{Tmax} specimens.

As for specimen No.2 with 2.00% C hardened from 1323K austenitizing, the smallest value of total wear loss was 237 mg of as-hardened, 311 mg of H_{Tmax}, 319 mg of L-H_{Tmax} and the largest 364 mg of H-H_{Tmax} specimen.

In the specimen No.3 with 2.34% C, the total W_l of 182 mg was smallest in as-hardened specimen and it increased in the order of in 204 mg of H_{Tmax}, 218 mg in L-H_{Tmax} and 275 mg in H-H_{Tmax} specimens.
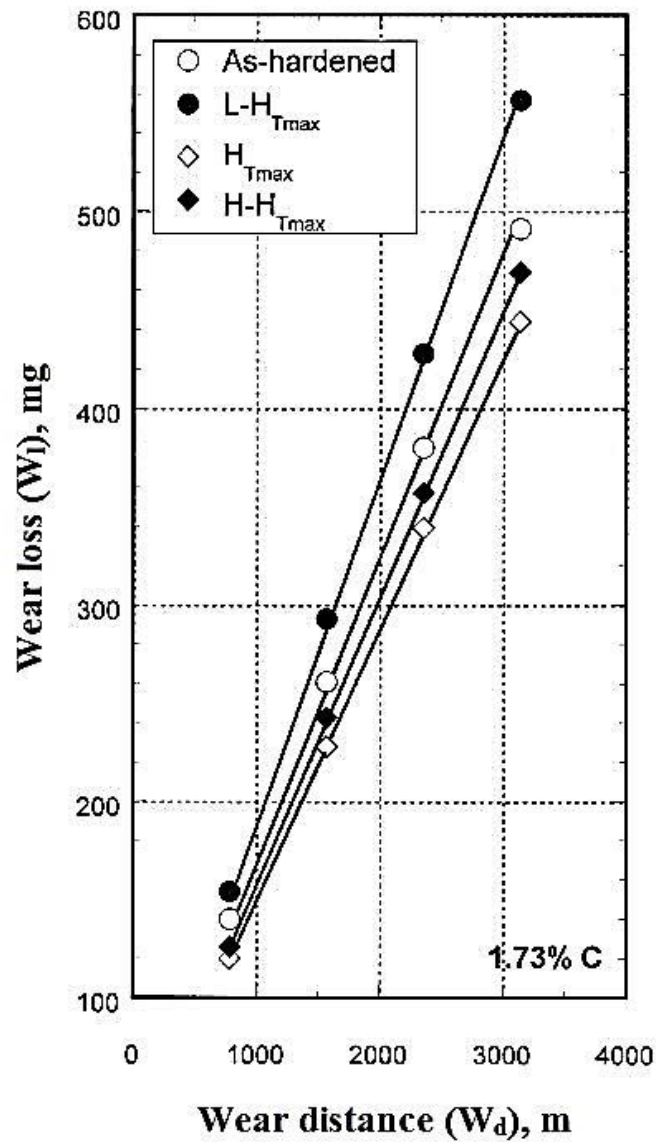
As-hardened	●	$W_l = 0.156 * W_d + 10.20$	$(R^2 = 0.99)$
L-H$_{Tmax}$	○	$W_l = 0.177 * W_d +$ 8.67	$(R^2 = 0.99)$
H$_{Tmax}$	◆	$W_l = 0.141 * W_d +$ 4.80	$(R^2 = 0.99)$
H- H$_{Tmax}$	◇	$W_l = 0.149 * W_d +$ 5.27	$(R^2 = 0.99)$

W_l : Wear loss, W_d : Wear distance

Fig. 4-14 Relationship between wear loss (W_l) and wear distance (W_d) of specimen No.1 tempered after hardening from 1323 K. Rubber wheel test (three-body-type) with load 85.3 N (8.7 kgf).
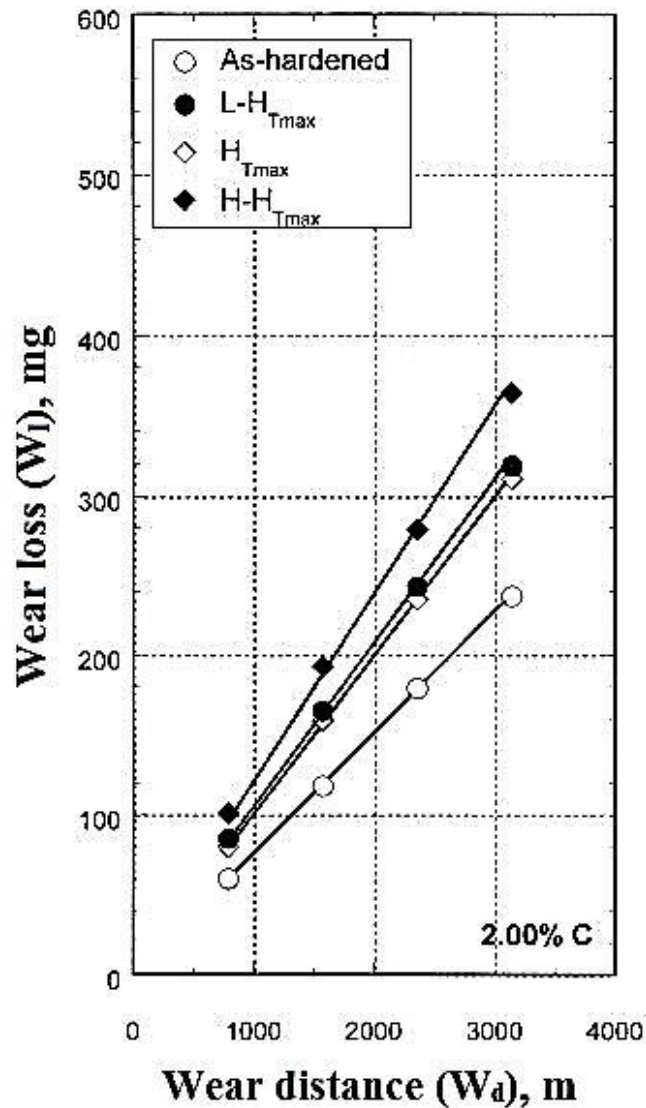
As-hardened	●	$W_l = 0.075 * W_d + 0.47$	$(R^2 = 1.00)$
$L\text{-}H_{Tmax}$	○	$W_l = 0.101 * W_d + 3.20$	$(R^2 = 0.99)$
H_{Tmax}	◆	$W_l = 0.099 * W_d + 1.60$	$(R^2 = 0.99)$
$H\text{-} H_{Tmax}$	◇	$W_l = 0.116 * W_d + 6.13$	$(R^2 = 0.99)$

W_l : Wear loss, W_d : Wear distance

Fig. 4-15 Relationship between wear loss (W_l) and wear distance (W_d) of specimen No.2 tempered after hardening from 1323 K. Rubber wheel test (three-body-type) with load 85.3 N (8.7 kgf).

As-hardened	●	$W_l = 0.058 * W_d + 5.47$	$(R^2 = 0.99)$
L-H$_{Tmax}$	○	$W_l = 0.069 * W_d + 2.33$	$(R^2 = 0.99)$
H$_{Tmax}$	◆	$W_l = 0.065 * W_d + 2.20$	$(R^2 = 0.99)$
H- H$_{Tmax}$	◇	$W_l = 0.087 * W_d + 2.60$	$(R^2 = 0.99)$

W_l : Wear loss, W_d : Wear distance

Fig. 4-16 Relationship between wear loss (W_l) and wear distance (W_d) of specimen No.3 tempered after hardening from 1323 K. Rubber wheel test (three-body-type) with load 85.3 N (8.7 kgf).

Table 4-2 Total wear loss (W_l) at 3140 m in rubber wheel abrasive wear test (three-body-type) of specimens with different heat treatment conditions. Load : 85.3 N (8.7 kgf).

Specimen	Total wear losses of rubber wheel abrasive wear test at 3140 m. (W_l : mg)			
	As-hardened	L-H_{Tmax}	H_{Tmax}	H-H_{Tmax}
No.1 (1.73% C)	491	557	444	469
No.2 (2.00% C)	237	319	311	364
No.3 (2.34% C)	182	218	204	275

(a) Austenitizing temperature : 1323 K

Specimen	Total wear losses of rubber wheel abrasive wear test at 3140 m. (W_l : mg)			
	As-hardened	L-H_{Tmax}	H_{Tmax}	H-H_{Tmax}
No.1 (1.73% C)	318	424	406	383
No.2 (2.00% C)	245	305	255	314
No.3 (2.34% C)	185	195	191	270

(b) Austenitizing temperature : 1373 K

4.3.2 In case of hardening from 1373 K austenitizing

Abrasive wear test results of tempered specimens after hardening from 1373 K are shown in Fig. 4-17 for specimen No.1, Fig. 4-18 for No.2 and Fig. 4-19 for No.3, respectively. The wear behavior shows the same manner in the case of 1323 K austenitizing, that is, the W_l increases proportionally to the W_d.

As shown in Table 4-2 (b); in the specimen No.1 with 1.73% C, the total W_1 increased in the order of the smallest loss of 318 mg in as-hardened, 383 in H-H_{Tmax}, 406 in H_{Tmax} and the largest of 424 in L-H_{Tmax} specimens.

In the specimen No.2 with 2.00% C, the wear behaviors were separated to two groups; one is more W_1 and the other is less W_1. From Table 4-2 (b), total wear loss increased in the order of the smallest of 245 mg in as-hardened, 255 in H_{Tmax}, 305 in L-H_{Tmax} and the largest of 314 in H-H_{Tmax} specimens.

As for the specimen No.3 with 2.34% C, the wear behaviors shows the same trend as specimen No.2, that is, they separated to two groups. The W_1 values were almost same as 185 in as-hardened, 191 in H_{Tmax} and 195 mg in L-H_{Tmax} specimens, respectively, and the W_1 was much larger in H-H_{Tmax} specimen with 270 mg.
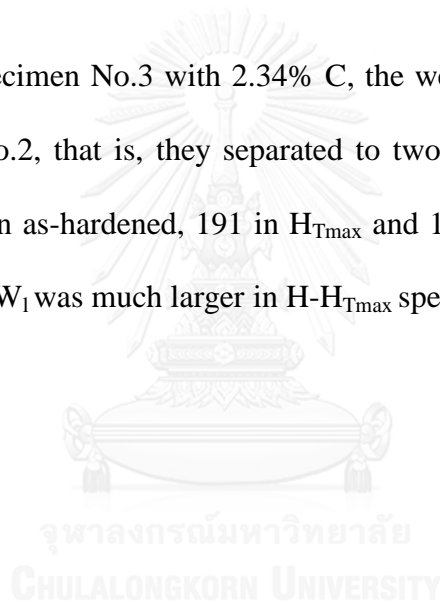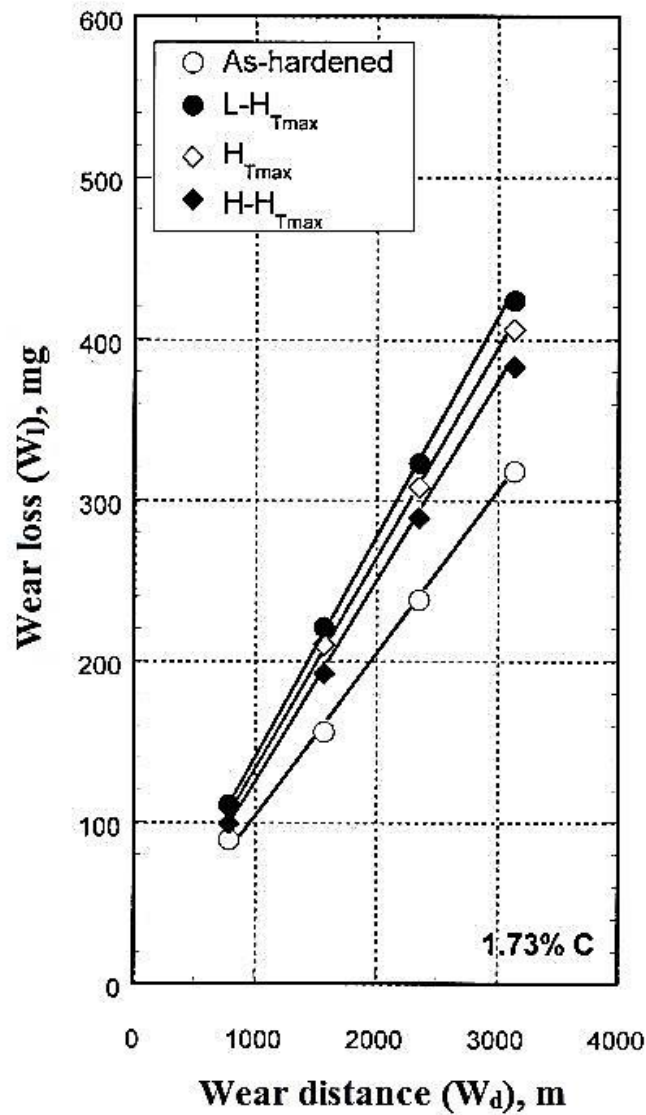
As-hardened	●	$W_l = 0.100 * W_d + 3.33$	$(R^2 = 0.99)$
L-H$_{Tmax}$	○	$W_l = 0.135 * W_d + 3.80$	$(R^2 = 0.99)$
H$_{Tmax}$	◆	$W_l = 0.129 * W_d + 4.40$	$(R^2 = 0.99)$
H- H$_{Tmax}$	◇	$W_l = 0.122 * W_d + 1.40$	$(R^2 = 0.99)$

W_l : Wear loss, W_d : Wear distance

Fig. 4-17 Relationship between wear loss (W_l) and wear distance (W_d) of specimen No.1 tempered after hardening from 1373 K. Rubber wheel test (three-body-type) with load 85.3 N (8.7 kgf).
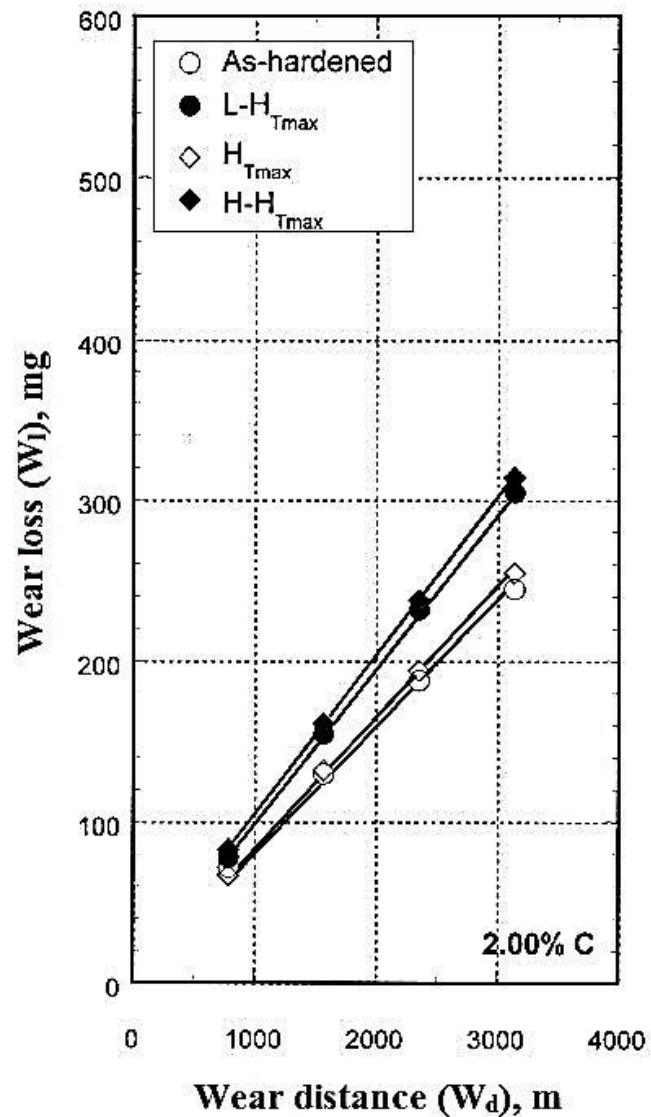
As-hardened	●	$W_l = 0.077 * W_d + 5.67$	$(R^2 = 0.99)$
L-H$_{Tmax}$	○	$W_l = 0.097 * W_d + 1.20$	$(R^2 = 0.99)$
H$_{Tmax}$	◆	$W_l = 0.081 * W_d + 2.20$	$(R^2 = 0.99)$
H- H$_{Tmax}$	◇	$W_l = 0.100 * W_d + 2.60$	$(R^2 = 0.99)$

W_l : Wear loss, W_d : Wear distance

Fig. 4-18 Relationship between wear loss (W_l) and wear distance (W_d) of specimen No.2 tempered after hardening from 1373 K. Rubber wheel test (three-body-type) with load 85.3 N (8.7 kgf).

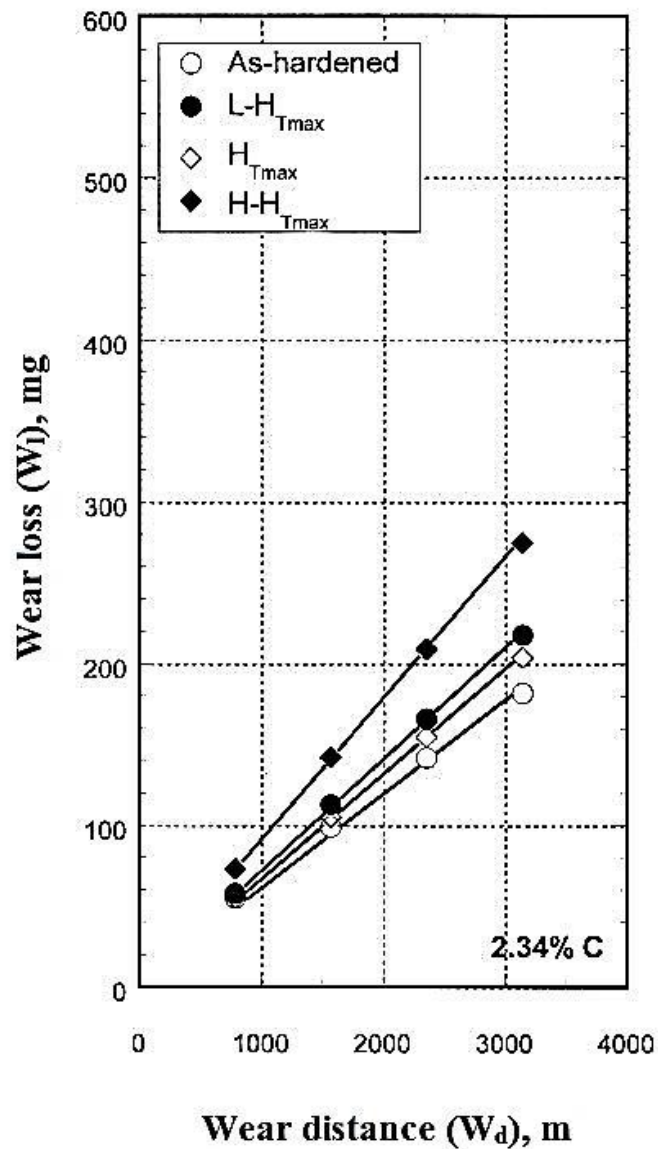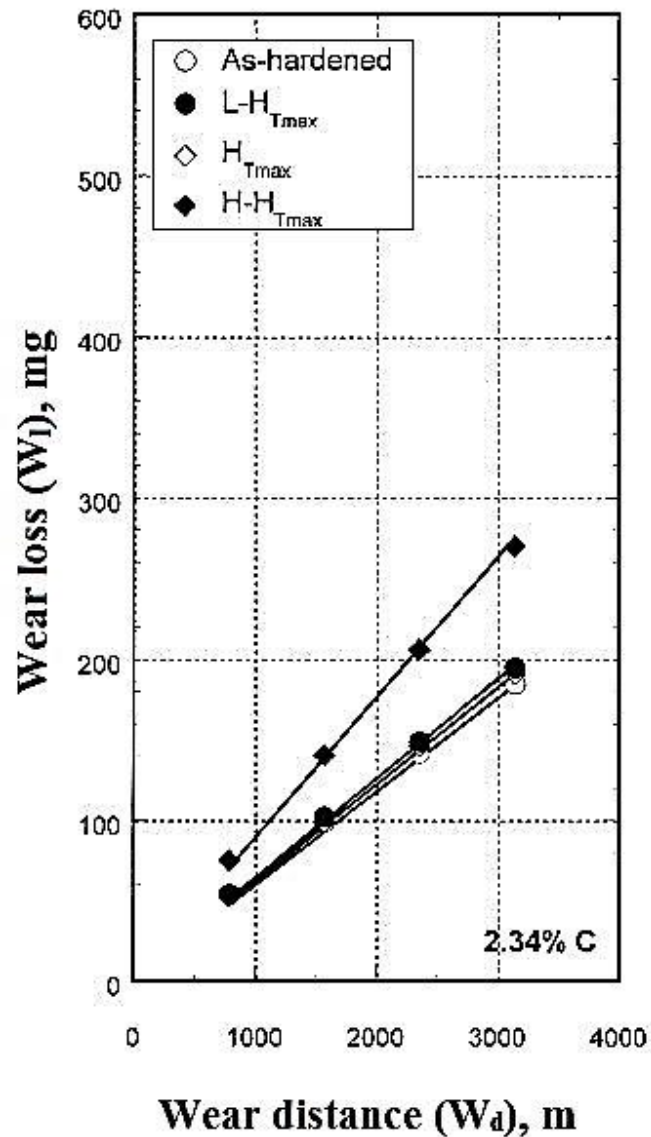| As-hardened	●	$W_l = 0.058 * W_d + 4.40$	$(R^2 = 0.99)$
L-H$_{Tmax}$	○	$W_l = 0.062 * W_d + 3.13$	$(R^2 = 0.99)$
H$_{Tmax}$	◆	$W_l = 0.061 * W_d + 2.80$	$(R^2 = 0.99)$
H- H$_{Tmax}$	◇	$W_l = 0.086 * W_d + 4.20$	$(R^2 = 0.99)$

W_l : Wear loss, W_d : Wear distance

Fig. 4-19 Relationship between wear loss (W_l) and wear distance (W_d) of specimen No.3 tempered after hardening from 1373 K. Rubber wheel test (three-body-type) with load 85.3 N (8.7 kgf).

Chapter V

Discussions

5.1 Behavior of heat treatment

5.1.1 As-hardened state

Relationship between macro- and micro-hardness, Vγ and C content are shown in Fig. 5-1 (a) for specimens hardened from 1323 K and (b) for those hardened from 1373 K austenitizing. In the case of specimens hardened from 1323 K, macro- and micro-hardness increased as C content rose. In the case of 1373 K austenitizing, both of hardness increased but they decreased greatly at high C content of 2.34% (specimen No.3). The behavior of macro- and micro-hardness varies in the same manner against the change in C content, irrespective of austenitizing temperatures. On the other side, the Vγ continues to increase with a rise of C content of specimens hardened from both of 1323 K and 1373 K austenitizing. The reason for the hardness of specimen No.3 dropped remarkably is due to that too much soft austenite existed against the amount of transformed martensite with high hardness. In cases of austenitizing temperature, the critical amount of austenite could be near 30%.

Since the macro-hardness is overall higher than the micro-hardness and the trend of Vγ associated with C content is very similar, it is reasonable that the higher macro-hardness is supported by the existence of eutectic carbides.
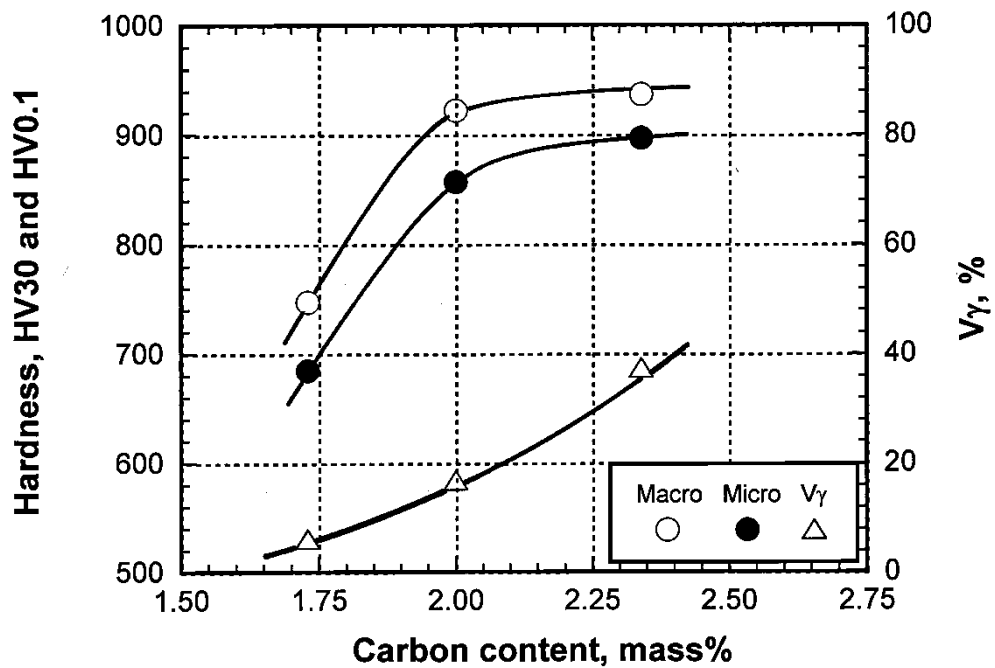
(a) 1323 K austenitizing temperature
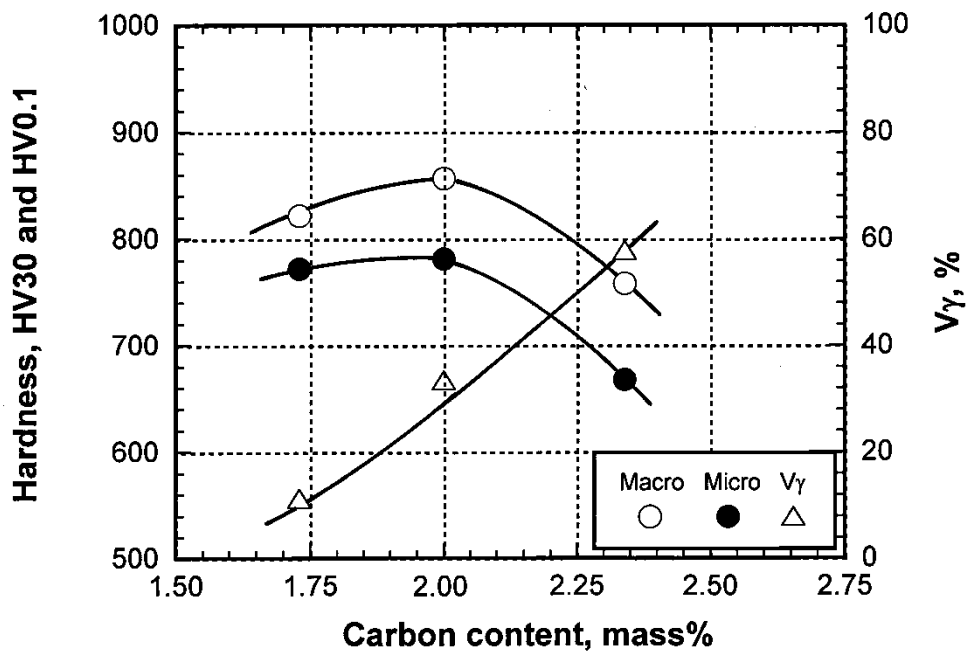
(b) 1373 K austenitizing temperature

Fig. 5-1 Relationship between macro- and micro-hardness, volume fraction of austenite (Vγ) and C content.

When compared the hardness at the same C content, the higher hardness was obtained in specimens hardened from 1323 K austenitizing except for specimen No.1 with lower C content of 1.73%. This can be explained by correlation between Vγ and amount of martensite. The Vγ value of specimen No.1 in 1323 K is lower than that of 1373 K austenitizing. This means that the amount of martensite is more and Vγ is less in the specimen hardened from 1323 K. In spite of the fact, the hardness of specimen hardened from higher austenitizing temperature of 1373 K is higher. It is considered that more C dissolved into martensite at higher temperature of 1373 K made the hardness of martensite increased greatly [30].

On the other side, the Vγ continuously increased as C content rose, regardless of austenitizing temperature and at the same C content, the higher austenitizing temperature caused higher Vγ. It can be explained that the solubility of C and alloying elements in austenite increased at an elevated temperature, and subsequently, these alloys lowered the Ms temperature. The relationship between Ms temperature and alloying elements for steel is expressed by the following equation [31]

$$Ms\ (^{o}C) = 545 - 330 \times (\%C) + 2 \times (\%Al) + 7 \times (\%Co) - 14 \times (\%Cr) -$$
$$13 \times (\%Cu) - 23 \times (\%Mn) - 5 \times (\%Mo) - 4 \times (\%Nb) -$$
$$13 \times (\%Ni) - 7 \times (\%Si) + 3 \times (\%Ti) + 4 \times (\%V) +$$
$$0 \times (\%W) \quad \quad \quad (5.1)$$

Though, this equation can avail to estimate the Ms temperature of steels, it can not do it for the alloyed white cast irons because added carbide forming elements combine preferably with C to form eutectic carbides during solidification. Therefore, the Ms temperature of multi-alloyed white cast iron will be calculated if the

concentrations of C and alloying elements in matrix can be analyzed quantitatively. As imagined from above equation, most of alloying elements added to the multi-alloyed white cast iron have effect to decrease the Ms temperature except for Co. Hence, C and alloying elements dissolved in the matrix promote to stabilize the austenite. This means that the retained austenite is increased by addition of C and alloying elements and by elevating the austenitizing temperature. It should be noted that the transformation behaviors including the change of Ms teamperature are determined by the total effects of alloying elements dissolved in the matrix and austenitizing temperature.
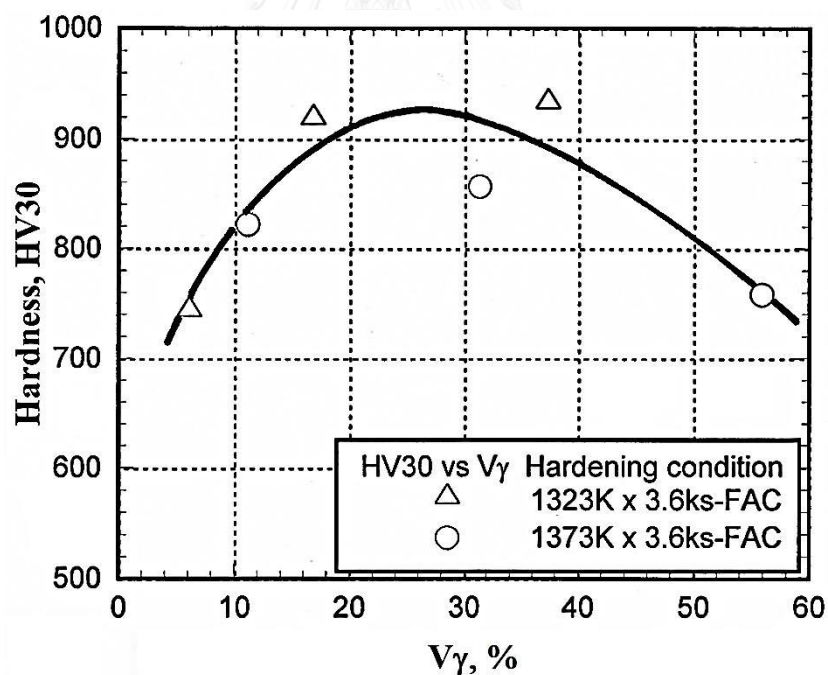
Fig. 5-2 Relationship between macro-hardness and volume fraction of retained austenite ($V\gamma$) in as-hardened state.

The relationship between the macro-hardness and the Vγ in as-hardened state is shown in Fig. 5-2. It is clear from the figure that the hardness increased with a rise of V$_\gamma$ up to 28% and then decreased as the Vγ gets over 28%. It is considered that the former occurred due to an increase in precipitation of carbides and the latter took place because of an excess of soft austenite and a reduction of hard martensite.

Therefore, the maximum hardness is obtained by the optimum balance of the Vγ and the amount of martensite.

5.1.2 In tempered state

5.1.2.1 Relationship between macro-hardness, micro-hardness and tempering temperature

In general, the amount of eutectic carbides does not change during usual heat treatment. Therefore, hardness varies mainly depending on the matrix structure. The macro-hardness measured by Vicker hardness tester shows the sum of the carbides and matrix while the micro-hardness measured by Micro-Vicker hardness tester does the hardness of matrix itself in which plural phases are co-existing.

The relationships between macro-, micro-hardness and tempering temperatures are shown in Fig. 5-3 (a) and (b) for specimen No.1, 5-4 (a) and (b) for specimen No.2 and 5-5 (a) and (b) for specimen No.3, respectively. The variation of macro-hardness shows similar trend to the micro-hardness against tempering temperature and the micro-hardness is overall lower than the macro-hardness in all the specimens. The differences in hardness between the macro- and micro-hardness are 30 to 70 HV30 in specimen No.1, 50 to 95 HV30 in No.2 and 40 to 105 HV30 in

No.3 for specimen hardened from 1323 K austenitizing. In case of the specimens hardened from 1373 K austenitizing, the differences are 35 to 50 HV30 in No.1, 30 to 75 HV30 in No.2 and 30 to 80 HV30 in No.3 specimens. This proves that higher macro-hardness is due to the eutectic carbides in microstructure in addition to the matrix hardness. When the trend is considered more in details, the macro- and micro-hardness change side by side in the range of lower tempering temperature until H_{Tmax}. Here, the reduction of $V\gamma$ in matrix could mainly contribute proportionally to the increase of hardness.
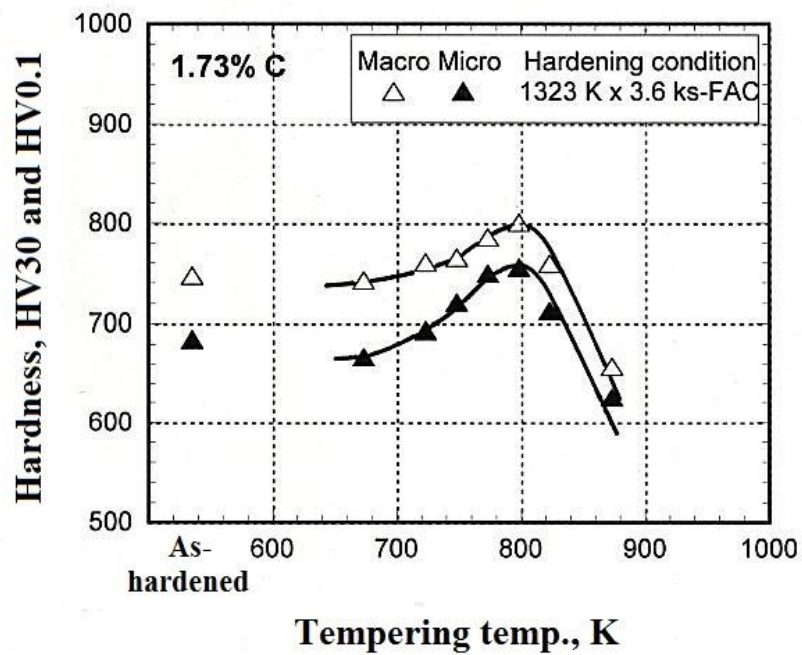
(a)
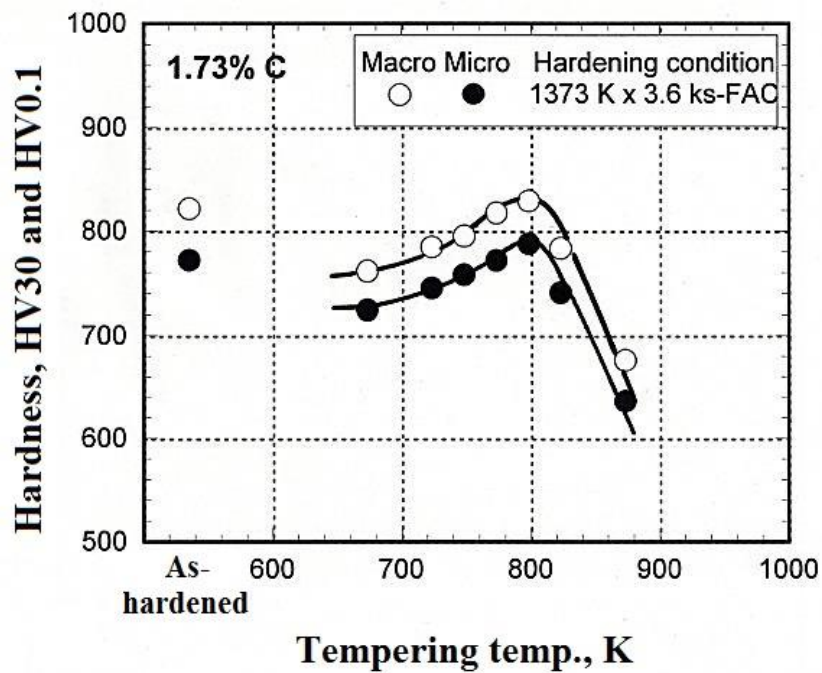
(b)

Fig. 5-3 Relationship between macro-hardness, micro-hardness and tempering temperatures of specimen No.1 with 1.73% C. Austenitizing temperature : (a) 1323 K and (b) 1373 K.
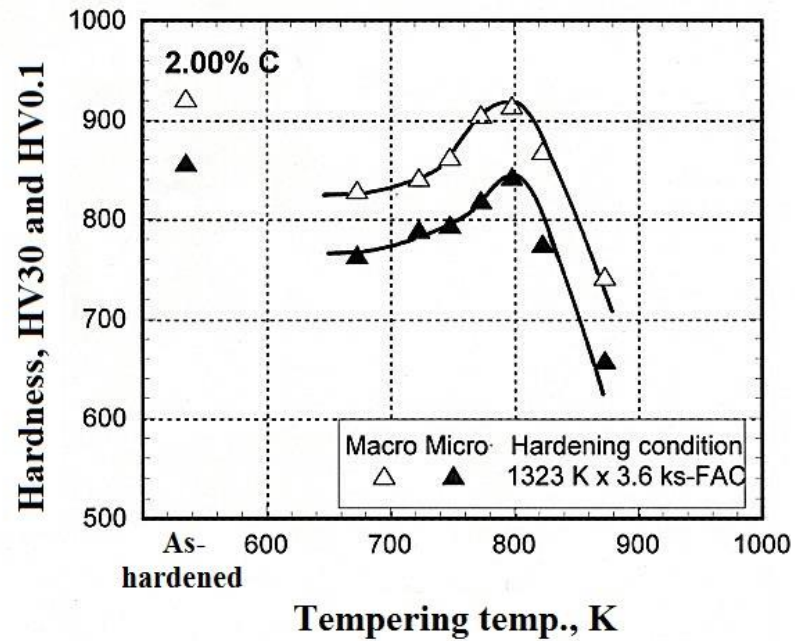
(a)
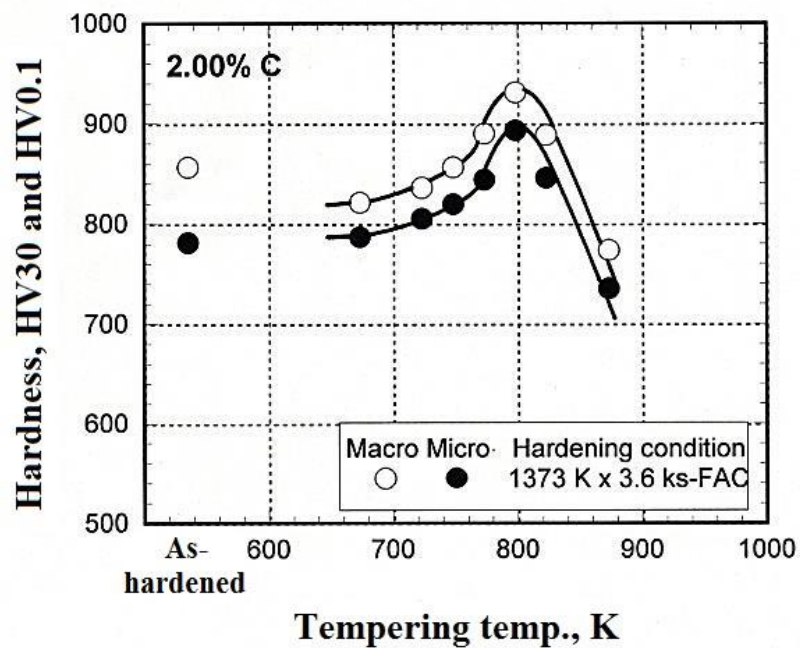
(b)

Fig. 5-4 Relationship between macro-hardness, micro-hardness and tempering temperatures of specimen No.2 with 2.00% C. Austenitizing temperature : (a) 1323 K and (b) 1373 K.
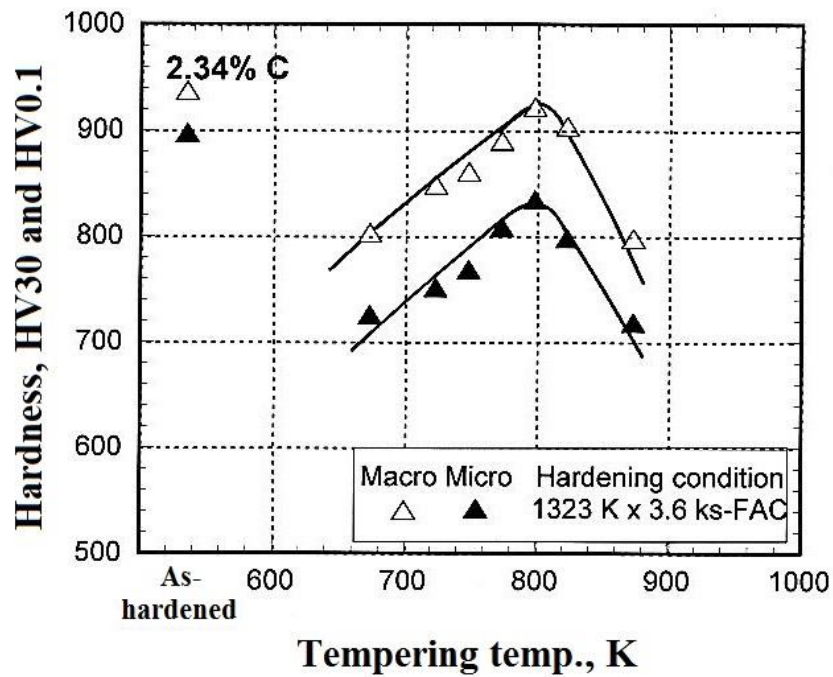
(a)
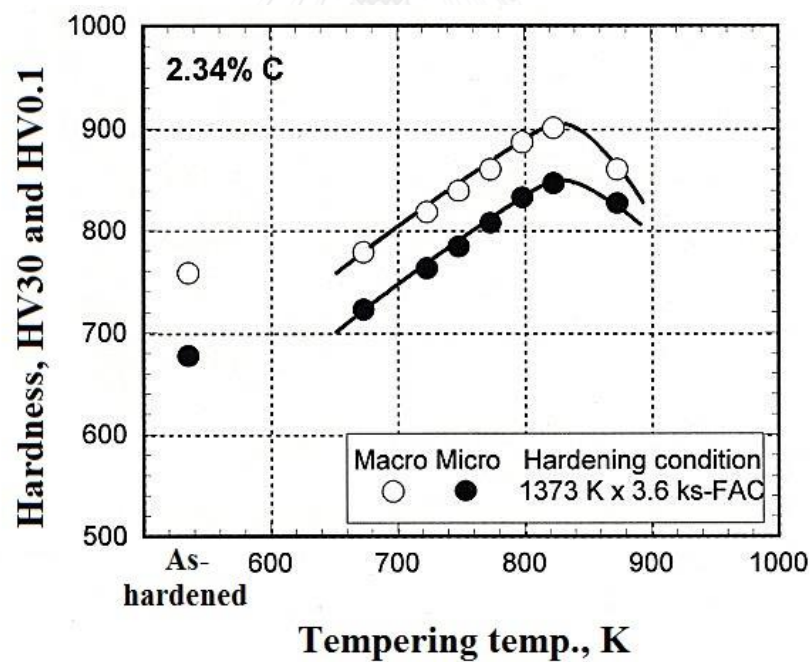
(b)

Fig. 5-5 Relationship between macro-hardness, micro-hardness and tempering temperatures of specimen No.3 with 2.34% C. Austenitizing temperature : (a) 1323 K and (b) 1373 K.

5.1.3 Relationship between hardness, volume fraction of retained austenite and C content

5.1.3.1 Relation of hardness and C content

The relationship between maximum tempered hardness (H_{Tmax}), volume fraction of retained austenite ($V\gamma$) and C content was shown in Fig. 5-6. As C content increased the H_{Tmax} rose until 2.00% C and decreased toward 2.34% C. The former phenomenon is explained by that the increasing of C content promoted an increase in secondary carbides precipitation and the transformation of retained austenite to martensite. The latter phenomenon occurs by that more $V\gamma$ existed in the matrix due to an increase in C content of specimen. It will be estimated the highest H_{Tmax} exists at C content 2.00% for 1323 K and 2.34% for 1373 K austenitizing in this experiment. According to detailed observation on the highest H_{Tmax}, however, the peak seems to shift to low C side by elevating the austenitizing temperature from 1323 K to 1373 K. This reason can be explained as follows. In order to get the same highest H_{Tmax} value as hardened from 1323 K by hardening from 1373 K, the amount of C content in the specimen is reduced to 2.00% under the basic alloy composition of this experiment.
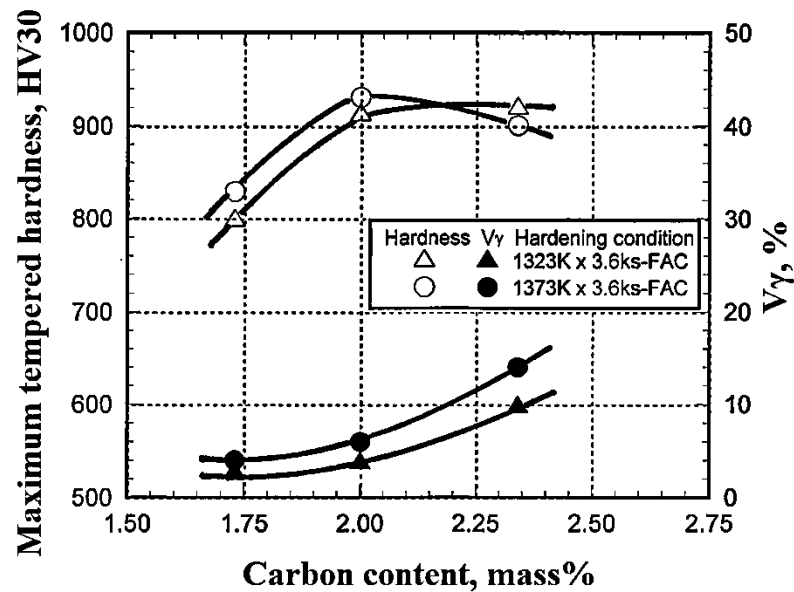
Fig. 5-6 Relationship between maximum tempered hardness (H_{Tmax}), volume fraction

of retained austenite (V_γ) and C content of specimens.

5.1.3.2 Relation of hardness and retained austenite

From the relation of H_{Tmax} vs. C content shown in Fig. 5-6, it was found that the $V\gamma$ values at H_{Tmax} increased continuously as the C content rises, regardless of austenitizing temperature. Higher austenitizing temperature produced overall higher $V\gamma$ value. It is understood from the equation 5-1 that the increasing of C content makes Ms temperature decrease and the austenite was stabilized to increase its amount.

As mentioned previously, the hardness of the cast iron depends on the eutectic carbides and the matrix structure. In general, the eutectic carbide changes little during tempering; the hardness is mainly influenced by the constituent phases in matrix. In the matrix structure, the volume fraction of austenite ($V\gamma$) affects the hardness greatly. Therefore, the relationships between macro-hardness and $V\gamma$ of all the tempered

specimens are summarized in Fig. 5-7. It is found that the hardness increases to the maximum value and then decreases as the Vγ increases. The maximum hardness more than 900 HV30 was obtained at about 4 to 14% Vγ. In the range of less than the maximum hardness, the hardness is low because the specimen was over-tempered, i.e., the fine secondary carbides agglomerated to large particles and this decreases the hardness of matrix. Over the maximum hardness, the hardness decreases gradually due to a rise of Vγ.
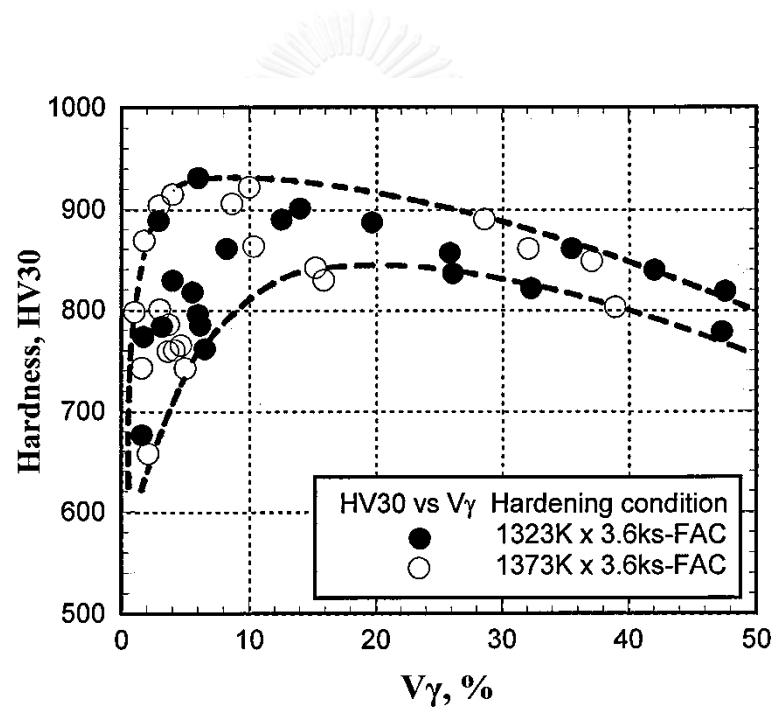
Fig. 5-7 Relationship between macro-hardness and volume fraction of retained austenite (Vγ) of tempered specimens.

5.1.4 Relationship between maximum tempered hardness and volume fraction of

retained austenite in heat treated state

In order to make sure which austenite remaining in tempered state or that in as-hardened state influenced more on the H_{Tmax}, the H_{Tmax} values were connected to the $V\gamma$ in the tempered and the as-hardened states. The former relation is shown in Fig.5-8 and the latter one in Fig.5-9, respectively. From Fig. 5-8, the maximum value of H_{Tmax} seems to exist near 6% $V\gamma$ in tempered state. In order to get H_{Tmax} values over 900 HV30, the tempering should be carried out so that the $V\gamma$ remains from 4 to 14% in tempered state. This result shows a good agreement with the relationship between all of macro-hardness and the $V\gamma$ values in the tempered state (Fig.5-7). In the as-hardened state, the H_{Tmax} increased first roughly in proportion to $V\gamma$ and then decreased moderately as the $V\gamma$ increased, regardless of difference in austenitizing temperatures. This tendency could be explained by that the softening due to the amount of retained austenite exceeded, the total hardening by the precipitation of secondary carbides and the transformation of retained austenite to martensite. From this result, it is found that the $V\gamma$ more than 15% in the as-hardened state is necessary for the cast iron to get the H_{Tmax} value over 900 HV30 in the tempered state. This proves that the retained austenite in as-hardened state contributes more to the secondary hardening during tempering, particularly precipitation of secondary carbides and formation of martensite.
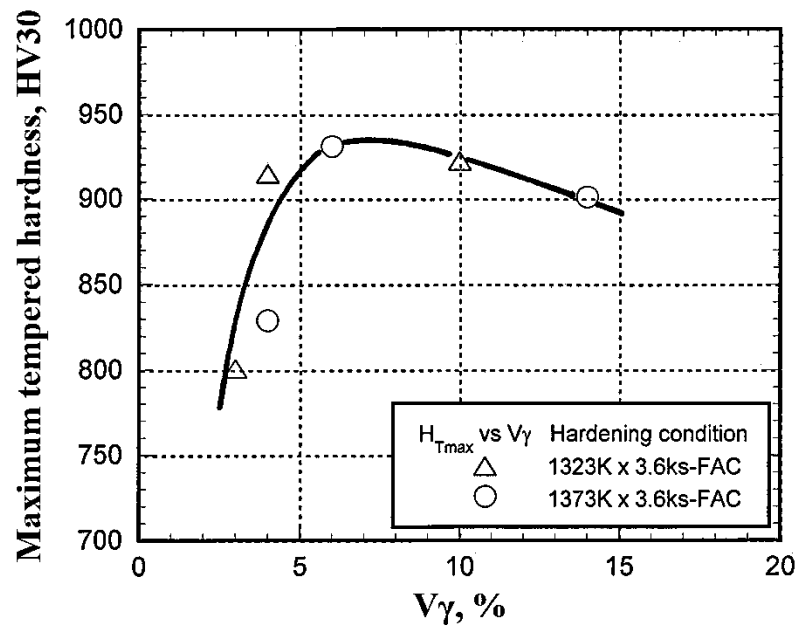
Fig. 5-8 Relationship between maximum tempered hardness (H_{Tmax}) and volume fraction of retained austenite ($V\gamma$) at H_{Tmax}.
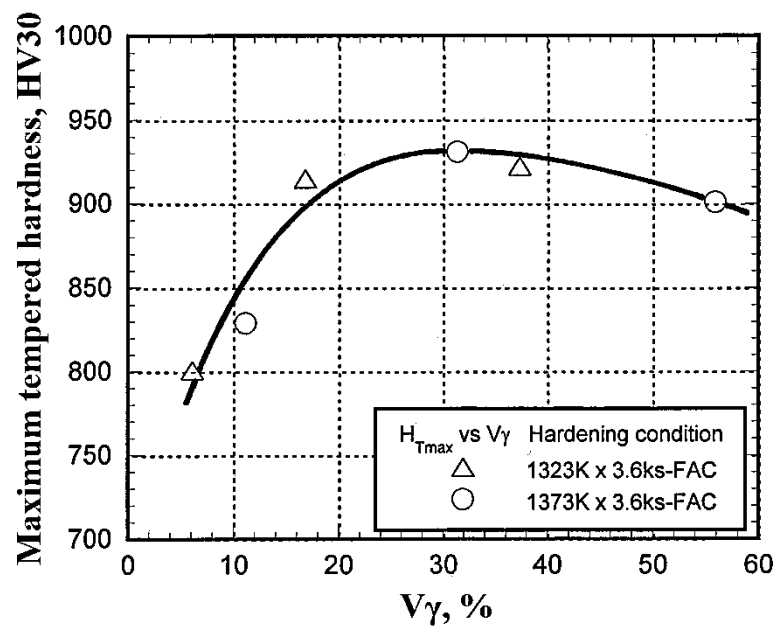
Fig. 5-9 Relationship between maximum tempered hardness (H_{Tmax}) and volume fraction of retained austenite ($V\gamma$) in as-hardened state.

5.2 Abrasive wear behavior

5.2.1 Rate of abrasive wear

Wear rate (R_W) values of specimen heat-treated by different conditions are summarized in Table 5-1 (a) for 1323 K and (b) for 1373 K austenitizing, respectively.

Table 5-1 Wear rate (R_W) in rubber wheel abrasive wear test (three-body-type) of specimens with different heat treatment conditions. Load : 85.3 N (8.7 kgf).

Specimen	Wear rate (R_W : mg/m)			
	As-hardened	L-H$_{Tmax}$	H$_{Tmax}$	H-H$_{Tmax}$
No.1 (1.73% C)	0.156	0.177	0.141	0.149
No.2 (2.00% C)	0.075	0.101	0.099	0.116
No.3 (2.34% C)	0.058	0.069	0.065	0.087

(a) Austenitizing temperature : 1323 K.

Specimen	Wear rate (R_W : mg/m)			
	As-hardened	L-H$_{Tmax}$	H$_{Tmax}$	H-H$_{Tmax}$
No.1 (1.73% C)	0.100	0.135	0.129	0.122
No.2 (2.00% C)	0.077	0.097	0.081	0.100
No.3 (2.34% C)	0.058	0.062	0.061	0.086

(b) Austenitizing temperature : 1373 K.

Here, the wear rate (R_W) which is expressed by the slope of the straight line obtained from the relationships between wear loss (W_l) and wear distance (W_d),

which are shown in Fig.4-14 to Fig. 4-19 was introduced as a parameter to evaluate the wear resistance.

Even if the straight line lies at higher position, it does not always mean a lower wear resistance. The importance is the slope of the straight line (R_W), because the W_l at primary stage or primary wear may be removed depending on the initial surface condition, and so constant wearing or proportional wear must be taken into consideration. Therefore, it can be said that the alloy with higher wear resistance should have lower R_W value.

In case of specimens hardening from 1323 K austenitizing, the R_W values are summarized in Table 5-1 (a). The wear resistance of specimen No.1 is largest in H_{Tmax} state with R_W of 0.141 mg/m, followed by the order of high wear resistance in H-H_{Tmax} with 0.149, as-hardened with 0.156 and the lowest in L-H_{Tmax} specimen with 0.177.

As for the wear resistance of specimens No.2, as-hardened specimen was best with R_W of 0.075 mg/m, and it decreased in the order of H_{Tmax} with 0.099, L-H_{Tmax} with 0.101 and the worst of H-H_{Tmax} specimen with 0.116.

With respect to specimens No.3, the wear resistance decreased in the order of as-hardened state with R_W of 0.058 mg/m, H_{Tmax} with 0.065, L-H_{Tmax} with 0.069 and H-H_{Tmax} specimen with 0.087.

On the other side, the R_W values of specimens hardened from 1373 K austenitizing are also summarized in Table 5-1 (b). The R_W values of specimens No.1 increased in the order of 0.100 mg/m of as-hardened state, 0.122 of H-H_{Tmax}, 0.129 of

H_{Tmax} and 0.135 of L-H_{Tmax} specimen. Therefore, the wear resistance is best in the as-hardened state and worst of H-H_{Tmax} specimen.

In specimens No.2, R_W was smallest in as-hardened specimen with 0.077 mg/m and it increased in the order of 0.081 in H_{Tmax}, 0.097 in L-H_{Tmax} and 0.100 in H-H_{Tmax} specimen. It can be said that the highest abrasive wear resistance was obtained in as-hardened specimen and the lowest one in H-H_{Tmax} specimen.

With respect to specimen No.3, the order of R_W value was 0.058 mg/m in as-hardened state, 0.061 in H_{Tmax}, 0.062 in L-H_{Tmax} and 0.086 in H-H_{Tmax} specimen, respectively, and therefore, the largest wear resistance was obtained in as-hardened state and the worst was H-H_{Tmax} specimen.

When the wear rate is come to think of synthetically, it can be said that the R_W values in as-hardened specimens are smaller than those in tempered specimens. Though the carbide structure is almost the same in each specimen, however, the component of phases in the matrix are quite different between the as-hardened and the tempered states even if the hardness is similar. The former consists of martensite, retained austenite and carbides precipitated during austenitizing, and the latter is composed of tempered martensite with very fine carbides, and small amount of retained austenite and martensite transformed from retained austenite during cooling. It is well known that the tempered martensite is very useful and effective phase for wear resistance, having high hardness and considerable toughness. Therefore, it will be reasonable to discuss the wear resistance separately according to the matrix microstructure.

In the as-hardened state, the R_W decreases in each austenitizing temperature, as the C content increases, that is, the wear resistance becomes better with an increase in C content. However, the problem of induced martensite transformation or work hardening of cast iron can leave behind while using. In case of tempered state, the highest wear resistance is obtained mostly in H_{Tmax} specimens, followed by L-H_{Tmax} and the lowest wear resistance in H-H_{Tmax} specimen. On the other side, the R_W decreases as the C content of specimen increases, i.e., the wear resistance is improved by increasing the C content.

These reasons can be explained that H_{Tmax} specimens have the tempered martensite, secondary carbides and 3 to 14% of retained austenite, and that H-H_{Tmax} specimens have over-tempered structure with coarse carbides and very less austenite. The L-H_{Tmax} specimens may be in the intermediate state.

5.2.2 Relationship between hardness, amount of residual austenite and wear rate

5.2.2.1 Effect of hardness on wear rate (R_W)

It is well known that hardness is one of factors to increases the wear resistance and the wear resistance is generally high in the cast irons with high hardness. The relationships between hardness and wear rate (R_W) are shown in Fig. 5-10 (a) for specimens hardened from 1323 K and Fig.5-10 (b) for those from 1373 K austenitizing, respectively. In each austenitizing temperature, the R_W decreases as the hardness of specimen increases and the decreasing rates are almost the same. From the positions of symbols, the specimens with higher C content, say, No.2 and No.3, have clearly, the lower R_W. This is because C combined with carbide formers to

produce more eutectic carbide during solidification and to promote the precipitation of secondary carbides and post transformation of retained austenite to martensite. These effects connect directly to an increase in hardness of specimens.
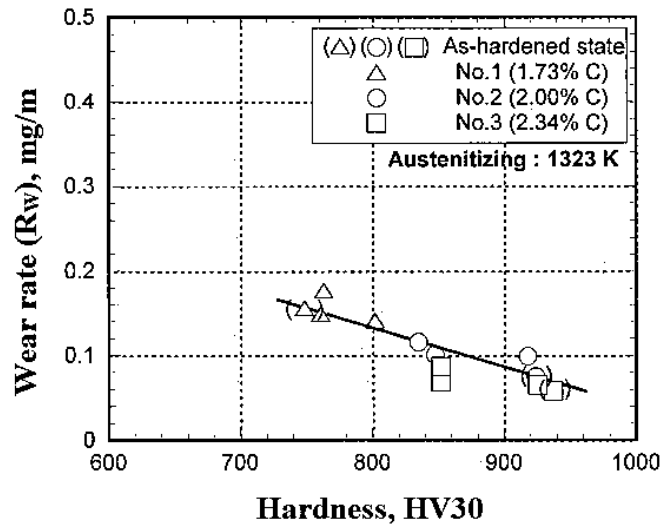
1323 K austenitizing	$R_W = -0.0005 * HV + 0.55$ ($R^2 = 0.81$)

(a)
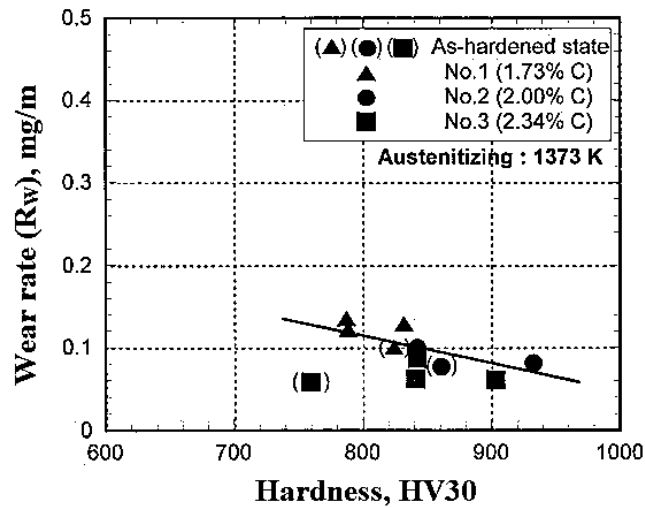
1373 K austenitizing	$R_W = -0.0004 * HV + 0.45$ ($R^2 = 0.51$)

(b)

Fig. 5-10 Relationship between wear rate (R_W) and hardness of tempered specimens after hardening from difference austenitizing temperatures.

5.2.2.2 Effect of volume fraction of retained austenite on wear rate

Higher wear resistance is relating to the types and amounts of hard carbides in eutectic structure and the precipitates in the matrix. If the matrix is soft or has low strength, it is easy for carbides to be worn out. Effect of volume fraction of austenite ($V\gamma$) on the wear rate (R_W) of tempered specimens hardened from 1323 K austenitizing is shown in Fig.5-11. The relation of R_W and $V\gamma$ is separated to two groups; one is in the lower $V\gamma$ values less than 5% and another is in the higher $V\gamma$ ones more than 5%. Within the $V\gamma$ values less than 5%, the R_W values cover a wide range from 0.08 to 0.18 mg/m, and over 5% $V\gamma$, the R_W decreases roughly in proportion to the increasing of the $V\gamma$.

To find the reason why the R_W values are spreading widely, the R_W values were related to hardness and the relation is shown in Fig. 5-12. It was clarified that the R_W depends on the hardness of specimens, that is to say, the wear resistance varies depending on the matrix microstructure that determines the hardness of specimens.

In case of specimens hardened from 1373 K austenitizing, very similar relation of R_W vs. $V\gamma$ is obtained as shown in Fig. 5-13. The R_W values from 0.08 to 0.14 mg/m were obtained in the $V\gamma$ lower than 5%. As the $V\gamma$ increases over 5%, the R_W lowers gradually with a rise of $V\gamma$. Within 5% $V\gamma$, it is obvious from Fig. 5-14 that the R_W decrease roughly in proportion to the increase of hardness which is mainly determined by the matrix structure.
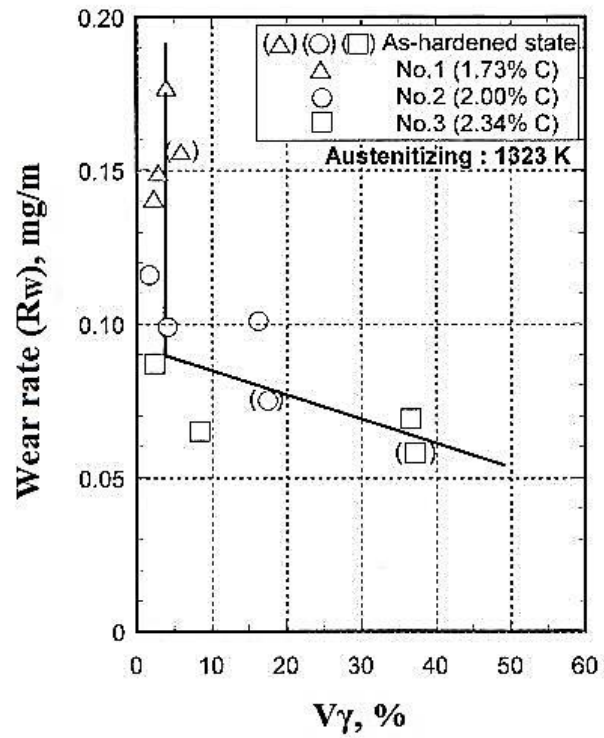
Fig. 5-11 Relationship between wear rate (R_W) and volume fraction of retained austenite ($V\gamma$) of tempered specimens after hardening from 1323 K.
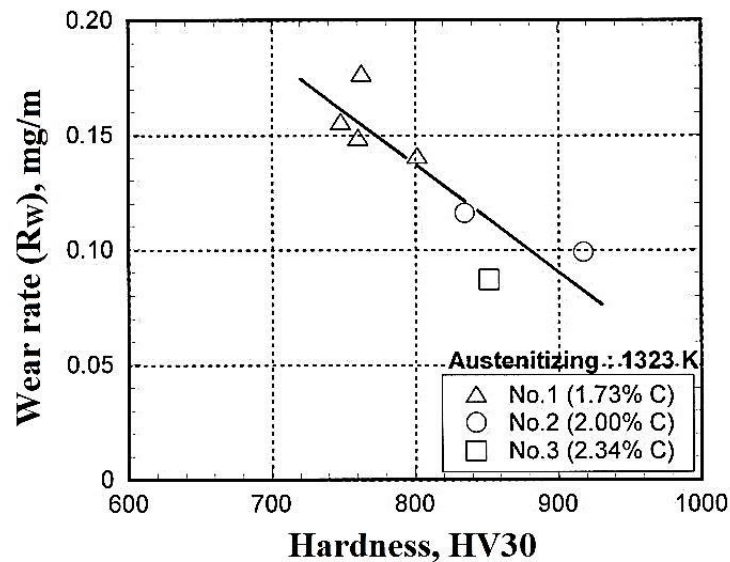
Fig. 5-12 Relationship between wear rate (R_W) and hardness of tempered specimens with volume fraction of retained austenite ($V\gamma$) less than 5% after hardening from 1323 K.
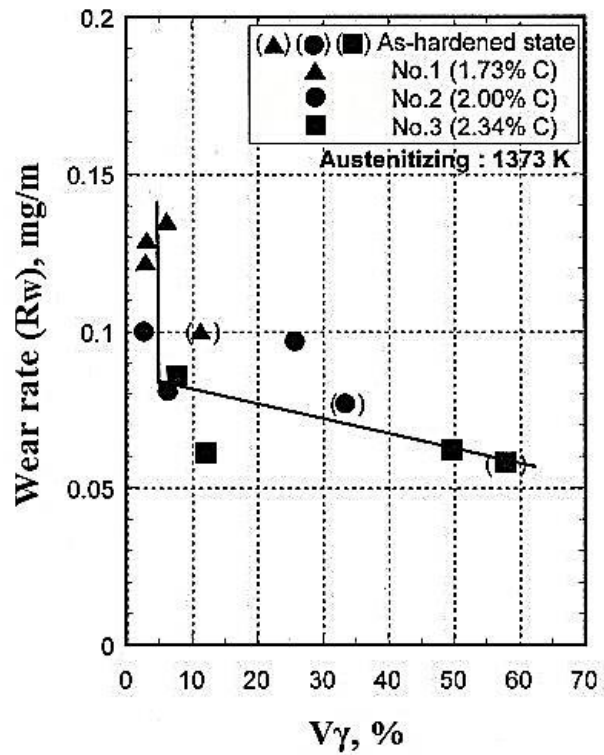
Fig. 5-13 Relationship between wear rate (R_W) and volume fraction of retained austenite ($V\gamma$) of tempered specimens after hardening from 1373 K.
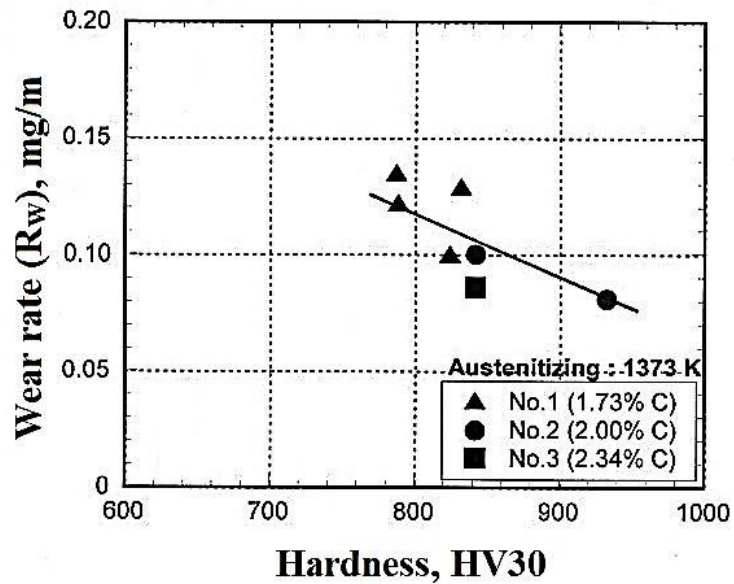
Fig. 5-14 Relationship between wear rate (R_W) and hardness of tempered specimens with volume fraction of retained austenite ($V\gamma$) less than 5% after hardening from 1373 K.

5.2.3 Application of multiple regression analysis to experimental results

In order to predict the wear rate (RW) of multi-alloyed white cast irons hardened from 1323 K and 1373 K austenitizing and tempered at 673 to 873 K, the multiple regression analysis was introduced for the results and the R_W was express by following equation;

$$R_W = - (55.22 \times 10^{-3}) \times (\%C) - (0.27 \times 10^{-3}) \times (T_\gamma) + (0) \times (t_\gamma)$$
$$- (7.22 \times 10^{-5}) \times (T_t) + (0.31 \times 10^{-3}) \times (t_t) - (0.26 \times 10^{-3}) \times (HV)$$
$$- (0.75 \times 10^{-3}) \times (V_\gamma) + 0.802 \quad\quad\quad\quad\quad\quad\quad\quad\quad (5.2)$$

Here, R_W = Wear rate of rubber wheel abrasive test (mg/m)

%C = Carbon content of specimen (%)

T_γ = Austenitizing temperature available : 1323 and 1373 (K)

t_γ = Holding time for austenitizing (min.)

T_t = Tempering temperature available : 673 to 873 (K)

t_t = Holding time for tempering (min.)

HV = Macro-hardness (HV30)

V_γ = Volume fraction of retained austenite available : 1.0 to 60.0 (%)

As shown in the equation, the R_W can be calculated by filling the data to the equation. It is found that most of the variables have effect to decrease the R_W except for the holding tempering time (t_t). Here, the equation was verified using four test pieces of specimen No.2 hardened from 1323 K and the results are displayed in the Table 5-2. It is evident from the table that the difference of R_W values between experimental and calculated results showed very less, and therefore, this equation can availed accurately predict the wear rate.

Table 5-2 Verification of experimental and calculated results for wear rate (R_W).

State	R_W (experimental)	R_W (equation)	Difference (%)
As-hardened	0.075	0.082	- 0.7
L-H_{Tmax}	0.101	0.114	- 1.3
H_{Tmax}	0.099	0.098	+ 0.1
H-H_{Tmax}	0.116	0.117	- 0.1

5.2.4 Observation of worn surface

As an example, a wear tested specimen with hardness of 755 HV30 and 1.17% Vγ was picked up and the worn surface appearance was observed by SEM. The SEM microphotograph is demonstrated in Fig.5-15. The direction of wearing by the sand abrasives is not clear, because the abrasives move freely on surface of specimen in the three-body-type abrasive wear test. This specimen was tempered at high temperature of 900 K and so it has lower hardness. The worn surface is rough and the scratchings are shown on the eutectic structure and the pittings are distributed randomly. This is because the scratching wear took place in the region of hard eutectics, and the pittings occurred mainly on the matrix areas when soft matrices were dug away by the abrasives and the pittings caused together with breaking away of eutectic carbides nearby.
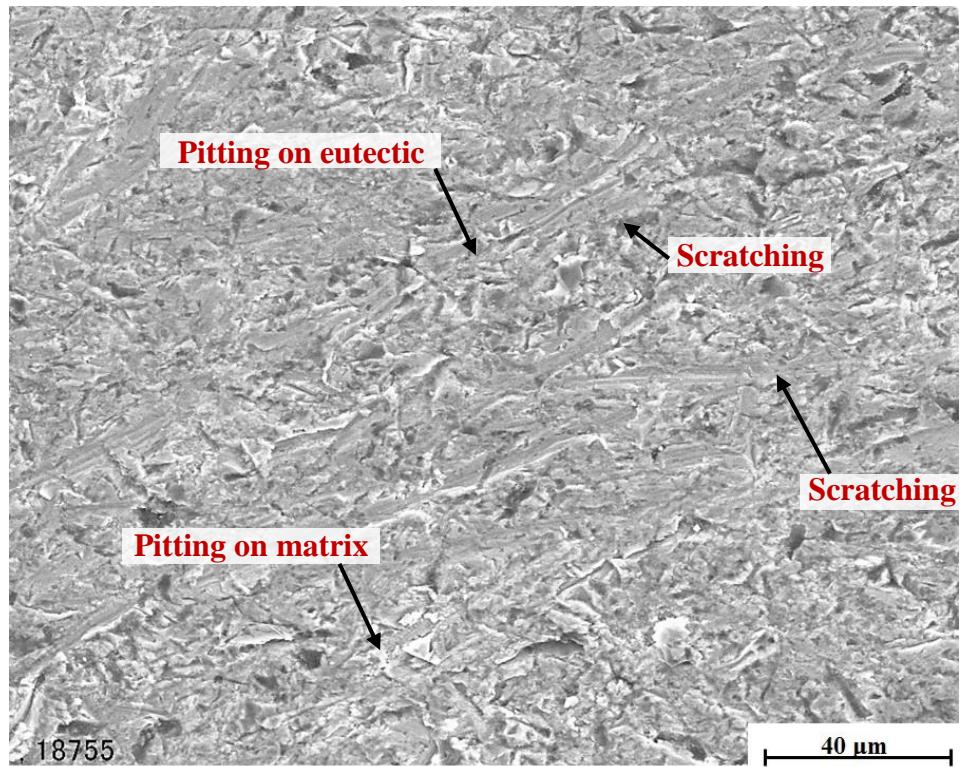
Fig. 5-15 SEM microphotograph of worn surface of specimen No.3 with 2.34% C hardened from 1373 K austenitizing and tempered at 900 K. Rubber wheel (three-body-type) abrasive wear test.

Chapter VI

Conclusions

Effects of carbon content on heat treatment behavior and abrasive wear resistance of multi-alloyed white cast iron with basic alloy composition were investigated. For the investigation of heat treatment behavior, specimens were hardened from two levels of austenitizing temperatures, 1323 K and 1373 K, and tempered at 50 K intervals from 673 to 873 K. In case of study for abrasive wear resistance, the hardened specimens were tempered at three levels of temperatures at maximum tempered hardness (H_{Tmax}), lower and higher temperatures than that at H_{Tmax} (L-H_{Tmax} and H-H_{Tmax}). Then, the wear rates (R_W) of specimens were evaluated using rubber wheel abrasive wear tester (three-body-type). The conclusions drawn from the experimental results and discussions are summarized as follows,

6.1 Effect of C content on variation of microstructures and heat treatment behavior

6.1.1 Microstructure of as-cast specimens

1) All the as-cast specimens show hypoeutectic structures composed of primary austenite dendrite and eutectic structures consisting of (γ+MC) and (γ+M_2C).

2) Area fraction of the eutectic increases as C content of specimens rises.

6.1.2 Microstructure of as-hardened specimens

1) Amount of austenite in primary area seems to be reduced compared with that in the as-cast state due to two reactions, the precipitation of secondary carbides and transformation of austenite to martensite.

2) Fine secondary carbides in as-hardened specimens decreased in number with an increase in C content. This is because the more martensite transformed at high C specimens. In high austenitizing specimens, the microstructure showed less secondary carbides, while the Vγ increases by dissolution of C and alloying elements into matrix and stabilized austenite.

3) Martensite was observed clearly in hardened specimen with higher C content.

6.1.3 Microstructure of tempered specimens

1) Microstructure of specimens observed by OM showed that fine precipitates or carbides were coarsened with increasing the tempering temperature.

2) Martensite were distinguished in the SEM microphotographs of specimen No.2 and No.3 with high C content, and the amount of fine secondary carbides decreased in the same way of as-hardened state as C content of specimen increased.

6.2 Effect of C content on macro- and micro-hardness and volume fraction of retained austenite (Vγ)

6.2.1 As-hardened state

1) In specimens hardened from 1323 K austenitizing, the macro- and micro-hardness increased as C content rose. In specimens hardened from 1373 K austenitizing, hardness dropped rapidly in specimen No.3 with highest C content of 2.34%.

2) The Vγ increased with an increase in C content, regardless of the difference in austenitizing temperatures. A critical value of Vγ in which the maximum hardness was obtained near 28%.

3) The maximum hardness could be obtained by an optimum balance of the Vγ and amount of martensite.

6.2.2 Tempered state

1) All of tempered hardness curves showed evident secondary hardening. The hardness increased first forward to the maximum hardness (H_{Tmax}) and then decreased as C content increased. This tells that the destabilization of retained austenite in the as-hardened state proceeded by both of precipitation of fine secondary carbides and martensite transformation from retained austenite as tempering temperature was increased. After the temperature was elevated over the H_{Tmax}, however, the hardness dropped remarkably due to the coarsening of fine secondary carbides.

2) The maximum tempered hardness (H_{Tmax}) was obtained at tempering temperature of 798 to 823 K.

3) Macro-hardness were higher than micro-hardness in all the specimens regardless of austenitizing temperatures.

4) Maximum tempered hardness (H_{Tmax}) increased with an increase in C content and the highest H_{Tmax} lay at C content 2.00% for 1323 K and 2.34% for 1373 K austenitizing. In order to get same highest H_{Tmax} value as the specimen hardened from 1323 K by hardening from 1373 K, the C content of specimen had to be reduced to low C content of 2.00%.

5) $V\gamma$ values of specimens austenitized at high temperature of 1373K were overall higher than those austenitized at lower temperature of 1323K. It is because more C and alloying elements dissolved into matrix and stabilized austenite at high temperature.

6) The $V\gamma$ value reduced greatly as tempering temperature elevated to 723 to 773 K.

6.2.3 Correlation between maximum tempered hardness (H_{Tmax}) and volume fraction of retained austenite ($V\gamma$) in heat treated state

1) The maximum hardness more than 900 HV30 were obtained at about 4 to 14% $V\gamma$ in tempered state.

2) The maximum tempered hardness (H_{Tmax}) seemed to be exist near 6% $V\gamma$.

3) The $V\gamma$ values more than around 15% in as-hardened state was needed to obtain high H_{Tmax} over 900 HV30.

6.3 Effect of heat treatment on abrasive wear behavior

6.3.1 Correlation between wear loss (W_l) and wear distance (W_d)

1)   Wear loss (W_l) was in proportion to wear distance (W_d) in every specimen even if specimen was tempered at different temperatures.

2)   The relationship between W_l and W_d was found to be linear function and wear rate (R_W) was expressed by the slope of linear relation.

6.3.2 Correlation between hardness, volume fraction of retained austenite ($V\gamma$)
       and wear rate (R_W)

1)   The wear resistance of as-hardened specimens was better than those of tempered specimens. The R_W in the as-hardened state decreased as C content increased. On the other side, the highest wear resistance is obtained mostly in H_{Tmax} specimens, followed by L-H_{Tmax} and the lowest wear resistance in H-H_{Tmax} specimen.

2)   In the relationship between R_w and hardness of specimens, the R_w decreased as hardness increased because the hard phases resisted the abrasive materials.

3)   When the effects of volume fraction of retained austenite ($V\gamma$) on R_W of tempered specimens was discussed, the R_W values of specimens with $V\gamma$ less than 5% covered in the wide range but it decreased with increasing of hardness. In the region of $V\gamma$ values over 5%, however, the R_W was decreased roughly in proportion to an increase in the $V\gamma$.

6.3.3 Application of multiple regression analysis to experimental results

1) The data of rubber wheel abrasive wear tests were summarized by using multiple regression analysis mothod, and the following equation was obtained to be able to predict the R_W accurately.

$$R_W = -(55.22 \times 10^{-3}) \times (\%C) - (0.27 \times 10^{-3}) \times (T_\gamma) + (0) \times (t_\gamma)$$

$$- (7.22 \times 10^{-5}) \times (T_t) + (0.31 \times 10^{-3}) \times (t_t) - (0.26 \times 10^{-3}) \times (HV)$$

$$- (0.75 \times 10^{-3}) \times (V_\gamma) + 0.802$$

6.3.4 Observation of worn surface

1) Worn surface appearance showed the scratching wear on eutectic areas and the pitting wear mainly in the matrix.
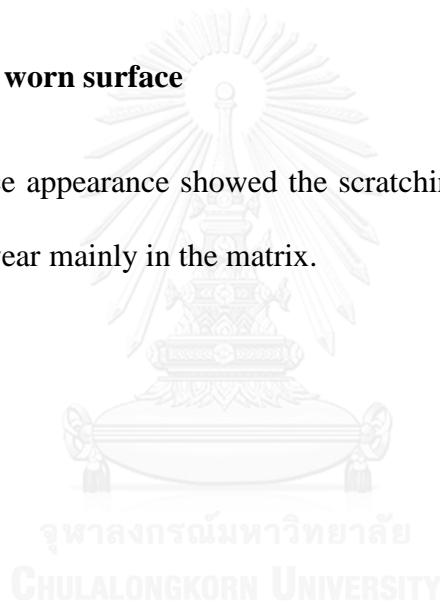
REFERENCES

[1]   M. Hashimoto, "Development of multi-component White Cast Iron (HSS) rolls and Rolling technology in steel rolling," *Abrasion Wear Resistant Alloyed White Cast Iron for Rolling and Pulverizing Mills,* pp. 1-23, 2008.

[2]   M. Boccalini Jr., "Overview : High speed steels for hot rolling mill rolls," *Abrasion Wear Resistant Alloyed White Cast Iron for Rolling and Pulverizing Mills,* pp. 123-142, 2011.

[3]   I. R. Sare and B. K. Arnold, "The influence of heat treatment on the high-stress abrasion resistance and fracture toughness of alloy white cast irons," *Metallurgical and Materials Transactions A,* vol. 26, pp. 1785-1793, 1995.

[4]   Y. Matsubara, N. Sasaguri, and M. Hashimoto, "The history and development of cast rolls for hot working mill," *The 4th Asian Foundry Congress-Australia,* pp. 251-261, 1996.

[5]   G. Laird, R. Gundlach, and K. Rohrig, *Abrasion-Resistance Cast Iron Handbook*: USA: American Foundry Society, 2000.

[6]   J. D. Watson, P. J. Mutton, and I. R. Sare, "Abrasive Wear of White Cast Irons," *Australian Institute of Metals Forum,* vol. 3, pp. 74-88, 1980.

[7]   K.-H. Zum Gahr and D. V. Doane, "Optimizing fracture toughness and abrasion resistance in white cast irons," *Metallurgical Transactions A* vol. 11, pp. 613-620, 1980.

[8]   O. Kubo, M. Hashimoto, and Y. Matsubara, "Influence of microstructure on wear resistance and crack propagation characteristics required for white iron rolling mill rolls," *Proceedings of The Science of Casting and Solidifications,* 2001.

[9]   W. Khanitnantharak, M. Hashimoto, K. Shimizu, K. Yamamoto, N. Sasaguri, and Y. Matsubara, "Effects of Carbon and Heat Treatment on the Hardness

and Austenite Content of a Multi-Component White Cast Iron," *AFS Transactions,* vol. 117, pp. 435-444, 2009.

[10]   H.-Q. Wu, N. Sasaguri, Y. Matsubara, and M. Hashimoto, "Solidification of Multi-Alloyed White Cast Iron : Type and Morphology of Carbides," *AFS Transactions,* vol. 140, pp. 103-8, 1996.

[11]   S. Karagoz, R. Riedl, M. R. Gregg, and H. Fischmeister, "The role of M2C carbides in high speed steels," *Sonderbande der Praktischen Metallographie,* vol. 14, pp. 389-362, 1983.

[12]   V. Raghavan, *Phase Diagrams of Ternary Iron Alloys*: Indian Institute of Metals, 1987.

[13]   G. V. Raynor and V. G. Rivlin, *Phase equilibria in iron ternary alloys* vol. 2. London The Institute of Metals, 1988.

[14]   G. Steven, A. E. Nehrenberg, and T. V. Philip, "High-performance high-speed steels by design," *Transactions of the ASM,* vol. 57, pp. 925-948, 1964.

[15]   M. Hashimoto, "Effects of Alloying Element on Compressive and Wear Properties of Multi-component White Cast irons for Steel Rolling Mill Rolls," *Abrasion Wear Resistant Alloyed White Cast Iron for Rolling and Pulverizing Mills,* pp. 183-192, 2011.

[16]   M. Boccalini Jr., A. Vicente De O Corrêa, and A. Sinatora, "Niobium in multi-component white cast iron," *Abrasion Wear Resistant Alloyed White Cast Iron for Rolling and Pulverizing Mills,* pp. 49-64, 2008.

[17]   J. Tchoufang Tchuindjang, M. Sinnaeve, and J. Lecomte-Beckers, "Influence of High Temperature Heat Treatment on in situ Transformation of Mo-rich Eutectic Carbides in HSS and Semi-HSS Grades," *Abrasion Wear Resistant Alloyed White Cast Iron for Rolling and Pulverizing Mills,* pp. 61-75, 2011.

[18] W. Theisen, "Design of wear resistant alloys against abrasion," *Abrasion Wear Resistant Alloyed White Cast Iron for Rolling and Pulverizing Mills,* pp. 128-138, 2008.

[19] J. D. B. De Mello and E. Canizza, "Influence of microstructural parameters on the tribological behaviour of multicomponent ferrous alloys," *Abrasion Wear Resistant Alloyed White Cast Iron for Rolling and Pulverizing Mills,* pp. 185-211, 2008.

[20] O. Joos, C. Boher, C. Vergne, C. Gaspard, T. Nylén, and F. RezaÏ-Aria, "Laboratory study of the wear and oxidation behavior of High Chromium Cast Iron and HSS material used for HSM work rolls," *Abrasion Wear Resistant Alloyed White Cast Iron for Rolling and Pulverizing Mills,* pp. 102-114, 2008.

[21] Y. Matsubara, N. Sasaguri, Y. Yokomizo, and H.-Q. Wu, "Continuous cooling transformation behavior of multi-alloyed white cast iron," *Journal of Japan Foundry Engineering Society,* vol. 71, pp. 183-189, 1999.

[22] M. Radulovic, M. Fiset, K. Peev, and M. Tomovic, "The influence of vanadium on fracture toughness and abrasion resistance in high chromium white cast irons," *Journal of Materials Science* vol. 29, pp. 5085-5094, 1994.

[23] H.-Q. Wu, M. Hashimoto, N. Sasaguri, and Y. Matsubara, "Solidification Sequence of Multi-Component White Cast Iron," *Journal of Japan Foundry Engineering Society,* vol. 68, pp. 637-643, 1996.

[24] H.-Q. Wu, N. Sasaguri, M. Hashimoto, and Y. Matsubara, "Practical Phase Diagram of Multi-Component White Cast Iron," *Journal of Japan Foundry Engineering Society,* vol. 69, pp. 917-923, 1997.

[25] E. Albertin and A. Sinatora, "Effect of carbide fraction and matrix microstructure on the wear of cast iron balls tested in a laboratory ball mill," *Wear,* vol. 250, pp. 492-501, 2001.

[26] R. J. Chung, X. Tang, D. Y. Li, B. Hinckley, and K. Dolman, "Effects of titanium addition on microstructure and wear resistance of hypereutectic high chromium cast iron Fe–25wt.%Cr–4wt.%C," *Wear,* vol. 267, pp. 356-361, 2009.

[27] Ö. N. Doğan, J. A. Hawk, and G. Laird II, "Solidification structure and abrasion resistance of high chromium white irons," *Metallurgical and Materials Transactions A* vol. 28, pp. 1315-1328, 1997.

[28] I. R. Sare, *Abrasion resistance and fracture toughness of white cast irons* vol. 6: Maney Publishing, 1979.

[29] N. Sasaguri, Y. Yokomizo, K. Yamamoto, and Y. Matsubara, "Influence of Cobalt Content on Heat Treatment Behavior and Abrasive Wear Characteristics of Multi-Component White Cast Iron," *Abrasion Wear Resistant Alloyed White Cast Iron for Rolling and Pulverizing Mills,* pp. 77-87, 2011.

[30] Y. Yokomizo, N. sasaguri, K. Nanjo, and matsubara Y., "Continuous Cooling Transformation Behavior of Multi-component White Cast Iron with Different Carbon Content," *JFS,* vol. 74, pp. 9-16, 2002.

[31] K. Ishida, "Calculation of the effect of alloying elements on the Ms temperature in steels," *Journal of Alloys and Compounds,* vol. 220, pp. 126-131, 1995.

APPENDIX

Macro-hardness, micro-hardness and volume fraction of retained austenite ($V\gamma$) of specimens at 1323 K austenitizing temperature.

Specimen No.	Tempering temperature (K)	Macro-hardness (HV30)	Micro-hardness (HV0.1)	Volume fraction of retained austenite ($V\gamma$) %
Specimen No.1 (1.73% C)	As-hardened	747.4	684.8	6.13
	673	742.6	667.2	5.00
	723	760.6	693.2	4.16
	748	765.2	720.4	4.65
	773	786	749.6	3.72
	798	800.6	755.4	3.08
	823	759.4	712.2	3.65
	873	657.6	625.6	2.12
Specimen No.2 (2.00% C)	As-hardened	922.4	857.0	16.83
	673	829.4	764.6	15.86
	723	842	789.6	12.40
	748	863.4	794.2	10.34
	773	905.8	819.2	8.65
	798	914.8	842.8	3.42
	823	869	775.6	1.79
	873	743.2	658.8	1.60

	As-hardened	937.2	897.2	37.37
	673	802.8	725.4	38.92
	723	848.6	751.4	37.08
Specimen No.3 (2.34% C)	748	860.6	768.2	32.08
	773	890	808.4	28.60
	798	922.2	834.2	14.82
	823	904	798.2	2.93
	873	798	718.6	1.00

Macro-hardness, micro-hardness and volume fraction of retained austenite (Vγ) of specimens at 1373 K austenitizing temperature.

Specimen No.	Tempering temperature (K)	Macro-hardness (HV30)	Micro-hardness (HV0.1)	Volume fraction of retained austenite (Vγ) %
Specimen No.1 (1.73% C)	As-hardened	821.8	772.5	11.13
	673	761.8	725.0	6.54
	723	784.8	745.7	6.18
	748	795.6	758.3	5.98
	773	817.4	772.2	5.56
	798	829.2	788.1	3.36
	823	783.6	741.5	3.19
	873	676.2	636.3	1.61
Specimen No.2 (2.00% C)	As-hardened	856.6	781.6	48.29
	673	821.4	787.1	32.30
	723	836.0	805.2	26.10
	748	856.4	819.8	25.85
	773	890.0	843.8	12.54
	798	931.2	893.4	5.00
	823	888.6	845.8	2.90
	873	774.0	735.5	1.74

	As-hardened	758.2	677.7	55.91
	673	778.8	723.0	47.29
	723	818.8	763.1	47.54
Specimen No.3 (2.34% C)	748	839.6	784.3	42.03
	773	860.6	807.8	35.49
	798	887.2	833.4	19.69
	823	901.2	847.2	9.78
	873	860.6	827.4	8.24

Wear loss (W_l) and wear distance (W_d) of specimen No.1. 1323 K austenitizing temperature.

Wear distance (W_d) (m)	Wear loss (W_l) of Rubber wheel abrasive wear test (mg)			
	As-hardened	L-H_{Tmax}	H_{Tmax}	H-H_{Tmax}
785	140	154	120	126
1570	261	293	228	243
2355	380	428	339	357
3140	491	557	444	469

Wear loss (W_l) and wear distance (W_d) of specimen No.2. 1323 K austenitizing temperature.

Wear distance (W_d) (m)	Wear loss (W_l) of Rubber wheel abrasive wear test (mg)			
	As-hardened	L-H_{Tmax}	H_{Tmax}	H-H_{Tmax}
785	60	85	80	101
1570	118	165	159	193
2355	179	243	235	279
3140	237	319	311	364

Wear loss (W_l) and wear distance (W_d) of specimen No.3. 1323 K austenitizing temperature.

Wear distance (W_d) (m)	Wear loss (W_l) of Rubber wheel abrasive wear test (mg)			
	As-hardened	L-H$_{Tmax}$	H$_{Tmax}$	H-H$_{Tmax}$
785	55	58	55	73
1570	99	113	105	142
2355	142	166	155	209
3140	182	218	204	275

Wear loss (W_l) and wear distance (W_d) of specimen No.1. 1373 K austenitizing temperature.

Wear distance (W_d) (m)	Wear loss (W_l) of Rubber wheel abrasive wear test (mg)			
	As-hardened	L-H$_{Tmax}$	H$_{Tmax}$	H-H$_{Tmax}$
785	89	111	109	99
1570	156	221	210	192
2355	238	323	308	289
3140	318	424	406	383

Wear loss (W_l) and wear distance (W_d) of specimen No.2. 1373 K austenitizing temperature.

Wear distance (W_d) (m)	Wear loss (W_l) of Rubber wheel abrasive wear test (mg)			
	As-hardened	L-H$_{Tmax}$	H$_{Tmax}$	H-H$_{Tmax}$
785	72	78	67	83
1570	130	155	132	161
2355	188	232	194	238
3140	245	305	255	314

Wear loss (W_l) and wear distance (W_d) of specimen No.3. 1373 K austenitizing temperature.

Wear distance (W_d) (m)	Wear loss (W_l) of Rubber wheel abrasive wear test (mg)			
	As-hardened	L-H$_{Tmax}$	H$_{Tmax}$	H-H$_{Tmax}$
785	54	54	53	75
1570	99	102	99	141
2355	142	149	146	206
3140	185	195	191	270

VITA

My name is Jatupon Opapaiboon. I was born on January 31, 1989 in Lopburi. I graduated with Bachelor degree of Engineering (Materials Engineering) from Kasetsart University (Bangkhen campus) in 2011. After graduation, I have been studying for Master degree of Engineering in Metallurgical Engineering at Chulalongkorn University. I was a research student at Department of Materials Science and Metallurgical Engineering, Kurume National College of Technology, Japan in July, 2014 until December, 2014.